Tamer Alsaeed Mahmoud Abdalrahman

Hierarchical fiber bundle strength statistics

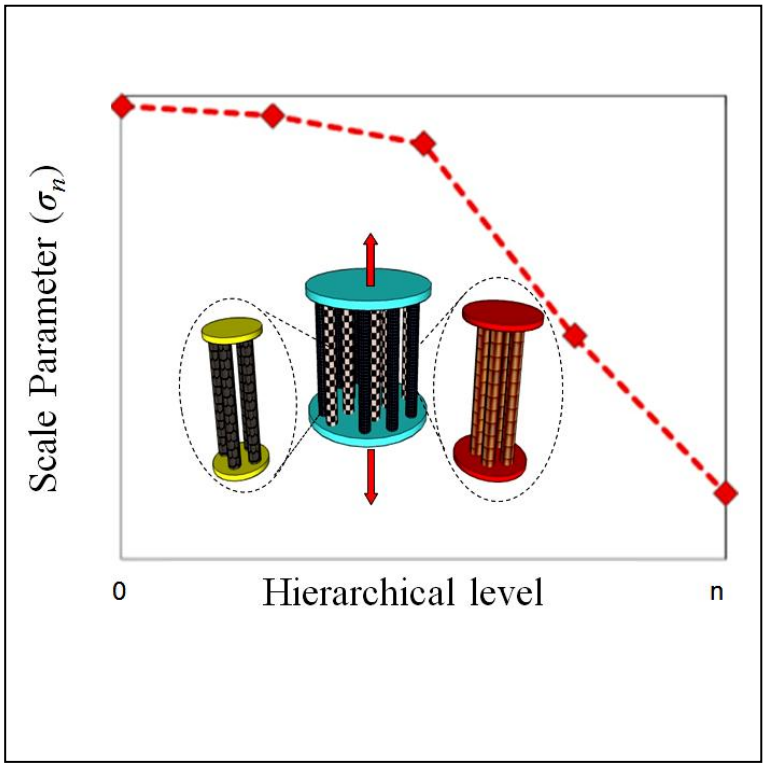

Dottorato di Ricerca in Ingegneria delle Strutture
Politecnico di Torino

Tamer Alsaeed Mahmoud Abdalrahman

Hierarchical fiber bundle strength statistics

Tesi per il conseguimento del titolo di dottore in Ricerca
XXIV Ciclo (2009-2010-2011)

Dottorato di Ricerca in Ingegneria delle Strutture
Politecnico di Torino

Dicembre 2011

Dottorato di ricerca in Ingegneria delle Strutture
Politecnico di Torino, Corso Duca degli Abruzzi 24, 10129 Torino, Italy.

Tutore: Prof. Nicola M. Pugno
Co-Tutore: Dr. Federico Bosia
Coordinatore: Prof. Alberto Carpinteri

Acknowledgments

It is a great pleasure to thank my supervisor, Prof. Nicola Pugno, for having offered me the chance of coming to the Politecnico di Torino and help me to get scholarship, that after three (largely enjoyable) years finally culminated in this Thesis. Prof. Nicola Pugno, I truly appreciated the amount of time and energy that you invested in guiding me throughout this work, your support in the most critical moments, the many enriching scientific discussions. Working with Federico Bosia has been an unforgettable experience, and I am deeply grateful for his untiring support.
Last, but not least, I would like to express my gratitude to those who encouraged and sustained me with their fondness and love. To my parents and my brother and my sisters who have been always at my side, even from a far. And, finally, I cannot imagine the past three years without my wife Hadeel, who exhorted and encouraged me in each and every moment.

Contents

Summary

Multi-scale modeling is currently one of the most active research topics in a wide range of disciplines. In this thesis we develop innovative hierarchical multi-scale models to analyze the probabilistic strength of fiber bundle structures.

The Fiber Bundle Model (FBM) was developed initially by Daniels (1945), and then expanded, modified and generalized by many authors. Daniels considered a bundle of N fibers with identical elastic properties under uniform tensile stress. When a fiber breaks, the load from the broken fiber is distributed equally over all the remaining fibers (global load sharing). The strength of fibers is assigned randomly most often according to the Weibull probability distribution. In chapter 2, we develop for the first time an ad hoc hierarchical theory designed to tackle hierarchical architectures, thus allowing the determination of the strength of macroscopic hierarchical materials from the properties of their constituents at the nanoscale. The results show that the mean strength of the fiber bundle is reduced when scaling up from a fiber bundle to bundles of bundles. The hierarchical model developed in this study enables the prediction of strength values in good agreement with existing experimental results. This new ad hoc extension of the fiber bundle model is used for evaluating the role of hierarchy on structural strength. Different hierarchical architectures of fiber bundles have been investigated through analytical multiscale calculations based on a fiber bundle model at each hierarchical level. In general, we find that an increase in the number of hierarchical levels leads to a decrease in the strength of material. On a more abstract level, the hierarchical fiber bundle model (HFBM), an extension of the fiber bundle model (FBM) presented in this thesis, can be applied to any hierarchical system. FBMs are an established method helpful to understand hierarchical strength.

Another extension of Daniels' theory for bimodal statistical strength has been implemented to model flaws in carbon nanotube fibers such as joints between carbon nanotubes, where careful analysis is necessary to assess the true mean strength. This model provides a more realistic description of the microscopic structure constituted by a nanotube-nanotube joint than a

simple fiber bundle model. We demonstrate that the disorder distribution and the relative importance of the two failure modes have a substantial effect on mean strength of the structure.

As mentioned, the fiber bundle model describes a collection of elastic fibers under load. The fibers fail successively and for each failure, the load is redistributed among the surviving fibers. In the fiber bundle model, the survival probability is defined as a ratio between number of surviving fibers and the total number of fibers in the bundle. We find that this classical relation is no longer suitable for a bundle with a small number of fibers, so that it is necessary to implement a modification into the probability function. It is possible to predict snap-back instabilities by inserting this modification in the theoretical expression of the load-strain (F-ε) relationship for the bundle, as discussed in chapter 4.

Scrutiny into the composition of natural, or biological materials convincingly reveals that high material and structural efficiency can be attained, even with moderate-quality constituents, by hierarchical topologies, i.e., successively organized material levels. This is shown in chapter 5, where a composite bundle with two different types of fibers is considered, and an improvement in the mean strength is obtained for some specific hierarchical architectures, indicating that both hierarchy and material “mixing” are necessary ingredients to obtain improved mechanical properties.

In Chapter 6, we consider a novel modeling approach, namely we introduce self healing in a fiber bundle model. Here, we further assume that failed fibers are replaced by new unstressed fibers. This process has been characterized by introducing a self healing parameter which has been implemented into the survival probability function of the fiber.

General conclusions of the research efforts presented in this thesis are given in chapter 7. This is followed by suggestions for further research and a brief outlook.

Chapter 1

Introduction

1.1 Introduction

Multiscale modelling has attracted increasing interest in past years in various fields, including solid mechanics. Until the late 1980s, it was widely recognized that any experimentally observed size effect on the nominal strength of structures was due to statistical reasons, i.e. related to random distribution in local material strength, described by the Weibull statistical theory.

As is well known, hierarchical structures have special designs with specific composition and microstructure morphology. For example, bone, shown in Fig. 1.1, is composed of hierarchical structures whose material properties change from nanoscale to macroscale.

Thus, these structures must be studied at each individual hierarchical level, in order to understand their intrinsic behavior as well as to determine appropriate design principles when manufacturing composite materials, which are generated using different fabrication technologies.

Hierarchy is an essential concept in order to understand the behavior of bio-tissues. At nanoscale, they are essentially material composites based on the interdigitation of the collagen, the most prevalent biopolymer in human body, and an apatitic mineralite (LeGeros, 1991; Eppell et al., 2001; Cowin, 2001; Katz, 1976; Katz, 1980). These nanoscale structures organize into microscale composites to resist loads, which is one of their primary functions (Cowin, 2001; Katz, 1976; Katz, 1980). For example, the macroscopic anisotropic properties of femoral cortical bone require that

both the haversian microstructure and the appropriate nanostructural organization of collagen and apatite (Eppell et al., 2001; Cowin, 2001; Katz, 1976; Katz, 1980) should provide appropriate macroscopic functions, the molecular structures of the collagen and apatite (nanoscale) must organize firstly; then, the structures to form the microscopic haversian system, which has fiber-like composite material behaviors (Cowin, 2001; Katz, 1976; Katz, 1980) and the system provides the bone microstructures with the required appropriate strength and stiffness (Eppell et al., 2001; Cowin, 2001; Katz, 1976; Katz, 1980).

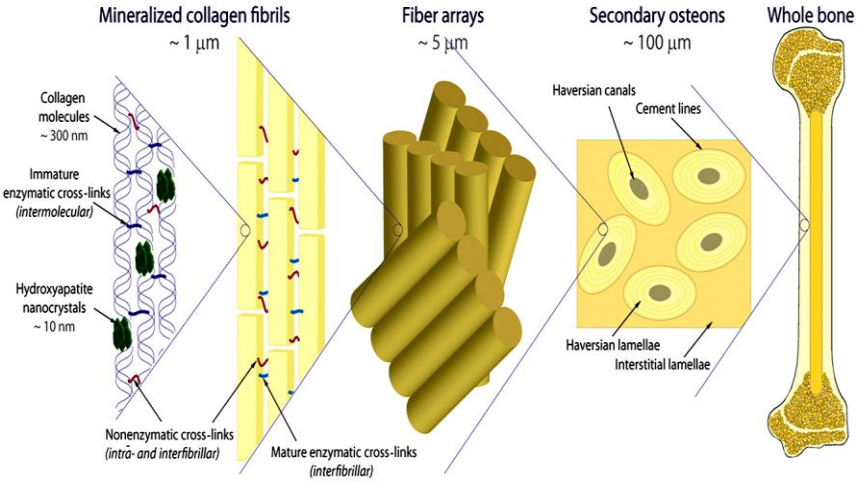

Fig. 1.1 Hierarchical structure of human bone (Ritchie, et. al).

Biological materials suggest a key to design new material with outstanding performance. Olson (1997) emphasized the existence of hierarchical design and distinguished the examples of top-down and goals/means approaches. The combination of bottom-up and top-down approaches has been the historical model for design new materials. Materials design depends on the process-structure and structure-property relations. The process of relating properties to performance is optimized. For example, the Ashby charts (Ashby, 1999) identify the existing material systems and properties that meet the needs of specific applications. This is always an initial step in solving any material design problem, and can be

conveniently done by searching for suitable tabulated properties of materials (Ashby, 1999), often using combinatorial search methods (Shu et al. 2003). Fig. 1.2 presents an example of the hierarchy of computational models.

In recent years, the hierarchical and multi-scale modeling methods for composites have attracted much attention. This is related to several factors. First, the investigations on microstructure–property relationships of natural materials (wood, bones, etc.) suggest that these materials represent hierarchical composites with fibrous reinforcement, and that their extraordinary properties (high strength, fracture toughness, etc.) are attributed to the hierarchical architectures of the materials (Fratzl and Weinkamer, 2007; Gao, 2006; Schmahl et al., 2008; Mishnaevsky, 2007).

Secondly, the optimization of composite properties by varying their structures at the microscale level is involved. Some properties (e.g., stiffness) are improved by increasing the volumetric fraction of hard reinforcement in composites, but this degrades other properties (namely fracture toughness). The idea to create a new family of materials with tailored properties, by controlling different structural elements, such as shape and size, at different levels; has been studied in the framework of the Japanese ‘‘Synergy Ceramics Projects’’ (Kanzaki et al., 1999), which presented an example of a ceramic material that has both high strength and toughness achieved by a combination of aligned anisotropic grains (at microlevel) with the intragranular dispersion of nanoparticles (at nanolevel).

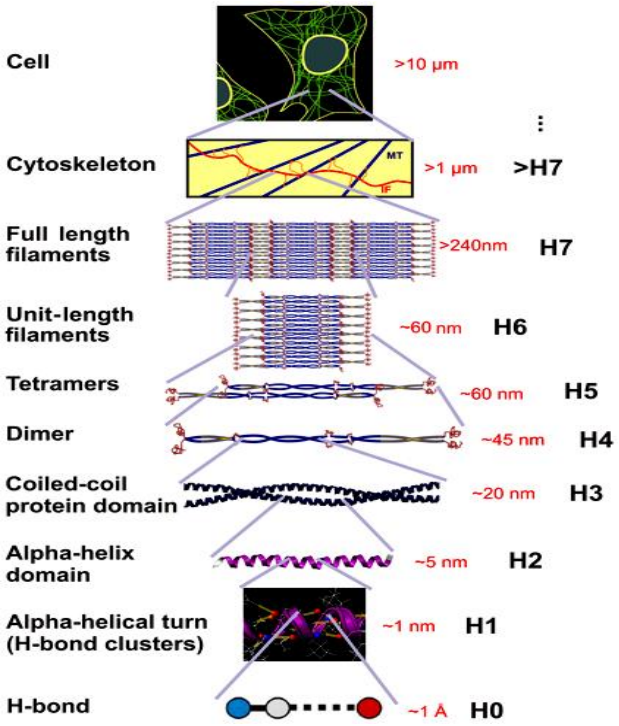

Fig. 1.2 Hierarchical structure of intermediate filaments, from the H-bond level (Angstrom scale) to the cell level (micrometer scale). (Qin, 2010).

Another example of a material with a hierarchical microstructure is a ‘‘trimodal’’ Al-composite, which has been developed by Ye et al., 2005 and has excellent properties (e.g. extremely high compressive yield strength). In this composite, coarse-grained Al is introduced into the nanocrystalline Al, which is reinforced with B_4C particles in order to achieve high strength and acceptable ductility. In general, multiscale composite design allows to improve different mechanical properties of different composites, for example fracture toughness in a carbon fiber reinforced epoxy composites is improved by 80% (Godara, 2009), and dramatic increases in elastic modulus, compressive strength and interlaminar strength of carbon fiber/polymer composites are obtained by dispersed carbon nanofibers (Iwahori, 2003); fracture toughness of carbon fiber reinforced epoxy/clay nanocomposites CFRENCs with the introduction of 4 phr nanoclay in epoxy

is increased by 85% (Xu and Hoa, 2008), flexural strength is increased by 38% due to a small amount of nanoclay (2 phr) added into the epoxy of carbon/epoxy composites (Xu and Hoa, 2008). Thus, tailoring material properties at different hierarchical levels makes it possible to improve mechanical properties of structures.

In order to analyze the effect of the hierarchical structures on the strength and mechanical properties, a number of mathematical models have been developed. Carpinteri and Paggi (2009) developed a model for a hierarchical, fractal grained composite, in which mesograins are composed of micrograins. Using a top down approach, rule of mixture and a generalized Hall–Petch relationship (for hardness), the authors studied the effect of the hierarchical levels on the material hardness and toughness. They demonstrated that a hierarchical material is tougher than its conventional counterpart, and that the material hardness increases with increasing hierarchical levels. Joshi and Ramesh (2007) developed a micromechanical model of particle reinforcement in multiscale composites, in which at least one phase is a composite at a finer scale. They used the multiscale secant Mori–Tanaka method and added subscale terms (in particular, grain size, particle size and dispersoid strengthening), and computed overall response of the material. Yao and Gao (2007) developed self-similar models of hierarchical materials: one was applied to gecko feet and the other one to the microstructure of bone. They demonstrated that a hierarchical material can be designed to achieve flaw insensitivity, using the ‘‘fractal bone’’ model (i.e. a multiple level self-similar composite structure). Gao also demonstrated that a hierarchical material with different properties at different length scales can tolerate crack-like flaws. Besides, a series of analytical models of hierarchical materials, based on fracture mechanics approaches, has been presented by Gao, (2006).

The general conclusion of these works is that the hierarchical structures have higher strength and damage resistance than common structures. This conclusion is compared with the numerical results from Gómez and Pacheco (1997) and with experimental and numerical observations from Newman and Gabrielov (1991), where it is shown that clustering and bundling of reinforcement in composites leaded to the lower damage resistance (Chapter 8 from Schmahl et al., 2008; Mishnaevsky et al., 2004; Segurado and Llorca, 2006).

Based on the fiber bundle model and renormalization methods, and another group of models seek to analyze the asymptotic strength distributions of fiber bundles (Phoenix and Taylor, 1973; Phoenix, 1974, 1975; Newman et al. 1994; Newman and Phoenix, 2001), taking into account the effects of time dependent behavior of fibers and different load sharing rules. A more detailed overview of various fiber bundle models can be found in the works by Newman, Phoenix, Hansen, Herrmann, Bazant and colleagues (Mishnaevsky, 2007).

An important class of hierarchical structures is the fibrous bundle (Schmahl et al. 2008). In general, such a structure consists of fibers, which are capable of sustaining the longitudinal stress. The structure properties are determined by the constituents' properties. Many factors can be adjusted in the manufacturing process, but a lack of control in the production gives rise to strong fluctuations of the mechanical properties in different samples. Generally speaking, a hierarchy of length scales can be identified in fibrous materials, which are illustrated in Fig. 1.3.

Technically, an important example of fibrous structure is the fiber bundle, which has been widely used for modelling in the field of aerospace, automotive and sporting goods. The simplest layout of a fiber is a unidirectional bundle, in which fibers are all arranged in parallel. Under external loading, fracture first appears at the lowest level, i.e. individual fiber fractures. The entire system and its elements experience a gradual reduction of stiffness as damage accumulates by nucleation of micro-damage. Finally, the whole bundle of fibers ruptures, and fails catastrophically. Even though the fiber bundle model is simple, it captures the essential elements of failure processes in a large number of materials. Also, the fiber bundle model is a useful tool for understanding phenomena such as creep, and fatigue.

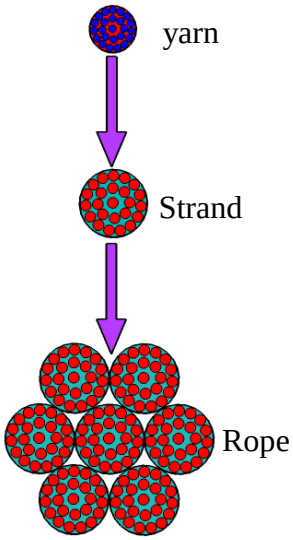

Fig. 1.3 The typical hierarchy ranking from the smallest level to the highest level fiber rope.

Usually, the starting point in the discussion of the failure characteristics of fibrous materials is to consider the macroscopic, volumetric-averaging loading behavior, which is represented by the stress-strain curve. This curve is the representative response obtained by loading a sample, typically by exerting a tension force on a long and macroscopically homogeneous structure. Three fundamental types of behaviors are usually categorized: a linear relation between stress and strain is called linear elastic behavior, where the Young's modulus completely characterizes the loading behavior, which is corresponding to the initial stage of the loading (Fig. 1.4). As loads increase, materials enter a nonlinear regime, a process that is called strain-hardening, and it is typically irreversible in the sense that after unloading, the sample will possess a reduced stiffness upon reloading. Other materials, however, display a behavior that is perfectly plastic after passing a material yield point, where the slope of the stress-strain curve vanishes; the behavior may be visualized as tearing apart a piece of chewing gum. This classification is also useful in terms of fracture: a brittle material breaks before reaching the yield point, whereas a ductile material reaches the plastic regime first.

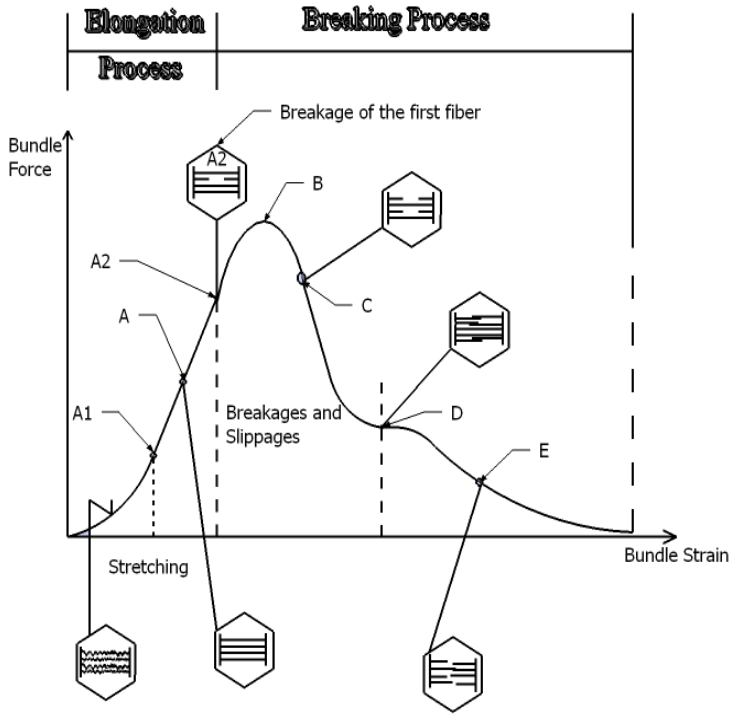

Fig. 1.4 Characteristic parts of a load–elongation curve obtained by tensile test (Grishanov, 1999).

1.2 State of research

Historically, the first appearance of the fiber bundle model can be dated back to 1927, when Peires introduced this approach in order to understand the strength of cotton yarns (Peires, 1926). Assuming equal load sharing after subsequent failure, the first consistent stochastic formulation of the model, together with a comprehensive study of bundles of threads was presented by Daniels (1945). Early attempts to capture fatigue and creep effects led Coleman to propose a time-dependent formulation of the model (Coleman, 1956). These first developments have been ensued by intensive research in both the engineering (Herrmann and Roux, 1990) and physics (LeGeros, 1991; Chakrabarti and Benguigui, 1997) communities. The main

scope is pedagogical and is at the same time an overview of fracture mechanics for physicists and an introduction to new concepts of statistical physics for mechanics engineers, so that nowadays fiber bundle models are considered one of the most important theoretical approaches to model hierarchical structures.

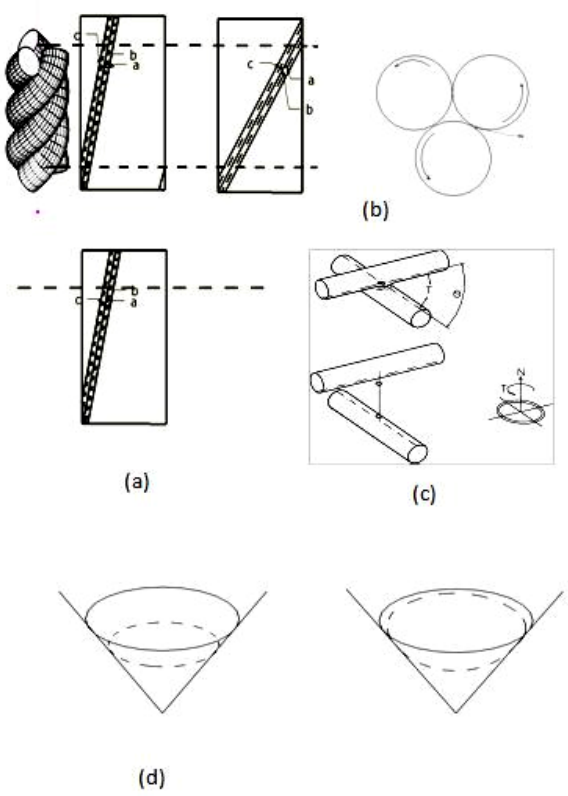

Fig. 1.5 Modes of slip (a) Mode 1 and Mode 2 stretching and twisting respectively. (b) Mode 3 rotating. (c)Mode 4 scissoring and mode 5 sawing. (d) Mode 6.

As mentioned before, FBMs are a useful for modeling fibrous structures under tensile loading, where the load is carried by the fibers. Fiber-fiber interface mainly determines the load transfer among fibers (Leech, 2002) and there are several modes as shown in Fig. 1.5: modes 1 and 2 involve axial sliding between fibers due to stretching and twisting; mode 3, rotation slip, is an end effect, modes 4 and 5 are scissoring and sawing at crossovers;

mode 6 is due to bulk compression or dilation. Fibers distortion was not explicitly included, but implicit in the change of packing geometry.

Still, some adaptations are necessary to make the model more realistic. The first is to find a way to interpolate between the limiting cases of global and local load sharing, which obviously constitute extreme abstractions of the finite range interaction present in a real material, such as the model was proposed by Hidalgo et al. (2002), where the load shared by the unbroken fibers decays as a power law with the distance from a broken fiber. They introduced a fiber bundle model where the interaction among fibers is modeled by an adjustable stress transfer function that can interpolate between the two limiting cases of load redistribution, i.e., the global and the local load sharing schemes. This model was subsequently applied to explain the size dependence of softwood samples under tension (Dill-Langer et al., 2003).

Phoenix and co-workers (Harlow and Phoenix, (1978a, b); Smith and Phoenix, 1981; Smith 1981; Phoenix and Smith. 1983; McCartney and Smith. 1983; Phoenix, 1983; Phoenix et al. 1997; Phoenix and Beyerlein, 2000; Mahesh et al., 2002) has investigated this approach in depth and has led it to high mathematical sophistication. Important mathematical results have been achieved for the statistical distribution of strength in tensioned parallel structural systems such as ropes consisting of fibers (or wires) obeying Weibull statistical distributions of strength.

Considering localization (Beyerlein and Phoenix, 1997), the effect of the matrix between the filaments (Phoenix et al., 1997) and nonlinear behavior (Krajcinovic and Silva, 1982), FBMs provided a basis for successful micro-mechanical models. Extensions of FBMs have been introduced taking into account the possible multiple cracking of the filaments by replacing the brittle filament failure with a continuous damage parameter (Kun et al., 2000).

When considering other sources of random behavior besides strength, the FBMs must be replaced by a deterministic micromechanical model with Monte-Carlo simulation techniques. This approach has been used in analyzing the influence of the distribution of the bundle strength for different fiber arrangements on the stress concentration around the broken

fibers (Ibnabdeljalil and Curtin, 1997). The prohibitive computational costs have been reduced by simplified micromechanical models, like break influence superposition-based on the shear-lag model (Beyerlein and Phoenix, 1996) or the lattice Green's function technique adapted to composite failure (Zhou and Curtin, 1995).

A fiber bundle model involving all the interaction effects occurring in tensile experiments with different specimen lengths paves the way for robust modeling of the failure process in the bond layer with cementations matrix. At present, fiber bundle models are regarded as a simple but elegant method to capture the most significant characteristics shared by disordered materials generally and fibrous composites, namely their inherently features, anisotropy and dynamical load transfer (Kun et al., 2006), which are the features in the breakdown of FRCs. Initially proposed as a model to capture the failure behavior of a bundle of fibers in textile yarns, the behavior of fiber composites can be described as follows: when a thread of parallel single fibers is under an external uniaxial tension, it deforms in a linear-elastic way until the fibers reach their respective failure thresholds, which are randomly distributed; if a fiber fails, the load drops to zero, and has to be redistributed to the remaining fibers. This can result in cascades of further breaking events. Obviously, fiber bundle models are therefore suitable for describing uniaxial composites under tension, and have been applied successfully for this loading condition, since the tensile load on a composite is sustained almost exclusively by the fibers.

Another important aspect that links composite materials to an advanced class of FBMs, i.e. continuous damage fiber bundle models (CDFBM) (Kun et al., 2000), is the inclusion of hierarchical failure levels. Experiments have revealed that long fiber composites loaded parallel to the fiber orientation experience a gradual degradation process so that the macroscopic stress-strain curve, $\sigma(\varepsilon)$, of the composites develops a plastic plateau and the global failure is preceded by a strain hardening regime.

Gücer and Gurland (1962) developed a model for ‘‘dispersed fracture” for a chain of elements, each of them considered as a fiber bundle. The strength of the bundles was analyzed using Daniels' theory, while the failure of the chain was studied using the weakest-link theory. The theoretical predictions of the strength of composites, using this theory, are generally

higher than corresponding experimental values. The model of Gücer and Gurland was developed further by Rosen (1964; 1965), who studied the damage in composite as a failure of chains of bundles with fibers of limited (critical) length. Zweben (1962) studied the influence of the stress concentration of a broken fiber on its closest neighbors, and demonstrated that failure of even a few fibers can lead to the failure of whole specimen. Recently, a number of FBM-based models were developed, which take into account the roles of the matrix and interfaces, nonlinear behavior of fibers and the matrix, and the real micromechanisms of composite failure (2000; 2002).

Krajcinovic and Rinaldi (2005) used the fiber bundle model (called "parallel bar model" in their works) to determine damage laws in materials taking into account the damage micromechanisms. They carried out thermodynamically analysis of the damage evolution in this system. Li and Li (2001) considered the tensile response of reinforced concretes using the parallel bar model by Krajcinovic and Silva, in which fibers and the matrix are connected by parallel series elements. Li and Li (2001) obtained tensile stress–strain curves for different volume contents of fibers by using the model with two damage parameters (for interfaces and for the concrete matrix).

This effect reflects the presence of a hierarchical organization in the materials, in which the failure mechanisms at the lower length scales (at the scale of fibers) gradually activate the breaking of higher order substructures (sub-bundles, bundles, and plies). With fibers embedded in a matrix material, the breaking of a fiber causes debonding along the fiber-matrix interface in the vicinity of the crack (Phoenix and Beyerlein, 2000). However, due to the frictional contact at the interface, the load of failed fibers builds up again over a certain length and consequently the broken fiber can still contribute to the overall load bearing capacity of the system.

As a common tool in computational material research, one can observe that fiber bundle models address two major challenges: on the one hand, they serve as a starting point to develop more realistic models of material failure, which comprise a detailed representation of the microstructure of a material, e.g. the local stress fields, and their complex transmission. Since efficient techniques have been developed to study large scale fiber systems through analytical calculations and simulations, FBMs and models based on

them allow investigating the influence of microscopic material parameters on the macroscopic response of disordered systems. On the other hand, the study on damage and fracture in disordered systems has evolved into a fascinating branch of statistical physics, where researchers have succeeded to find a link between breakdown phenomena, phase transitions, as well as critical phenomena in general. To pursue this analogy, there is now ongoing research to embed fracture phenomena into the framework of statistical physics.

1.3 Fiber bundle model applications

Because the uncertainty in current empirical strength predictions for hierarchical structures is far larger than in the classical structural analysis, statistical approaches offer great promise. One of characteristics for hierarchical fiber structures of positive geometry, the statistical parameters for structural strength cannot be constant but must be increased with increasing structures size. The statistical analysis of structure strength has so far been generally considered to be independent of mechanics, but further progress requires the cumulative distribution function (cdf) to be derived from the mechanics and physics of failure. The structure size effect on the modulus of rupture of plain concrete beams as well as other Quasi-Brittle materials (such as rocks, composites, ceramics or ice) has explained the randomness of the intrinsic material strength in a purely statistical manner (Bazant and Planas, 1998).

However, as revealed by the finite element analyses by Hillerborg et al. (1976) and Petersson, (1981), the statistical explanation ignores the stress redistributions caused by crack propagation prior to the maximum load, and the mean observed size effect can be described deterministically by the cohesive (or fictitious) crack model. A simple analytical formula based on this redistribution was derived by Bazant et al. (1995) and it showed that all the important test data matched very well. On an empirical basis, the same formula was proposed by Rokugo et al., (1995) and Bazant, (1997).

Traditionally, size effects have been explained by Weibull's statistical weakest link model (Fisher and Tippett, 1928; Weibull, 1939; 1949; 1951;

Epstein, 1948; Freudenthal, 1956; Freudenthal and Gumbel, 1953; Gumbel, 1958; Saibel, 1969; Weibull, 1956). Its basic hypothesis is that failure occurs fail as soon as the material strength is exceeded at one point of the structures. In summary, to capture the salient properties of Quasi-Brittle cohesive fracture in two or three dimensions expanding the probabilistic load-sharing concepts for parallel systems is one of the fiber bundle model applications.

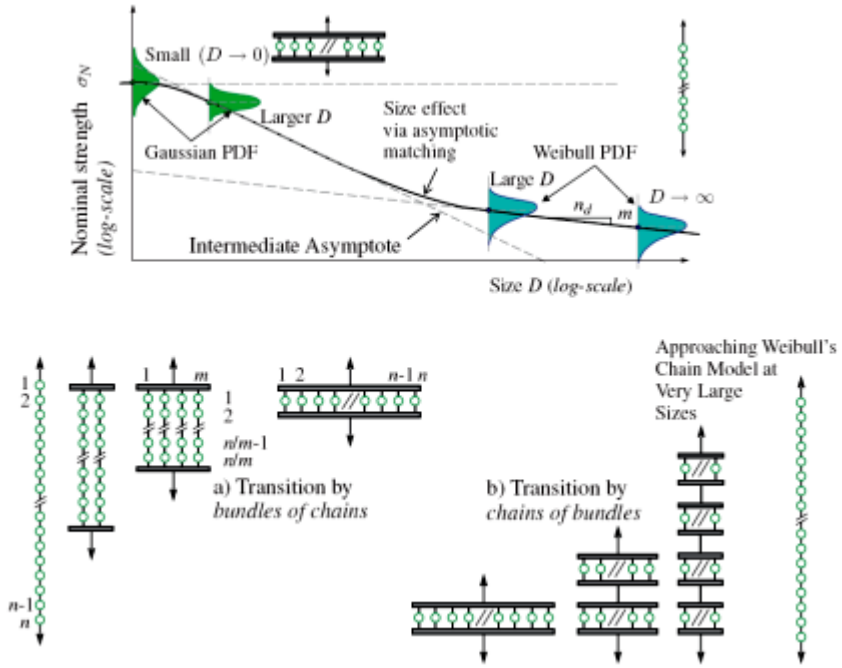

Fig. 1.6 Curve of mean size effect for structures failing at macroscopic fracture initiation, and its probability distributions for various sizes (Bazant, 2002).

Several novel aspects of breakdown phenomena have been revealed by the study of FBMs in recent years. The introduction of thermal noise leads to the reduction of the strength of materials. And in the presence of thermally activated cracking sub-critical crack growth, a finite lifetime of materials is observed (Roux, 2000; Scorretti et al., 2001). The healing effect

of microscopic cracks has also been addressed by thermodynamic fiber bundle models (Virgilii et al., 2007).

A crossover in the avalanche size distribution D (Δ) from the power law with exponent 5/2 to another power law regime with a lower exponent 3/2 has been observed, when the avalanches of fiber failures are only recorded in the vicinity of the point of macroscopic failure, i.e., the strength distribution of the remaining intact fibers is close to critical (Pradhan et al., 2005a, b). The connectivity properties of the bundle turned out to play an important role in breakdown processes, i.e., considering locally interacting fibers of a bundle on the nodes of a Barabasi-Albert network (instead of placing them on lattice sites) substantially alters the failure process (Kim et al., 2005); these models are closely related to the statistical properties of social interactions (da Silveira, 1999). Similarly, a random fuse model on a network may be applicable to predict the failure of electric grids (Bakke, 2006) and has been applied for biological materials (Nukala et al., 2005a, b).

The appropriate structural design of tissue engineering scaffolds and prosthetic grafts is critical to restoring native functionality thus determining the long-term success of the implant. Both cellular biocompatibility as well as mechanical compatibility must be considered within the engineering approach to tissue design (Wintermantel et al. 2000). Scaffolds and grafts with a wide range of properties (e.g., pore size, porosity, strength, elasticity, void volume, adaptability, and size) are needed to accommodate the range of tissue types currently being engineered, e.g., ligaments, tendons, urinary incontinence devices, soft-tissue reinforcement meshes, and blood vessels. In developing fibrous grafts for these applications, yarn design has been shown to be a major factor in tensile and burst strength, as well as flexure rigidity, of higher order constructs such as meshes and superstructures used for soft tissue reinforcement (Cosson et al., 2003).

A particular clinical need for advanced yarn design is evident in ligament and tendon tissue engineering, as previous failures have forced the field to readdress graft and yarn design (Guidoin et al., 2000). The need for reducing ligament graft stiffness to avoid the stress shielding of forming tissue has long been recognized and explored previously through braided designs; however, native tissue properties were not restored (Chvapil et al.,

1993). These braided prostheses failed due to the lack of biodegradation, as well as the geometry and resultant load distribution in the structure. Analysis of failed polyester grafts implanted for several years demonstrated insufficient and unorganized ingrowth throughout the structures. An example of a more appropriate anterior cruciate ligament (ACL) graft design was composed of silk wire-rope yarns where a combination of a long-term degradable biomaterial and appropriate geometry demonstrated a significantly reduced stiffness while maintaining strength (Altman et al., 2002).

Techniques including braiding, twisting, cabling, texturing, and plying have been explored to generate yarns for grafts or building blocks of grafts (e.g., weave, or non-woven structure).
An infinite number of yarns demand an understanding of how each yarn behaves mechanically relative to each other. The ability to predict changes in mechanics on the basis of changes in yarn geometry (e.g., increasing twisting angel or the number of fibers per yarn) will decrease the need for significant trial and error testing. However, it is important to note that for each specific goal, correlations must be established between the specific material of choice, yarn design, and structural design, in order to fully assess the impact of the yarn design on final properties. Our theory could be used to further understand the impact of yarn design and the methods of analysis to extrapolate predictions for specific structural and functional needs in tissue engineering.

The hierarchical structure of yarns can be described according to the following levels:
-Bundle: fibers can be maintained in parallel or twisted to one another to form a multifiber yarn.
-Cabled: A bundles of fibers held independently while they can be wrapped around each other or paralleled. Each hierarchical level consist of the filaments or bundles (Fig. 1.7).

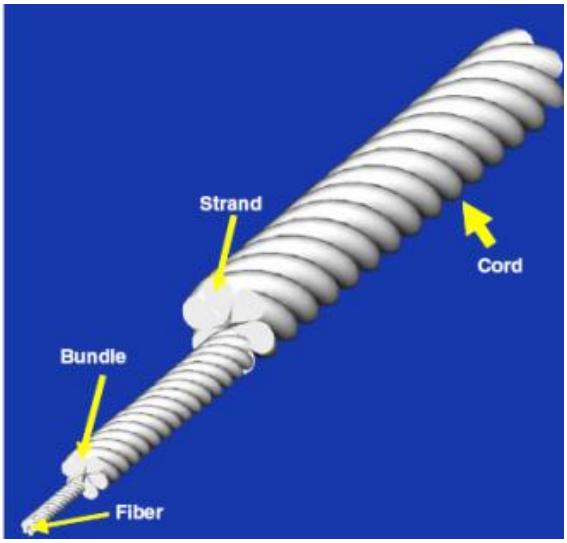

Fig. 1.7 Hierarchal organization of a twisted or cabled yarn. Fibers are combined to form bundles, bundles to form strands, and strands to form cords.

Kolařík et al. (1984) presented an application of fiber bundles for modeling synthetic tendons. They used Poly (ethylene terephthalate) fibers to prepare on a pilot-plant scale by additional drawing of commercial textile fibers texturized by false twist. Another example of application of fiber bundles in tissue engineering is for the design of synthetic tendons. By the varying fiber volume fraction, it is possible to adjust the required mechanical properties of these synthetic tendons (Kolarík et al. 1981).

1.4 The classical fiber bundle model

In this section, we will outline the main properties of the classical fiber bundle model in order to facilitate the comprehension of the modified FBMs presented in the subsequent chapters.

To generate a computationally feasible fiber bundle model, a couple of simplifying assumptions have to be made (Daniels, 1945; Phoenix, 2000; Closter et al. 1997; Pradhan et al., 2003; Cornett 1989; Andersen, 1997): The constituent fibers have a perfectly brittle behavior under an incremental load, which means they deform in a linear elastic manner until they break at their respective failure loads σ_i, $i = 1, \ldots, N$. The Young's modulus E is

identical for all fibers. The failure process of a single fiber is instantaneous and irreversible, so that the load on a broken fiber vanishes (see Fig. 1.8). Broken fibers in the classical FBM cannot be restored, i.e. there is no healing.

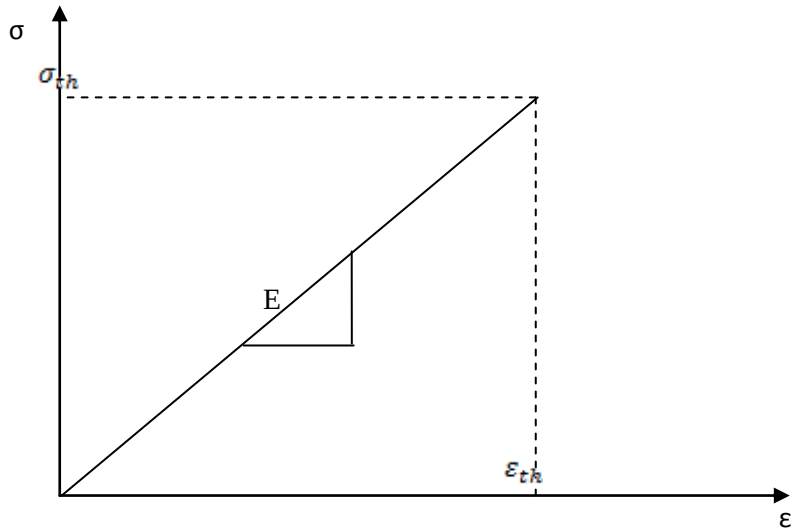

Fig. 1.8 Linear elastic loading characteristic of a single fiber, which breaks when its failure load σ_{th} is reached.

The significance in the construction of the fiber bundle model is the range of load redistribution after fiber failure, which obeys the load sharing rule. Two extreme cases for the interaction form have evolved as standards, and they constitute two sub-classes of fiber bundle models with substantially different micro- and macro-behaviors. The first form is global load sharing (GLS), sometimes termed equal load sharing (ELS), characterized by the fact that the load on a failed fiber is redistributed on all intact fibers in the array, regardless of their distance from the failed fiber. It reflects the experimental condition of loading a set of parallel fibers between two rigid plates, and usually it serves as a starting point for investigating more complex variations of this type, since GLS models usually can be treated analytically (Pradhan, 2005a; Kloster et al., 1997; Pradhan and Chakrabarti, 2003; Sornette, 1989; Hemmer and Hansen, 1992).

For the contrary case of local load sharing (LLS), the load of a failed fiber is shared equally by the neighboring intact fibers. The load redistribution evokes a high stress concentration around failed regions. The accompanying correlations set prohibitive limitations towards an analytical treatment of this problem (Phoenix and Beyerlein, 2000; Harlow and Phoenix, 1978; G´omez, 1993), so that large scale simulations have to be employed (Harlow and Phoenix, 1978; Hidalgo et al., 2002; Hansen and Hemmer, 1994; Curtin, 1998). The experiment corresponding to this situation is the stretching of a bundle of fibers between plates having finite compliance (Hansen and Roux, 2000; Batrouniet al., 2002; Delaplace et al., 1999).

The degree of disorder in a material is modeled by assigning randomly distributed failure thresholds σ_{th}^{i} to the fibers, for which the probability density is $w(\sigma_{th})$ and the distribution function is $W(\sigma_{th}) = \int_{\sigma_{min}}^{\sigma_{max}} w(x)dx$. This is very important in modeling heterogeneity and deeply influences the overall response of the model: in fact, it is the only component of the classical FBM that represents material dependent features.
Typically, two types of random distributions are employed. The first one is a uniform distribution between 0 and 1 with the density and distribution functions, which serves as a starting point for analytical solutions.

$$w(\sigma_{th}) = 1, \qquad W(\sigma_{th}) = \sigma_{th}, \tag{1.1}$$

A distribution with a better physical foundation (Dill-Langer et al., 2003) is the Weibull distribution

$$W(\sigma) = 1 - \exp[-(\frac{\sigma}{\sigma_0})^m] \tag{1.2}$$

where m and σ_0 denote the Weibull index and scale parameter, respectively. It should be noted that the amount of disorder can easily be controlled by tuning the Weibull index m. Some general features of FBMs will be mentioned in the following sections, as they are shared by most variants and are important in models for the understanding the breakdown of heterogeneous materials.

Loading on a bundle is usually performed quasi-statically, and can be controlled in two substantially different ways: first, if the strain ε of the bundle is controlled externally, the stress on single fibers σ_i at each loading stage is determined by $\sigma_i = E\varepsilon$; consequently, no load sharing occurs and the fibers break subsequently in the order of increasing breaking thresholds. Hence, for a given strain ε, only those fibers with breaking thresholds $\sigma_{th}^{\,i} < E\varepsilon$ fail, and the intact fibers sustain an equal stress $E\varepsilon$. Then, macroscopic constitutive behavior of the FBM can be expressed as:

$$\sigma(\varepsilon) = E\varepsilon\,[1 - W(E\varepsilon)] \tag{1.3}$$

where $[1 - W(E\varepsilon)]$ is the fraction of intact fibers at ε (da Silveira, 1999; Sornette, 1989). For the case of Weibull distributed strength values with m = 2.7 and σ_0= 34MPa, the constitutive curve is shown in Fig. 1.9.

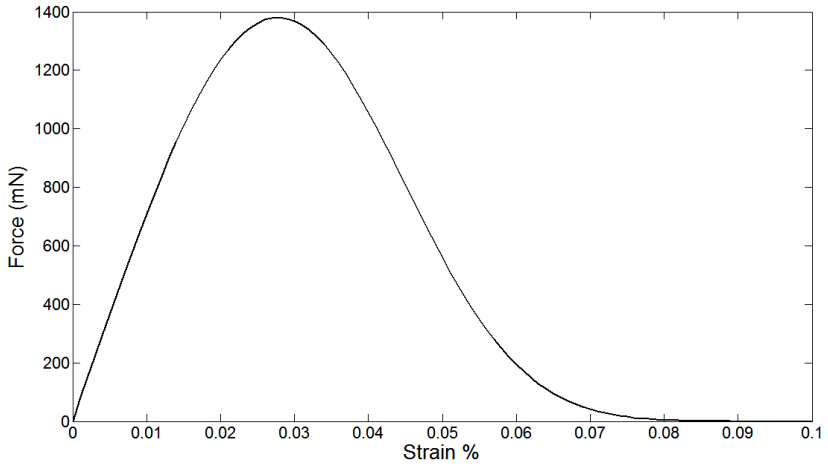

Fig. 1.9 Macroscopic constitutive behavior of a fiber bundle with global load sharing Eq. (1.3) using Weibull distributed strength values σ_{th} (m = 2.7 and σ_0=34 GPa).

The second type of loading configuration is the stress-controlled case. Here, the damage process is more complex, due to the load redistribution following a fiber breaking. The load by the remaining fibers, both in the cases of GLS or LLS, can result in secondary fiber breaking. These failures can then either stop after a certain number of broken fibers, or continue as a catastrophic event resulting in the macroscopic failure of the entire system

and in this case, all remaining intact fibers are destroyed (Pradhan et al., 2005a; Kloster et al., 1997; Hemmer and Hansen, 1992; Hidalgo, 2001).

One of the advantages of fiber bundle models are that they allows the simple incorporation of statistical and probabilistic effects, easy implementation of different probability laws and conditions, and even the simulation of complex dynamical patterns of damage evolution in composites. The weakness of initial fiber bundle models (which however tend to be overcome in recent models) was that the FBM (which is not based on continuum mechanics) does not include the strain continuity, deformation laws and other basic continuum mechanical laws. Thus, the nonlinear behavior of components, interface effects, and multiple cracking had to be introduced in the model, using additional assumptions and generalizations.

Chapter 2
A new hierarchical fiber-bundle model theory for the calculation of the strength of bioinspired nanomaterials

2.1 Introduction

In civil engineering ropes made from high-strength synthetic fibers are ideal for many applications. For instance, they may be used to replace high tensile steel strands, particularly where low weight and corrosion resistance are of prime concern. Ropes with parallel components have been identified for use in cable-stayed and suspension bridges, prestressed concrete structures, prestressed brickwork, cable supported roofs, deep water platforms and retaining walls. The individual elements (yarns or bundles) are arranged in parallel to the rope axis throughout the entire length. In this parallel construction there is little interaction between elements and statistics can easily be applied.

The tensile behaviour of parallel fiber bundles has always been an interesting topic for textile researchers. It is well known that the tensile properties of a fiber bundle are greatly influenced by those of the constituent fibers which form the bundle. Theoretical work has dealt with the mechanics of parallel fiber bundles, on the basis of the fact that each fiber in the bundle possesses a different tensile behaviour (Neckář and Das, 2006). In general, the fiber bundle model is one of the most important theoretical approaches to investigate the fracture and breakdown of disordered media, extensively used by both the engineering and physics communities.

The principal idea underlying statistical models for individual fibers is the "weakest link" concept. This was apparently introduced by Chaplin (1882; 1880) (see review by Harter, 1950) and further developed by Peirce (1926) and Weibull (1939). The connection with the statistical theory of extreme values was then exploited by Epstein (1948 a, b), Gumbel (1954) and Coleman (1958). Different aspects of the theory, as applied to brittle materials, have been investigated by McClintock and Argon (1966), Argon (1974) as well as Hunt and McCartney (1979).

In general, the theoretical model of a fiber bundle consists in a set of N parallel fibers with statistically distributed strengths. The sample is loaded parallel to the fiber direction and the fibers fail if the load on them exceeds their threshold value. An extensive mathematical investigation of failure properties of bundles of fibers was first carried out by Daniels (1945). He used a stochastic process to study bundles of threads made by a parallel construction, which is now generally referred to as the "classical" fiber bundle theory, investigating the relation between the strength of a bundle and the strength of its constituent threads. The main features of Daniels' model are discussed in Section 2.

Further, Harlow and Phoenix (1978) proposed the concept of the chain-of-bundles model for the strength of fibrous structures, to tackle the issue of the statistical nature of the strength of an individual filament, the size (length) effect on filament strength and the load-sharing mechanism during structure breakage. Porwal et al. (2006) also extended Daniels' method to analyze twisted fiber bundles by incorporating fiber helical paths into their model. However, the exclusion of fiber interactions, such as friction and lateral constraint, imposes limits to their model.

Research has since gone into more sophisticated models with more realistic hypotheses. One such direction of research has been the relaxation of the "equal load-sharing" assumption, e.g. to consider random slack of fibers (Phoenix and Taylor, 1973) or inter-fiber frictional forces (Smith and Phoenix, 1981). Also, much attention has been given to the development of models for composite materials when the fibers are embedded in a matrix, e.g. see Harlow and Phoenix (1978, 1981 a, b), as well as Smith (1980). These models generally focus on the influence of fiber strength, bundle

length, bundle size, fiber packing and role of a matrix. For example, a large scale Monte Carlo simulation was performed to study the fracture process in a fiber composite material, in which fibers are arranged in parallel in a hexagonal array and their strengths are given by a two-parameter Weibull distribution function (Mahesh et al., 1999); also, dynamic tensile properties of Ultra High Molecular Weight Polyethylene (UHMWPE) fiber bundles were studied at two strain rates and two temperatures (Huang and Wang, 2004).

There are various notable statistical strength theories for twisted fiber bundles, namely by Phoenix (1979) and Pan (1993). Although using different approaches, both have extended Daniels' parallel bundle theory. Gegauff (1907) was the first to theoretically analyze yarn strength in terms of yarn structure. He derived a simple mathematical relationship between twist angle and yarn strength. Gurney (1925) extended that relationship by taking into account the length and frictional properties of fibers, in addition to the twist angle. He argued that in a cotton yarn under tension, there are two kinds of forces present, i.e. forces that tend to press the fibers normally, and forces that tend to cause slipping. He suggested that when the ratio of the forces tending to cause the slipping to the normal forces exceeds a certain critical value, which corresponds to the friction coefficient (μ), then slipping would occur. He derived expressions for calculating stress developed in individual fibers, which take fiber length and coefficient of friction into consideration. Hua and Xin (2005), particularly, studied the strength of staple fibers using the Weibull distribution. Pan (1993) derived and directly applied an orientation efficiency factor to Daniels' mean and standard deviation, to account for the effect of an average twist. Recent attempts to model twisted ropes, including work on impregnated yarns, can be found in Porwal et al., (2006), where the strength of an impregnated yarn was estimated using an effective shear traction and fiber obliquity factor.

Further improvements to model construction can be achieved, for instance, by generalizing the damage law, constitutive behaviour, deformation state and interaction law of the fibers (Kun et al., 2007). The improvement in performance of high-modulus and high-strength yarns not only puts stronger demands on yarn manufacturing processes but also on the scientific community to develop more accurate descriptions of the structure and properties of filaments composing the yarn.

The high variability in strength found in brittle fibers is well described by a Weibull distribution function. This variability is due to randomly distributed flaws in the fibers. The assumptions generally used in this analysis, i.e. the so-called Coleman's conditions, are: (1) the filament length is constant within the bundle, (2) the stress–strain relationship for a single fiber follows Hooke's law up to failure, (3) the load released with the fracture of one fiber is uniformly distributed among the surviving fibers, and (4) phenomena that could lead to premature failure of the fibers are absent. The Weibull model was used to describe the intrinsic statistical nature of fracture strength and also the relation between material properties and size-scale (Sybrand van der Zwaang, 1989). The Weibull distribution is widely used to describe tensile strength of brittle materials (Coleman, 1958; Peirce, 1926) such as carbon (Pickering and Murray, 1999) and glass fibers (Andersons et al., 2002; Paramonov and Andersons, 2007). Recently, the Weibull theory was also used for the analysis of the tensile properties of bast fibers such as jute (Loan et al., 2006), hemp (Pickering et al., 2007), flax (Zafeiropoulos and Baillie, 2007) and for carbon nanotubes (Pugno and Ruoff, 2004, 2006) or carbon nanotube bundles (Pugno, 2006a, 2007a, b).

In this chapter, we develop a new theory, basically the hierarchical extension of Daniels' pioneering model, and complementary to a recently-introduced numerical hierarchical fiber bundle model (Pugno et al., 2008). This theory allows us to carry out statistical and reliability analysis on hierarchical structures, typically bio-inspired materials, in order to estimate their statistical parameters of structural response and/or theoretical failure probability. Thus, a purely analytical theory can be of great help in a domain where time-consuming numerical studies are usually employed.

2.2 Hierarchical fiber bundle theory

A rope, as well as many fibrous biological materials, can be seen as a hierarchical ensemble of fibers, organized as schematically shown in Fig. 2.1: the rope is composed of various strands, in turn composed of yarns, in turn composed by fibers. Each can be seen to correspond to a different hierarchical level, starting from single fibers (level 0): a bundle of fibers corresponds to a yarn (level1), a bundle of yarns corresponds to a strand

(level 2), and a bundle of strands corresponds to a rope (level 3). In Fig. 2.1 "Twisting" can be introduced at any level, and in the general case, the hierarchical structure can extend over many more levels than those shown in Fig. 2.1. This hierarchical arrangement suggests the use of a hierarchical procedure to determine higher-level properties only from level 0 constituent fiber properties, as discussed below.

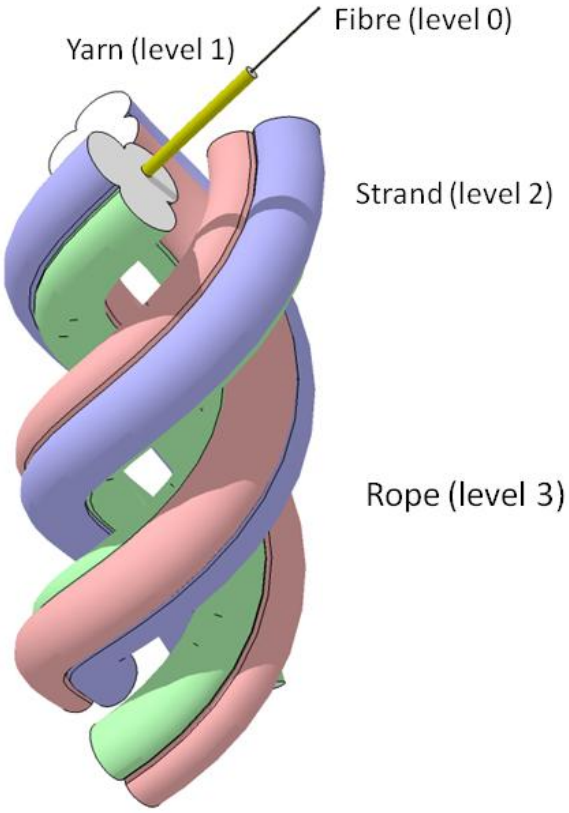

Fig. 2.1 Hierarchical organization of a rope

2.2.1 Single level statistics

The strength distribution of a single element composing a fiber bundle is assumed to be described by means of a two-parameter Weibull distribution $W(\sigma)$ as:

$$W(\sigma) = 1 - e^{-\frac{l}{l_c}(\frac{\sigma}{\sigma_0})^m} \tag{2.1}$$

where l is the element length, l_c is a characteristic internal length, σ is the stress applied in the longitudinal direction, whereas σ_0 and m are the scale and shape parameter respectively. It is seen that when the fiber length decreases, the statistical strength of the element will increase. The mean strength $< \sigma_W >$ is given by:

$$< \sigma_w >= \left(\frac{l}{l_c}\right)^{\frac{-1}{m}} \sigma_0 \Gamma\left(1 + \frac{1}{m}\right) \tag{2.2}$$

whereas the standard deviation is:

$$\theta_w = < \sigma_w > \sqrt{\frac{\Gamma(1+\frac{2}{m})}{\Gamma^2(1+\frac{1}{m})} - 1} \tag{2.3}$$

The shape parameter, m, represents the dispersion of the strength. A greater m value indicates a small strength variation and when m tends to infinity the strength becomes deterministic.

Now, let us consider a bundle made of a very large number, N, of parallel elements of Weibull type with equal length, l. Because it is a parallel bundle without any twist, we can expect all elements to have the same strain $\varepsilon_e = \varepsilon_b$ where ε_e, ε_b are the elements' and bundle's strains respectively. It is evident that if all elements had the same strength, the bundle strength would be equal to that of its constituents. However, because in reality there is certain

dispersion in the strength of the elements, the bundle strength will be statistically distributed, too. This problem was first tackled by Daniels (1945). In his analysis, it is assumed that when an element breaks, the load it was carrying is instantaneously shared equally among all the surviving elements. Thus, neither stress concentrations nor dynamic wave propagation effects are considered. Based on Daniels' analysis, the density distribution function for the strength of the bundle approaches a normal form:

$$D(\sigma) = \frac{1}{\sqrt{2\pi}\theta_D} e^{-\frac{(\sigma - <\sigma_D>)^2}{2(\theta_D^2)}} \tag{2.4}$$

where $<\sigma_D>$ is the mean bundle strength:

$$<\sigma_D> = \sigma_0 \left(\frac{l}{l_c} m \right)^{-1/m} e^{-1/m} \tag{2.5}$$

and θ_D is the standard deviation of the bundle strength, given by:

$$\theta_D = \sqrt{\frac{<\sigma_D>^2 \left(1 - e^{-1/m}\right)}{N e^{-1/m}}} \tag{2.6}$$

Note that for m tending to infinity a deterministic strength is predicted.

For a normal distribution, $<\sigma_D>$ will be the maximum likelihood estimate of the bundle strength. It can be seen, by comparing Eqs. (2.2) and (2.5), that due to the element strength dispersion, the mean bundle strength $<\sigma_D>$ is smaller than the mean fiber strength $<\sigma_W>$. The difference between the two will diminish when the shape parameter m tends to infinity.

2.2.2 Hierarchical extension of Daniels' theory

The equations in Section 2.1 can be exploited to derive strength distributions for hierarchical structures such as that shown in Fig. 2.1. To do this, we assume that each hierarchical level can be represented as a bundle of fibers, of which each constituent fiber can in turn be represented by a

bundle of lower level fibers, and so on. The structure is schematically represented in Fig. 2.2. It is reasonable to assume that at each level n in the structure the strength of the constituent fibers is Weibull distributed, i.e. is described by Eqs. (2.1) - (2.3) with scale and shape parameters σ_{0n} and m_n and length parameters l_n and l_{cn}.

We now exploit the fact that analytical results show a transition of the strength distribution function for a fiber bundle from a Weibull to a Gaussian form for large values of the number of fibers N_n. Therefore, the mean strength $<\sigma_{Wn}>$ and standard deviation θ_{Wn} of the fibers at level n should coincide with those calculated using Daniels' theory (Eqs. (2.5) and (2.6)) applied at level (n-1). Therefore, the Weibull parameters of the constituent fibers at each hierarchical level can be determined those at the lower level, down to level 0 (single fiber), where the distribution parameters are usually known or can be inferred.

Accordingly, we impose:

$$< \sigma_{Wn+1} >=< \sigma_{Dn} > \tag{2.7}$$

$$\theta_{Wn+1} = \theta_{Dn} \tag{2.8}$$

thus linking two adjacent hierarchical levels and extending Daniels' theory.

The two equations lead to

$$\frac{\Gamma\left(1+\frac{2}{m_{n+1}}\right)}{\Gamma^2\left(1+\frac{1}{m_{n+1}}\right)} = \left(\frac{\theta_{Dn}}{< \sigma_{Dn} >}\right)^2 + 1 \tag{2.9}$$

$$\sigma_{0(n+1)} = \frac{< \sigma_{Dn} > \left(l_{n+1} / l_{c(n+1)} \right)^{1/m_{n+1}}}{\Gamma\left(1 + \frac{1}{m_{n+1}} \right)} \tag{2.10}$$

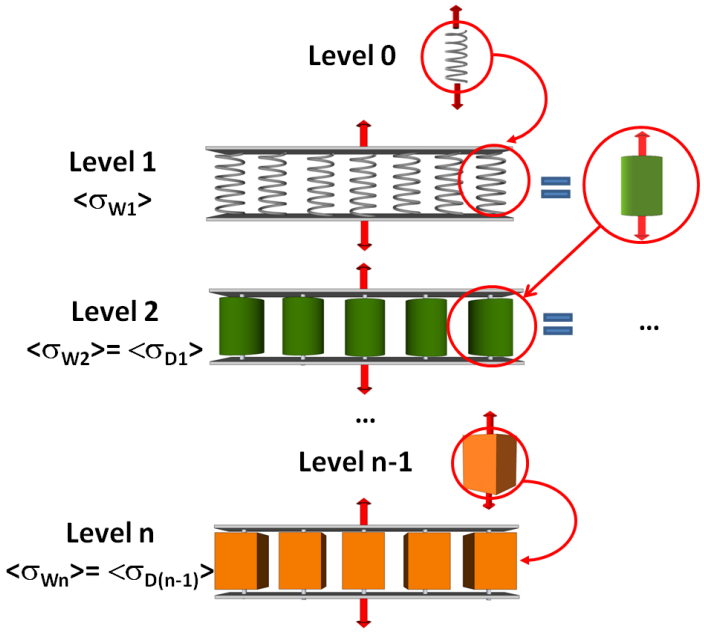

Fig. 2.2 Schematic representation of a hierarchical structure and of the procedure to determine the Weibull strength distribution at level *n* from Daniels' theory applied to the fiber bundle at level (*n-1*)

The shape factor m_{n+1} for level $(n+1)$ can be easily numerically calculated from Eq. (2.9), and the scale factor $\sigma_{0(n+1)}$ can be obtained from Eq. (2.10). This procedure can be repeated for each hierarchical level, i.e. starting from the Weibull distribution at level 0, Daniels' theory can be applied to derive the strength at the first hierarchical level, and so on up to level *n*. Notice that this hierarchical procedure amounts to relaxing the equal-load-sharing (ELS) hypothesis, because load sharing applies only to single fiber bundles. This provides more realistic strength distribution

estimations than "single level" estimations, because in real materials some form of "local load sharing" takes place.

2.3 Modifications to the hierarchical theory

Clearly, the procedure described in Section 2 can be refined by including corrections for various effects, e.g. bundles with a small number of fibers, fiber twisting, friction etc. These corrections are introduced below.

2.3.1 Bundles with a small number of fibers

The asymptotic value $<\sigma_{Dn}>$ is independent from N_n, since the number of fibers in the bundle is assumed to be large. However, when dealing with hierarchical architectures, structures represented by bundles made up of a small number of fibers are commonplace (see e.g. Ackbarow 2009), and approximations used in Daniels' theory could no longer be acceptable. Smith (1982) found a way to eliminate the discrepancy between the real Gaussian distribution and the Daniels' normal approximation, by deriving a correction factors that depend on the number of fibers N_n, in order to improve the accuracy of the strength estimation for relatively small bundles.

The improved $<\hat{\sigma}_{Dn}^{(N_n)}>$ and $\hat{\theta}_{Dn}^{(N_n)}$ estimations according to McCartney and Smith (1983) are given by:

$$<\hat{\sigma}_{Dn}^{(N_n)}>=f_{N_n}<\sigma_{Dn}>=\left(1+C_1\sqrt[3]{\frac{e^{2/m_n}}{N_n m_n}}\right)<\sigma_{Dn}> \tag{2.11}$$

$$\hat{\theta}_{Dn}^{(N)}=g_{N_N}\theta_{Dn}=\sqrt{1-C_2\left(\frac{e^{2/m_n}}{{N_n}^2 m_n}\right)^{2/3}\left(\frac{<\sigma_{Dn}>}{\theta_{Dn}}\right)^2}\,\theta_{Dn} \tag{2.12}$$

where f_{Nn} and g_{Nn} are the correction factors for mean strength and standard deviation, and C_1=0.992 and C_2=0.317 are numerical coefficients.

In order to improve these estimations, we can use the hierarchical theory outlined in Section 2.2 in the limiting case of a bundle composed of single

fiber (in the following we omit the subscript *n*, as this procedure is valid at any hierarchical level). Using Eqs. (2.5) and (2.10) for N=1, and having set for simplicity $l=l_c$, we have:

$$f_1 = \frac{\Gamma(1+\frac{1}{m})}{m^{-1/m}e^{-1/m}} \tag{2.13}$$

Similarly, from Eqs. (2.6) and (2.9) for N=1:

$$g_1 = \sqrt{\frac{\left(1+\frac{2}{m}\right)^{-2}(1+\frac{1}{m})}{e^{-1/m}\left(1-e^{-1/m}\right)}} \tag{2.14}$$

To check the validity of these relations, we use numerically calculated results using a Hierarchical Fiber Bundle Model (HFBM) previously developed by the authors and described in Pugno (2008). Fig. 2.3 illustrates the results for f_1 and g_1 as a function of m in the three cases: 1) Hierarchical theory (Eqs. 2.13 and 2.14), 2) McCartney/Smith theory (Eqs. 2.11 and 2.12), and 3) HFBM simulations. It is apparent that the correction factor proposed by McCartney/Smith overestimates the actual value above and below $m=2$, whilst there is an excellent agreement between 1) and 3), thus confirming the validity of the proposed hierarchical approach. There is also good agreement between 1) and 3) in the case of the correction factor for the standard deviation, while the McCartney/Smith value displays an altogether different behaviour.

Numerical HFBM simulations are also used to derive f_N and g_N, i.e. the dependence of the correction factors on the number of fibers N. In the case of the mean strength, the power-law dependence on N proposed by McCartney/Smith is consistent with HFBM results, and Eq. (2.13) can therefore be generalized to:

$$f_N = 1+\left(f_1-1\right)N^{-\frac{2}{3}} \tag{2.15}$$

In the case of the correction factor for the standard deviation, the expression by McCartney/Smith is inadequate in reproducing results from numerical calculations, and therefore the dependence on N is derived from the latter as best fit, in the form:

$$g_N = g_1 N^{(am+b)} \tag{2.16}$$

where a=0.01, b=-0.05 are the numerically derived coefficients. The comparison of the results for mean strength and standard deviation are illustrated in Fig. 2.4 (McCartney/Smith values are not reported, since the discrepancies are considerable).

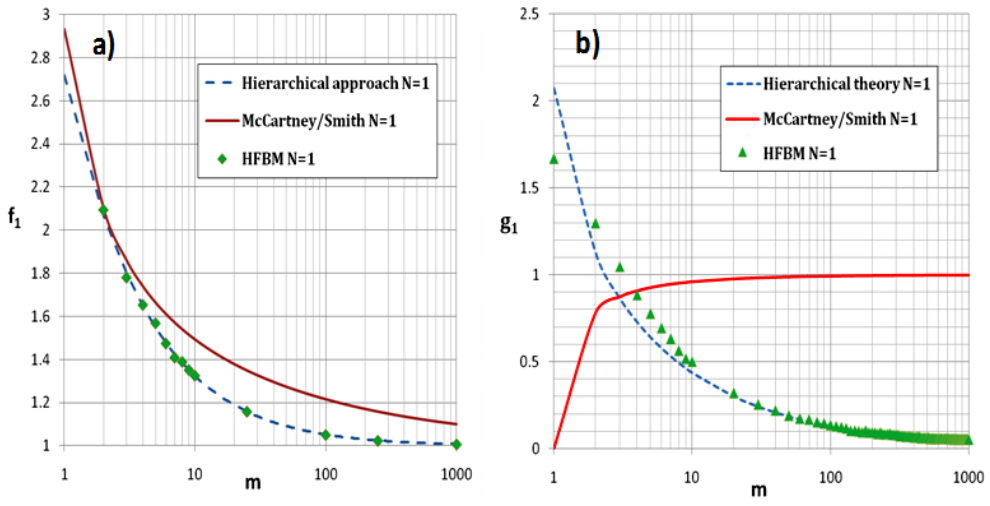

Fig. 2.3 Analytically and numerically derived correction factors for a) mean strength and b) standard deviation for N=1.

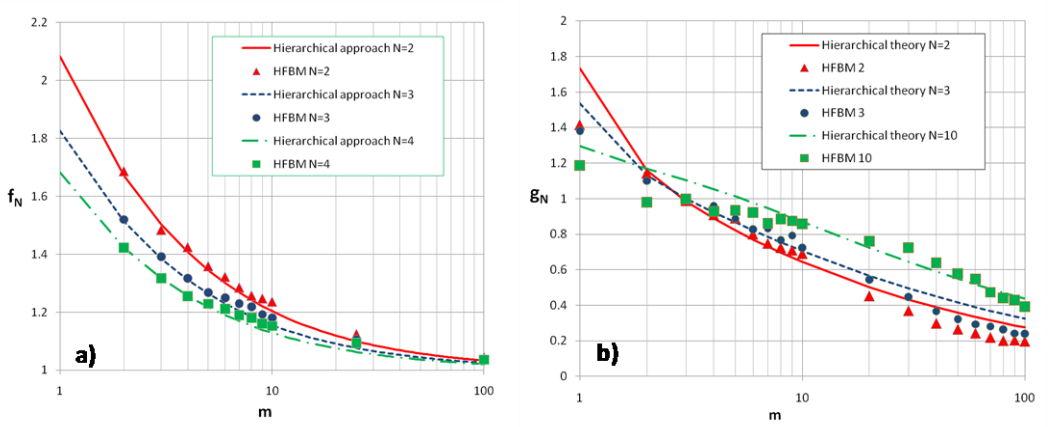

Fig. 2.4 Analytically and numerically derived correction factors for a) mean strength and b) standard deviation for $N>1$.

2.3.2 Twisting angle

As mentioned previously, the effect of fiber twisting must also be considered. The strength distribution and size-effect for a twisted-fiber rope are generally more complicated than for a parallel structure because twisted structures are heterogeneous in microstructure. This can be understood by envisioning fibers in layers following concentric helical paths about the central axis of the fiber bundle, with helical angles varying from zero, for the central fiber, to ψ_s, for fibers at the surface. Under the action of an applied load, the stresses or strains sustained by individual fibers differ, depending on their helical angle, with respect to the loading direction and the angles of the surrounding fibers. In addition, their stresses will depend on the actual distribution of neighbouring fiber breaks.

The most commonly analyzed geometry of a twisted fiber bundle or yarn is the one in which the fibers lie in concentric cylindrical layers (Fig. 2.1). Within each layer, fibers follow ideal helical paths with the same helical angle, but this angle differs from layer to another. In this idealization, fibers in different layers must necessarily have different lengths to be strain-free and without slack. This implies that between two yarn cross-sections, fibers

(other than the central fiber) will have lengths (when straight) equal to their helical path lengths, and thus, will be longer than the distance between these cross-sections.

In our model, we apply a probabilistic bundle strength model developed by Porwal et al. (2006) to the hierarchical structure of a twisted rope, which averages the fiber helical paths across the bundle to obtain uniform bundle geometry. In doing so, the mean helical angle for the ideal helical structure is calculated as:

$$\overline{\psi}_n = \cos^{-1}\left(\frac{\sum_i^z z_{kn}\cos\psi_{kn}}{z_n}\right) \tag{2.17}$$

where z_n and z_{kn} are the total number of elements in the rope and in the k-th concentric layer, respectively; thus $\overline{\overline{\overline{\psi}}}$ is weighted by the fraction of elements in each layer with respect to the total, namely z_{kn}/z_n, which increases when travelling from the centre to the surface of the bundle.

Let us assume that any level of the hierarchical structure is made up of a large number, N_n, of twisted elements of Weibull type. Based on Porwal et al. (2006), Eq. (2.1) can be modified as:

$$W_n(\sigma) = 1 - \exp\left[-\frac{l_n}{l_{cn}}\left(\frac{\sigma}{\left(\cos\overline{\psi}_n\right)^2\sigma_n}\right)^{m_n}\right] \tag{2.18}$$

thus the mean strength, $<\sigma_{Dn}^{(\psi)}>$, is given by:

$$<\sigma_{Dn}^{(\psi)}> = <\sigma_{Dn}>\cos^2\overline{\psi}_n \tag{2.19}$$

and the standard deviation, $\theta_{Dn}^{(\psi)}$, is given by:

$$\theta_{Dn}^{(\psi)} = \theta_{Dn} \cos^2 \overline{\psi_n} \tag{2.20}$$

2.3.3 Friction

According to Pan's (1993) theory, twisted yarns with friction can be treated as a chain of short twisted frictionless fiber bundles of length l_{cn} (Fig. 2.3), where the critical length l_{cn} is given by the Kelly and MacMillan equation (1986):

$$l_{cn} = \frac{r_n \sigma_{bn}}{\mu_n g_n} \tag{2.21}$$

where μ_n is the friction coefficient, g_n is the local lateral pressure, σ_{bn} is the tensile stress which causes the element to break and r_n is the element radius.

The length of each small bundle, l_{bn}, is geometrically related to the critical length of the element by:

$$l_{bn} = l_{cn} \cos \psi_{sn} \tag{2.22}$$

where ψ_{sn} is the helical angle on the surface (at the hierarchical level n).

Accordingly, we calculate the cumulative distribution function of the strength of this twisted yarn at any hierarchical level, n, simply by:

$$W_n(\sigma) = 1 - \exp\left(-\frac{l_n}{l_{bn}} \left(\frac{\sigma}{\sigma_n}\right)^{m_n}\right) \tag{2.23}$$

where l_n is the length of the twisted yarns, and σ_n and m_n are the scale and shape parameters of short bundles. They can be calculated by applying our hierarchical Daniels' theory (Eqs. (2.9) and (2.10)), based on the critical length, the fiber length and the scale and shape parameters of the single fiber, including the twisting angle modification (Eqs. (2.15) and (2.16)).

The expected values of the strength and standard deviation of the twisted yarn are given by Eqs. (2.2) and (2.3), based on the scale and shape parameters in Eq. (2.23).

2.3.4 Chains of bundles

In many cases, standard or hierarchical materials are schematically represented in the form of a chain of bundles, rather than simple fiber bundles. In this case, the procedure outlined in Section 2.2 can still be applied, with the necessary modifications.

The material at level *n* can in this case be discretized in N_{xn} fibers in parallel (bundles) and N_{yn} bundles in series (chain). As shown in Fig. 2.5, a N_{x1} by N_{y1} chain of bundles at level 1 becomes a fiber in a N_{x2} by N_{y2} chain of bundles at the next hierarchical level, and so on. The Weibull strength distribution for a bundle at level *n* is given by:

$$W(\sigma) = 1 - \exp\left(- \frac{l_n}{l_{cn}} \left(\frac{\sigma}{\sigma_{0n}} \right)^{m_n} \right) \tag{2.24}$$

We can now use the weakest link theory (Peirce 1926, Paramonov 2007) to derive the strength distribution of the chain of bundles as:

$$W(\sigma) = 1 - \exp\left(- N_{yn} \frac{l_n}{l_{cn}} \left(\frac{\sigma}{\sigma_{0n}} \right)^{m_n} \right) \tag{2.25}$$

and the mean strength of the chain of bundles is thus:

$$< \sigma_{Wn} >= (N_{yn} \frac{l_n}{l_{cn}})^{\frac{-1}{m_n}} \sigma_{0n} \Gamma(1 + \frac{1}{m_n}) \tag{2.26}$$

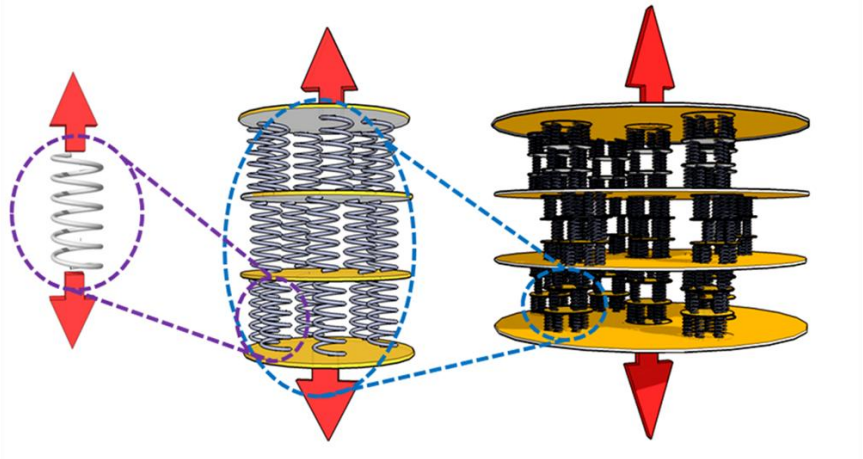

Fig. 2.5 Schematic representation of hierarchical procedure for chains of bundles

For each bundle of the next hierarchical level (n+1), we can apply Daniels' theory based on Weibull scale and shape parameters calculated at level n, and calculate their mean strength and standard deviation, which will correspond to the level (n+1) Weibull mean strength and standard deviation, according to our hierarchical theory. The Weibull strength distribution for the (n+1)-level chain of bundles can again be determined as for level n by as a function of the number of bundles $N_{y(n+1)}$, and so on.

2.4 Results

2.4.1 Size effects

First, we investigate the size-effects predicted by the theory. The level 0 fiber properties used here are provided in Table 2.1 (Pan, 1993) with consider l=1mm. The strength and standard deviation can be calculated from Eqs. (2.2) and (2.3) as $<\sigma_{W0}>$ = 72.4 MPa, θ_{W0} = 37.98 MPa. From the fiber properties we predict for the bundle (Eqs. (2.5) and (2.6)) $<\sigma_{D1}>$ = 35 MPa, θ_{D0} = 2.161 MPa. By applying the hierarchical theory (Eqs. (2.9) and (2.10)) we calculate the shape and scale parameters, m_1 and σ_1, at the first hierarchical level, finding m_1 = 18 and σ_1 = 50 MPa; then we calculate the mean and standard deviation for the second hierarchical level, and so on.

Table 2.1. Fiber properties (Pan, 1993).

Item	Typical value	unit
Fiber radius, r_0	30	μm
Characteristic length, l_{c0}	1	mm
Fiber number, N_0	200	
Fiber shape parameter, m_0	2	
Fiber scale parameter, σ_0	82	MPa

We applied this procedure to the extensive data by Amaniampong and Burgoyne (1994), reporting statistical strength of aramid and polyester yarns, described by a Weibull distribution, Gumbel distribution, Gaussian distribution and log-normal distribution (see Table 2.2), for 4 hierarchical levels. For the first and second levels we used N_1=N_2=30 and for third and fourth levels N_3=N_4=20.

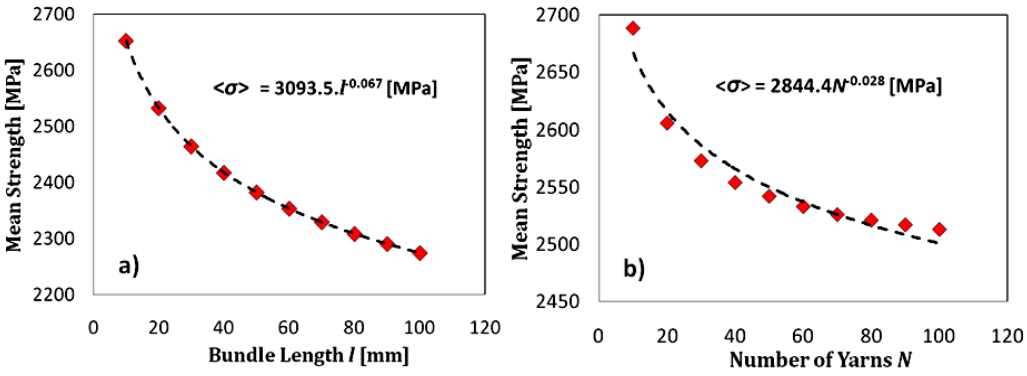

Fig. 2.6 Variation of the mean strength bundle as a function of (a) length or (b) number of yarns, at the first hierarchical level.

The variation of the bundle mean strength with the bundle length and number of fibers in the bundle is shown in Fig. 2.6 for the first hierarchical level for the first type of fiber described in Table 2.2 (KR145). The strength decrease with increasing length/number of fibers can be adequately fitted by a power law (included in the Figs.).

Table 2.2. Comparison between experimental and present theory for the strength of hierarchical fibers (all strengths and standard deviations are given in MPa).

Type of fiber	Mean and standard deviation, fitted by a Gaussian distribution. (Exp.)		Parameters of a conventional Weibull distribution, fitted by the cumulative distribution function $W_1 = 1 - \exp(-(\frac{\sigma}{\sigma_1})^{m_1})$. (Exp.)		Parameters of the Weibull distribution, predicted by our model from the mean and standard deviation of the Gaussian distribution. (Theo.)	
	θ_{D0}	$<\sigma_{D0}>$	m_1	σ_1	m_1	σ_1
KRI45	220	2477	16	2566	15	2565
KRI34	224	2461	15	2554	14	2555
KRI24	246	2467	15	2563	13	2564
KRI14	221	2520	16	2608	15	2608
KRII45	230	2299	14	2393	13	2392
KRII34	223	2270	13	2365	12	2363
KRII24	166	2384	21	2451	20	2449
KRII14	179	2417	18	2491	18	2492
PR50	52	920	20	944	21	943
PR40	57	879	18	904	18	906
PR30	67	887	16	916	16	916
PR20	63	909	16	937	17	937

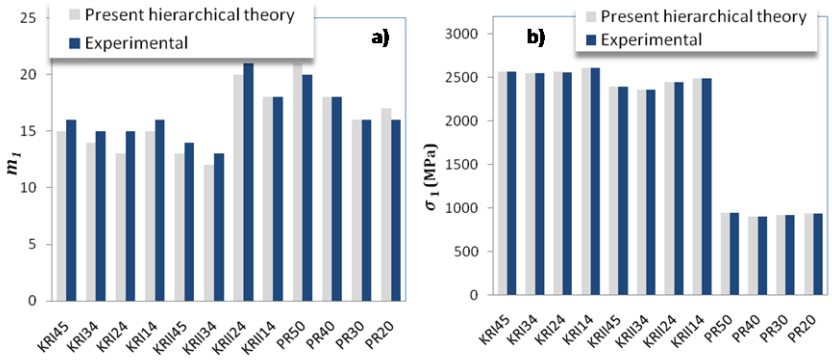

Figure 3: Comparison between predicted ("Present hierarchical theory") and experimentally derived ("Experimental") shape and scale parameters m_1 and σ_1 for the first-level Weibull distribution of various types of fibres (see Table 2)

Next, we wish to investigate the influence of the various factors considered (number of fibers in the bundle, bundle length, frictional critical length, fiber twisting). Figs. 2.7-2.9 show the expected shape and scale parameters for the second hierarchical level, by varying the length, number of yarns, twisting angle or friction critical length, respectively. Power law fits are included in Figs. 2.7 and 2.8.

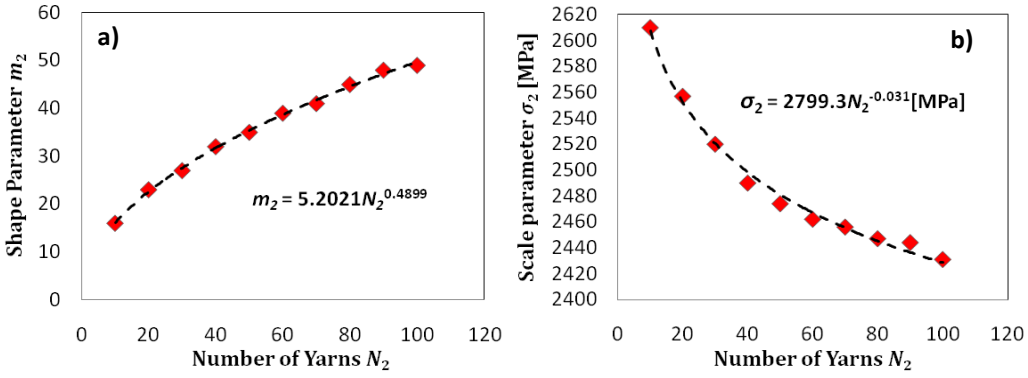

Fig. 2.7 Variation of the shape parameter (a) and scale parameter (b) of the bundle as a function of number of yarns at the second hierarchical level.

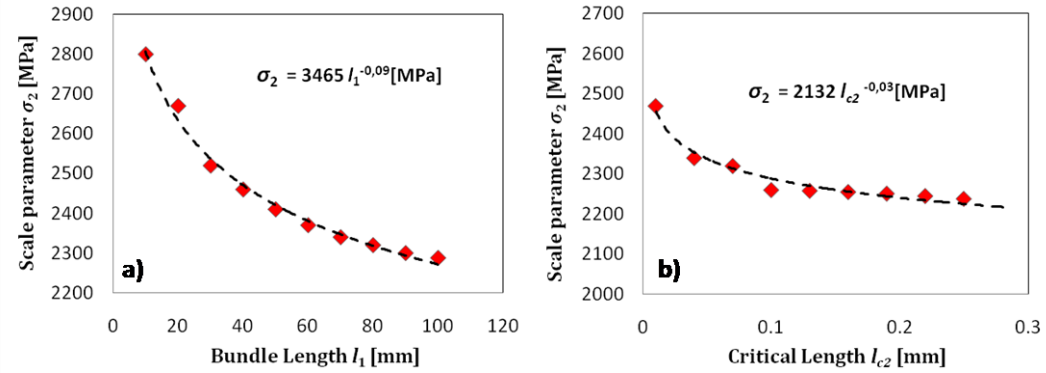

Fig. 2.8 Variation of the scale parameter σ_2 of the bundle at the second hierarchical level as a function a) of its length and b) of its critical length.

We notice that the shape parameter increases with the number of yarns but is constant with respect to the fiber length, twisting angle and frictional critical length. Finally, the variation of shape and scale parameters is evaluated as a function of hierarchical level as shown in Fig. 2.10. The decrease in scale parameter implies a decrease in mean strength with increasing hierarchical levels.

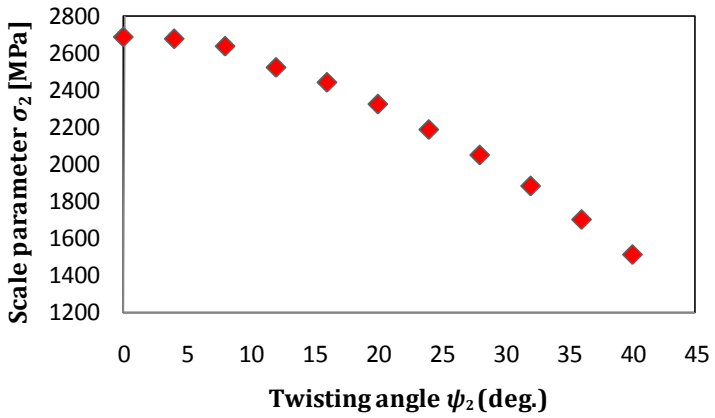

Fig. 2.9 Variation of the scale parameter of the bundle as a function of its twisting angle at the second hierarchical level.

It is important to emphasize that the size-scale effects predicted in this section naturally emerge from the theory, without the need of introducing best-fit or unknown parameters. Notice the agreement of the values of the power exponents when compared to those predicted by different approaches (Carpinteri, 1994; Carpinteri and Pugno, 2005; Pugno, 2007 a, c).

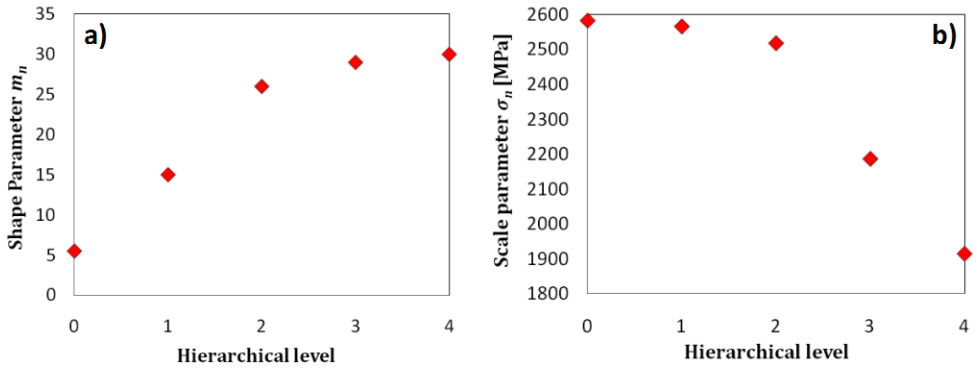

Fig. 2.10 Variation of shape parameter (a) and the scale parameter (b) as a function of the hierarchal level.

2.4.2 Comparison with numerical and experimental results

To check the validity of the proposed approach, we now compare some calculations to numerical or experimental results in the literature.

First, we wish to analyse the strength of various chain-of-bundles architectures composed of a constant number of fibers. This is a useful study when evaluating the influence of structure in hierarchical architectures, which is a problem of paramount importance in the study of biological and bio-inspired materials. We consider various 128-fiber structures, organized in 1 or 2 hierarchical levels, for simplicity. As mentioned previously, this is a typical case where correction factors for bundles with a small number of fibers are particularly important. For simplicity, in this case we choose to neglect the effect of fiber twist or friction. Analytical calculations are compared to numerical simulations carried out with the afore-mentioned Hierarchical Fiber Bundle Model (HFBM). Level 0 fiber properties are σ_0=34GPa and m_0=3, and the labelling scheme for the considered structures is as follows:

(a,b) Single level chain of bundles: $N_{x1}=a$, $N_{y1}=b$.
(a,b);(c,d) 2nd level chains of bundles: $N_{x1}=a$, $N_{y1}=b$, $N_{x2}=c$, $N_{y2}=d$.

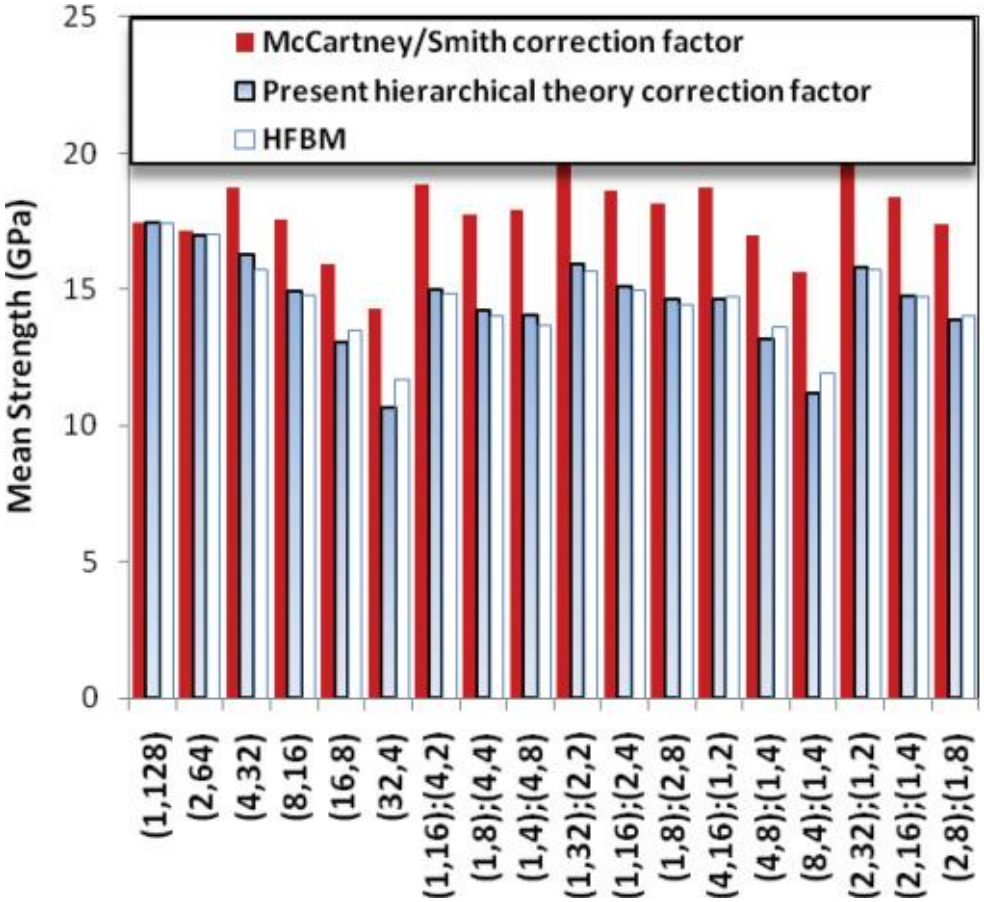

Fig. 2.11 Comparison between strength predictions for different first-and second-level, 128-fiber chain of bundle architectures: values are calculated using McCartney/Smith correction factors, hierarchical theory correction factors, and Fiber Bundle Model (FBM) numerical simulations.

Results are shown in Fig. 2.11 and display considerable agreement between analytical and numerical calculations. Furthermore, the correction factor introduced in Section 2.3.1 provides to be more reliable than that suggested by McCartney/Smith.

It is worth noting how the highest strength is achieved in the structures that maximize the number of parallel fibers, a fact that is of interest when evaluating optimization issues in hierarchical bioinspired materials.

Next, we consider the experiments on *Bombyx mori* silkworm yarns (Horan, 2006) that we compare with our theoretical predictions. In this case, too, no best-fit parameters are present since the statistical data for *Bombyx mori* silk (Rigueiro et al., 2006), listed in Table 3, was used to predict the mean strength of the strands at different hierarchal levels.

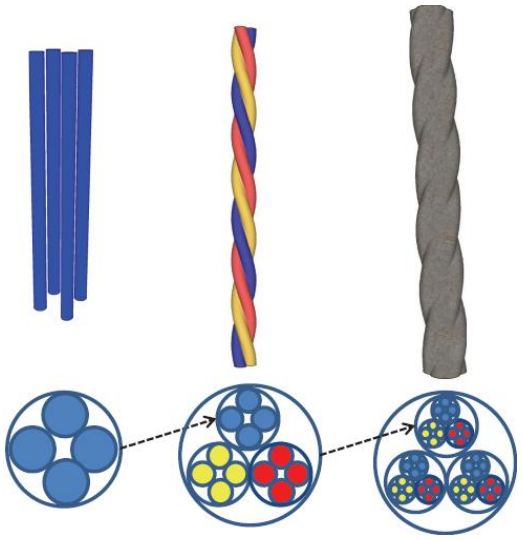

Fig. 2.12 Hierarchal organization of the twisted cabled yarn.

Table 3. *Bombyx mori* silk fiber properties (Rigueiro et al., 2006).

Item	Typical value	unit
Fiber length, l_0/l_{c0}	1	
Fiber number in bundle, N_0	According to level, see Fig. 2.12	
Fiber shape parameter, m_0	5.4	
Fiber scale parameter, σ_0	402	MPa

Strands were labelled as: A (a) x B (b) x C (c), where A, B, C represent the number of fibers, bundles and strands in the final structure, respectively, and a, b, c are the number of turns per unit length at each hierarchical level. This type of structure is illustrated in Fig. 2.12.

The comparison between experimental and theoretical values is graphically shown in Fig. 2.13. Theoretical values underestimate slightly the real values, however considerable agreement is achieved. In particular, the hierarchical theory calculations are able to capture the non-monotonic behaviour, i.e. the decrease in Ultimate Tensile Force (UTF) for the highest hierarchical structure 4(0) x3(10) x3(9).

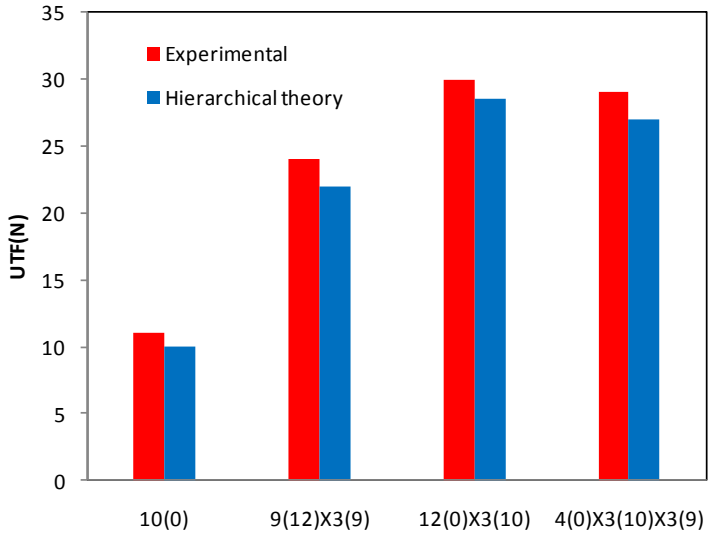

Fig. 2.13 Comparison between hierarchical model predictions and experimental measurements (Horan et al., 2006) for the ultimate tensile force (UTF) of different hierarchical architectures.

In addition, a close resemblance of fiber bundle model for modeling the biological structures (Erdmann et al., 2004) has recently been discovered.

An interesting example of complex composite hierarchical structure is that of bamboo, constituted by nano to micro fibrils which further build up macro fibers and bundles, making it strong and tough. According to the data

regarding the structure and mechanical properties at each hierarchical level given in (Wan et al., 2006), we can determine single fiber Weibull parameters m_0=2.474 and σ_0=1040MPa, and therefore calculate a bundle shape parameter of m_1=5.681, which is close to the experimental value of m_1=5.140. This is an example of how the model could also be used to deduce material parameters which might be hard to determine experimentally. Another example is a tissue used as replacement for ACL, i.e. a braid-twist scaffold based on Poly(L-lactic acid) (PLLA) (Freeman et al., 2007), our hierarchical theory predicts a mean strength of 40 MPa which is close to the experimental value about 46 MPa, and here neglecting fiber twisting would yield a further 10% underestimation of this value. In this study, a preliminary framework of probabilistic upscaling is presented for hierarchical fiber bundle modelling of mean strength across nano-micro-macro scales.

2.5 Conclusions

A hierarchical model has been presented to predict the strength of hierarchal ropes. The proposed procedure can be considered a hierarchical extension of the classical Daniels' theory. In particular, we assumed that at the first level, the fiber strength is normally distributed, and used the related mean and standard deviation to calculate the scale and shape parameters of an equivalent Weibull distribution with the same mean and standard deviation, thus linking two adjacent hierarchical levels. This procedure can be repeated at various hierarchical levels, up to the desired final structure of interest. Modifications have also been introduced in order to account for finite size, twisted configurations and friction. Strong size-effects, e.g. on mean strength and Weibull modulus, emerge naturally. Comparison with numerical simulations and experiments on hierarchical fibers display good agreement. Our theory could be useful for designing high-strength and toughness (e.g. bio-inspired) hierarchical ropes.

Chapter 3

Multimodal Daniels' theory: an application to CNT twisted strands

3.1 Introduction

Research on carbon nanotube (CNT) synthesis and on CNT fibers are interdependent, and drive new discoveries in CNT catalysis and growth. Many of the key advances in CNT synthesis led immediately to new results in fiber production. Various synthesis techniques can produce either shorter nanotubes (including arc-discharge, laser oven, high-pressure CO conversion (HiPco), fluidized bed Chemical Vapor Deposition (CVD)) or longer nanotubes (substrate growth CVD, catalytic gas flow CVD).
The Weibull distribution has been widely used to describe the strength of brittle materials (Danzer, 1992; Sigl, 1992; Junget et al., 1993; Helmer et al., 1995; Peterlik, 1995). It is now well-known that a Weibull distribution of strength values necessarily arises, if the distribution of defects obeys the following three conditions: (Danzer, 1992; Danzer and Lube 1996) (1) the defects are independent from each other, i.e. they are not interacting; (2) the material obeys the weakest-link hypothesis; i.e. the weakest link causes failure of the whole structure; (3) a critical defect density can be defined, and the size of a critical defect is uniquely related to the strength.

The strength of a fiber is an extreme-value property, depending only on the strength of the weakest link. This is the basis of the so-called weakest link theory of brittle materials, which has been extensively discussed in the literature (Phoenix, 1975; Kasa and Saito, 1979; Hitchon and Phillips, 1979). The most well-known one is due to Weibull (1951). The importance of weakest link theories is twofold: first, the theories are experimentally statistically verifiable and secondly, they provide a mechanism for extrapolating fiber strength to experimentally inaccessible gauge lengths.

Carbon fiber strength distributions have been analyzed with single modal distributions, even though in many cases the measured distributions were clearly multimodal. Accordingly, we here extend the Daniels' theory (Daniels, 1945) to multi-modal failure. As an example, we apply the theory to predict the strength of CNT twisted strands and of the related CNT-CNT junctions, complementary to previous analyses (Pugno and Ruoff, 2004; Pugno and Ruoff, 2006; Pugno, 2006b; Pugno, 2007 a,b).

3.2 Multimodal Daniels' Theory

Daniels (1945) considered Z parallel fibers with given cross-sectional area, linear elastic constitutive law and single modal Weibull distribution. Tensile strength distributions have more than one mode of failure are now considered in extending the Daniels' theory. The presence of several modes in the strength distribution implies the existence of several distinct types of strength-limiting defects in the fiber structure. Accordingly, we consider a multi-modal Weibull distribution for each fiber. For a multi-modal distribution, the probability function is given by:

$$W(\sigma)=1-(\left[1-W_1(\sigma)\right]\left[1-W_2(\sigma)\right]\ldots\ldots\ldots\ldots\ldots\left[1-W_n(\sigma)\right]) \quad (3.1)$$

where $W_1(\sigma)$, $W_2(\sigma)$ ….., $W_n(\sigma)$ are the statistical probabilities of each modal failure.

The probability density for the strength of a fiber is illustrated in Fig. 3.1. In a bundle, the fibers with strength larger than the applied stress, P, sustain

the stress. On other hand, the fibers with the strength lower than *P*, will break and the stress of broken elements becomes zero.

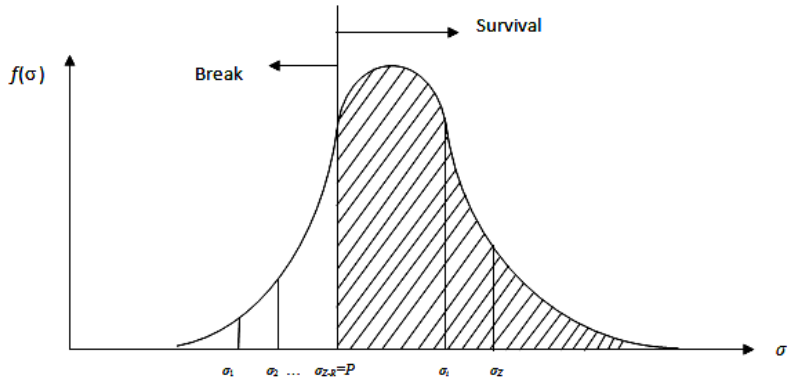

Fig. 3.1 Probability density for the strength of each fiber in the bundle.

Assuming $W_i(\sigma)$ of Weibull type, the cumulative probability function is thus given by:

$$W(\sigma) = 1 - \exp\left(\sum_{i=1}^{n} - \frac{l}{l_{0i}} \left(\frac{\sigma}{\sigma_i} \right)^{m_i} \right) \tag{3.2}$$

where l is the fiber length, l_{0i} is the characteristic length, σ is the stress applied in the longitudinal direction, whereas σ_i and m_i are the scale and shape parameters respectively.

Accordingly, the probability density is

$$w(\sigma) = \sum_{i=1}^{n} \frac{l}{l_{0i}} \left(\frac{m_i}{\sigma_i} \right) \left(\frac{\sigma}{\sigma_i} \right)^{m_i - 1} \exp\left(\sum_{i=1}^{n} - \frac{l}{l_{0i}} \left(\frac{\sigma}{\sigma_i} \right)^{m_i} \right) \tag{3.3}$$

Fig. 3.2 shows the stress condition of the bundle. If *R* is the current number of surviving fibers in the bundle, then assuming the Equal Load Sharing (ELS), the average stress of the bundle is defined as

$$\sigma = \frac{R}{Z} P \tag{3.4}$$

where P is the stress sustained by the survival fibers.

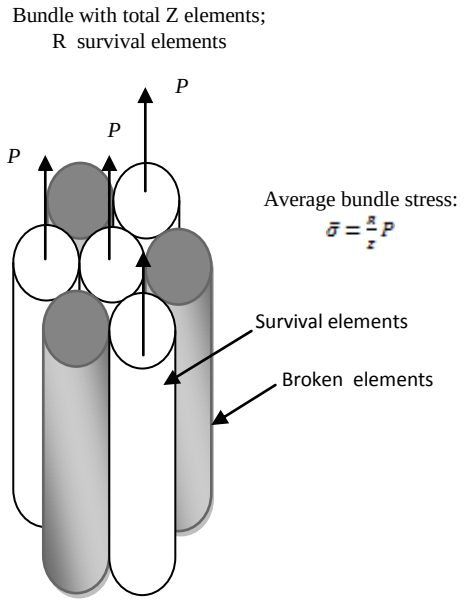

Fig. 3.2 Stress condition of the bundle.

The maximum value of $\bar{\sigma}$ gives the strength of the bundle. Hence the strength of the bundle is obtained from $\frac{d\bar{\sigma}}{dP} = 0$.

The ratio of the number of sustain fibers R to the total number of fibers Z, when Z is high and when fiber failures are equally probable events, is (Figs. 3.1 and 3.2)

$$\frac{R}{Z} = \int_{P}^{\infty} w(\sigma)\, d\sigma \tag{3.5}$$

and, considering Eq. (3.3), becomes:

$$\frac{R}{Z} = \exp\left(\sum_{i=1}^{n} -\frac{l}{l_{0i}} \left(\frac{P}{\sigma_i} \right)^{m_i} \right) \tag{3.6}$$

Thus:

$$\sigma = P \exp\left(\sum_{i=1}^{n} -\frac{l}{l_{0i}} \left(\frac{P}{\sigma_i} \right)^{m_i} \right) \tag{3.7}$$

The maximum value of $\overline{\sigma}$ is given by:

$$\frac{\mathrm{d}\sigma}{\mathrm{d}P} = 0 \tag{3.8}$$

namely:

$$\exp\left(\sum_{i=1}^{n} -\frac{l}{l_{0i}} \left(\frac{P}{\sigma_i} \right)^{m_i} \right) + P \sum_{i=1}^{n} -\frac{l}{l_{0i}} \left(\frac{m_i}{\sigma_i} \right) \left(\frac{P}{\sigma_i} \right)^{m_i - 1} \exp\left(\sum_{i=1}^{n} -\frac{l}{l_{0i}} \left(\frac{P}{\sigma_i} \right)^{m_i} \right) = 0 \tag{3.9}$$

This equation can be solved numerically yielding P_f, which gives the mean strength of the bundle as:

$$\sigma = P_f \exp\left(\sum_{i=1}^{n} -\frac{l}{l_{0i}} \left(\frac{P_f}{\sigma_i} \right)^{m_i} \right) \tag{3.10}$$

The standard deviation of the strength is predicted to be

$$\theta = \sqrt{\frac{(\sigma)^2 \; Z^{-1}}{\exp\left(\sum_{i=1}^{n} -\frac{l}{l_{0i}}\left(\frac{P_f}{\sigma_i}\right)^{m_i}\right)}\left(1-\exp\left(\sum_{i=1}^{n} -\frac{l}{l_{0i}}\left(\frac{P_f}{\sigma_i}\right)^{m_i}\right)\right)} \tag{3.11}$$

Eqs. (3.10) and (3.11) for n=1 correspond to the results of the classical single modal Daniels' theory.

3.3 An application to carbon nanotube ropes

CNTs are an extremely interesting type of material due to their unique one dimensional structure, and their excellent mechanical properties (Dresselhaus et al., 2001; Bratzel et al., 2010). To exploit their excellent physical properties at a macroscopic level, it is desirable to create CNTs with macroscopic length. However, it has been very challenging to grow arbitrarily long CNTs (Cheng et al., 1998). An alternative approach is to create long nanotube structures with many of them aligned into continuous yarns or ropes (Liu, et al., 2000; Jiang, et al., 2002; Zhang, et al., 2004; Zhang, et al., 2005; Shanov, et al., 2006).

Due to the high-strength constituent CNTs and their twisted nanostructure, CNT yarns can potentially be made much stronger and tougher than Kevlar. When the twisted yarn is pulled, the CNTs attempt to straighten, invoking a locking mechanism used to make ropes stronger. CNTs have a finite length, l, but twisting prevents a bundle of CNTs (much longer than l) from falling apart. Like most advanced fibers, it has been shown that CNT strength can also be described by a Weibull distribution: (Barber et al., 2006; Pugno and Ruoff, 2004, 2006)

$$W(\sigma) = 1-\exp\left(-\frac{l}{l_0}\left(\frac{\sigma}{\sigma_0}\right)^{m}\right) \tag{3.12}$$

where l_0 is the length of the individual CNT, σ is the applied fiber axial stress, m and σ_0 are the Weibull shape and scale parameter, for a given fiber length l.

The mean strength $< \sigma_W >$ is given by:

$$< \sigma_w >= (\frac{l}{l_0})^{\frac{-1}{m}} \sigma_0 \Gamma(1+\frac{1}{m}) \tag{3.13}$$

whereas the standard deviation is:

$$\theta_w =< \sigma_w > \left(\frac{\Gamma(1+\frac{2}{m})}{\Gamma^2(1+\frac{1}{m})} - 1 \right)^{1/2} \tag{3.14}$$

The situation can additionally turn out to be still more complex, if the strength distribution is not unimodal. Moreover, bimodal Weibull distributions were observed for carbon (Helmer et al., 1995) and silicon carbide fibers (Lissart and Lamon, 1997) and for certain ceramics (Orlovskaja et al., 1997).

Experimentally, (Zhang et al., 2004; Zhang et al., 2006) CNT yarns are peeled off from the super-aligned arrays, thanks to a strong binding force between the fibers. Also, the bundles were joined end to end forming a continuous yarn, Fig. 3.3. Intrinsic nanotube fracture, and nanotube sliding at the fronts suggest a bimodal failure. Accordingly, Eq. (3.12) becomes:

$$W(\sigma) = 1 - \exp\left(-N_{CNT} \left(\frac{\sigma}{\sigma_{CNT}} \right)^{m_{CNT}} - N_p \left(\frac{\sigma}{\sigma_p} \right)^{m_p} \right) \tag{3.15}$$

where σ_{CNT}, m_{CNT} are the scale and shape parameter of single carbon nanotube whereas σ_p, m_p are the scale and shape parameters of the peeling joint failure.

The hierarchical structure of CNT strand is shown in Fig. 3.3. It starts from level 0, a CNT fiber; this fiber consists of carbon nanotubes connected together end by end. We consider level 1 as a bundle of parallel CNT fibers. In level 2, a CNT strand, is a twisted bundle of CNT yarns. We model this complex hierarchical structure with our theory.

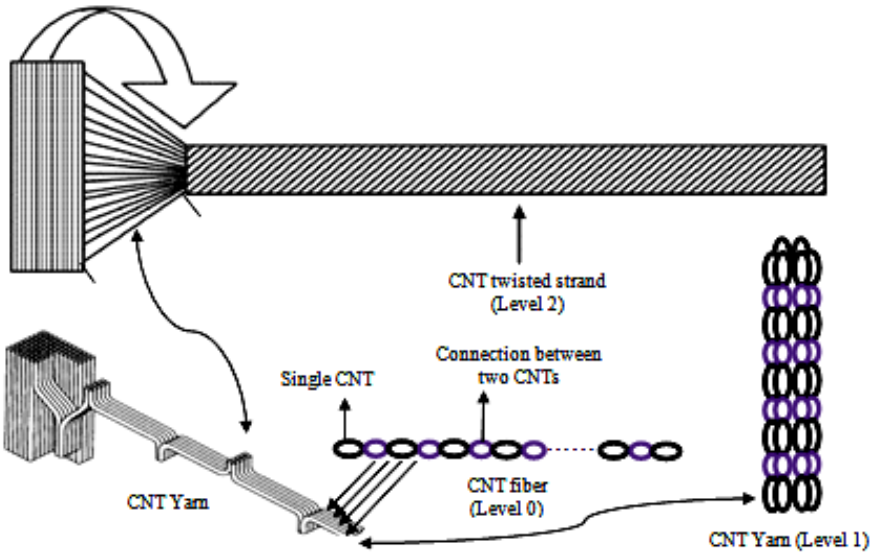

Fig. 3.3 Hierarchical twisted strand CNT model.

By differentiating Eq. (3.15), the probability density function is derived as

$$w(\sigma) = \left[N_{CNT}\alpha_{CNT} m_{CNT} \sigma^{m_{CNT}-1} + N_p \alpha_p m_p \sigma^{m_p - 1} \right] \exp\left(-\left(N_{CNT}\alpha_{CNT}\sigma^{m_{CNT}} + N_p \alpha_p \sigma^{m_p} \right)\right) \tag{3.16}$$

where $\alpha_{CNT} = (1/\sigma_{CNT})^{m_{CNT}}$ and $\alpha_p = (1/\sigma_p)^{m_p}$.

Accordingly,

$$\frac{R}{Z} = \exp(-\left(N_{CNT}\alpha_{CNT}P^{m_{CNT}} + N_p\alpha_p P^{m_p} \right)) \tag{3.17}$$

By substituting Eq. (3.15) into Eq.(3.4), the average stress of CNT yarn is calculated as

$$\sigma = \exp(-\left(N_{CNT}\alpha_{CNT}P^{m_{CNT}} + N_p\alpha_p P^{m_p} \right)) P \tag{3.18}$$

The maximum value of $\overline{\sigma}$ is given by:

$$\frac{\mathrm{d}\sigma}{\mathrm{d}P} = 0 \tag{3.19}$$

namely:

$$\exp(-\left(N_{CNT}\alpha_{CNT}P^{m_{CNT}} + N_p\alpha_p P^{m_p} \right) - P\left[N_{CNT}\alpha_{CNT}m_{CNT}P^{m_{CNT}-1} + N_p\alpha_p m_p P^{m_p-1} \right]$$
$$\exp\left(-\left(N_{CNT}\alpha_{CNT}P^{m_{CNT}} + N_p\alpha_p P^{m_p} \right) \right) = 0 \tag{3.20}$$

i.e.:

$$1 - \left[N_{CNT}\alpha_{CNT}m_{CNT}P^{m_{CNT}} + N_p\alpha_p m_p P^{m_p} \right] = 0 \tag{3.21}$$

Eq. (3.21) can be solved numerically to obtain P_f ; by substituting P_f into Eq. (3.18), the strength of CNT yarn, σ_{yD}, is finally calculated:

$$\sigma_{yD} = \exp(-\left(N_{CNT}\alpha_{CNT}P_f^{m_{CNT}} + N_p\alpha_p P_f^{m_p} \right)) P_f \tag{3.22}$$

whereas the standard deviation, θ_{yD}, of the strength is

$$\theta_{yD} = \sqrt{\frac{(\sigma_{yD})^2 Z^{-1}}{\exp(-\left(N_{CNT}\alpha_{CNT}P_f^{m_{CNT}} + N_p\alpha_p P_f^{m_p} \right))} \left(1 - \exp(-(N_{CNT}\alpha_{CNT}P_f^{m_{CNT}} + N_p\alpha_p P_f^{m_p})) \right)} \tag{3.23}$$

where Z is the number of the CNT fibers in the CNT yarn, level 1.

In the case of a hierarchical rope (Gautieri et al., 2011) we can use our recently developed theory (Pugno et al., 2011), implying:

$$\sigma_{yW} = \sigma_{yD} \tag{3.24}$$

$$\theta_{yW} = \theta_{yD} \tag{3.25}$$

where σ_{yW} and θ_{yW} are the mean strength and standard deviation of the CNT yarn in the Weibull form; σ_{yD} and θ_{yD} are the mean and standard deviation of CNT yarn in Daniels' form.
From Eqs. (3.22) and (3.23), we deduce:

$$\frac{\Gamma(1+\frac{2}{m_y})}{\Gamma^2(1+\frac{1}{m_y})} = \left(\frac{\theta_{yD}}{\sigma_{yD}}\right)^2 + 1 \tag{3.26}$$

where m_y is the shape parameter of the CNT yarn and can be calculated numerically. Then σ_{0y}, the scale parameter of the CNT yarn, can be calculated as:

$$\sigma_{0y} = \frac{<\sigma_{yD}>(l_y)^{\frac{1}{m_y}}}{\Gamma(1+\frac{1}{m_y})} \tag{3.27}$$

where l_y is the length of the CNT yarn.

According to Daniels' theory, the mean strength and standard deviation, σ_{st} and θ_{st}, of the CNT strand (level. 2), based on the shape and scale parameter of the CNT yarn, are predicted to be:

$$\sigma_{st} = (l_y m_y)^{-1/m_y}(\sigma_{0y})\exp(\frac{-1}{m_y}) \tag{3.28}$$

$$\theta_{st} = \sqrt{\frac{<\sigma_{st}>^2}{[\exp(\frac{-1}{m_y})]}[1-\exp(\frac{-1}{m_y})]K^{-1}} \tag{3.29}$$

where K is the number of yarns inside the CNT strand.

The most commonly analyzed geometry of a twisted strand is the one in which the yarns lie in concentric cylindrical layers. Within each layer, yarns follow ideal helical paths with the same helix angle but the angle differs from layer to layer. In this idealization, yarns in different layers necessarily must have different lengths to be strain-free yet without slack. This implies that between two strand cross-sections, yarns will have lengths when straight equal to their helical path lengths, and thus, will be longer than the distance between these cross-sections.

Let us consider that any level of the hierarchical structure of CNT strand is made of a large number, *K*, of twisted CNT yarn of Weibull type. Based on Porwal et al. (2006), the mean strength, $\sigma_{st}^{(\psi)}$, is given by:

$$\sigma_{st}^{(\psi)} = \sigma_{st} \cos^2 \overline{\psi} \tag{3.31}$$

whereas the standard deviation, $\theta_{st}^{(\psi)}$, becomes:

$$\theta_{st}^{(\psi)} = \theta_{st} \cos^2 \overline{\psi} \tag{3.32}$$

3.4 Characterizing the nanotube-nanotube joint

Interfacial strengths between carbon nanotubes (CNT) in contact were studied by using atomic mechanics by Li, et al. (2010). These results are important and may thus be used as a basis for explaining the observed tension strengths of CNT bundles and films that are mainly bonded by van der Waals interactions and the mechanical behaviors of composite materials with highly concentrated CNTs.

Now, we calculate the scale and shape parameters of the junctions between carbon nanotubes in the yarn, shown in Fig. 3.3. We apply a reverse process, from the experimental data, which allow us to extract these two values. The mean strength and standard deviation of dry-draw CNT strand are 0.35 GPa and 0.023 GPa respectively (Zhang et al., 2008) (level 2). The scale and shape parameter of CNT are σ_{CNT} = 34 GPa and $m_{\mathrm{CNT}} \approx$ 2.7 (Pugno and Ruoff, 2006). The characteristic number of CNT fibers in a

yarn is of the order of 100 and $N_{CNT} \approx N_P = 500$. Accordingly, solving Eqs. (3.21), (3.22) and (3.23) we deduced m_p=3.86 and σ_p= 3.36 GPa. These two parameters play a fundamental role in characterizing the statistical properties of the CNT fiber, yarn and strand. Figs. 3.4-3.5 show the effect of m_p and σ_p on the overall performances, suggesting that our model is a new useful tool for design CNT strands.

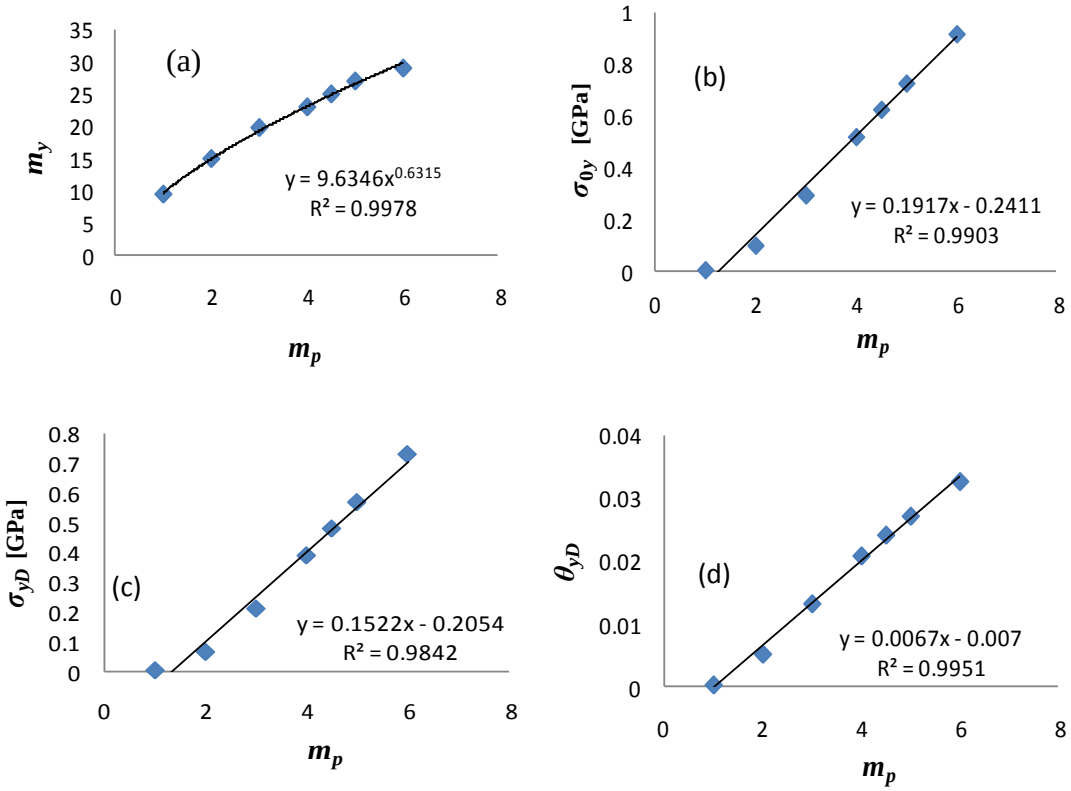

Fig. 3.4: Variation of CNT yarn's (a) shape parameter, (b) scale parameter, (c) mean strength and (d) standard deviation of, with shape parameter of the connection between carbon nanotubes in yarn.

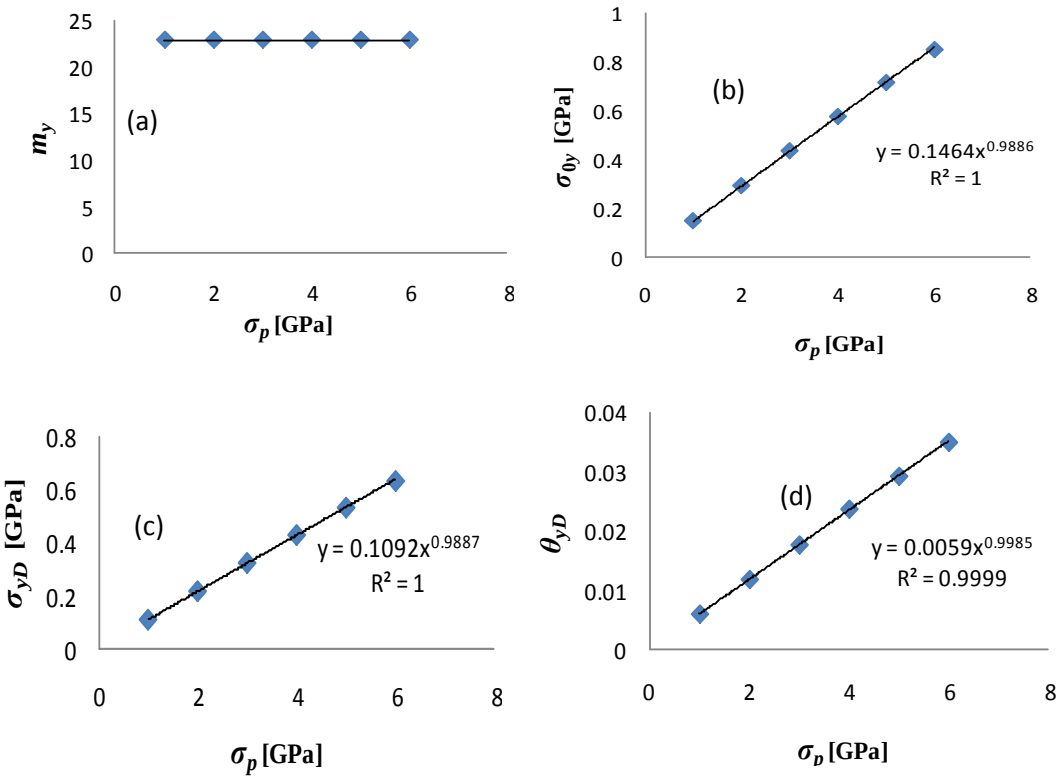

Fig. 3.5: Variation of CNT yarn's (a) shape parameter, (b) scale parameter, (c) mean strength and (d) standard deviation, with scale parameter of connection between CNTs in yarn.

3.5 Conclusion

The density of joints between CNTs decreases with the CNT length. These joints are defects because the intermolecular interaction between CNTs at the joints is much weaker than the chemical bonds within a single molecule. Decreasing the density of joints should yield CNT yarn with higher tensile strength. Thus the producing super long carbon nanotubes (with defect density less than proportional to CNT length) is crucial in this context.

Chapter 4
Catastrophic failure of nanotube bundles, interpreted with a new statistical nonlinear theory.

4.1 Introduction

In fibers of quasi brittle materials, such as carbon or glass, the strength is normally limited by the most severe defect present and, for a set of apparently similar fibers, the strength distribution can often be represented by a two-parameter Weibull function (Weibull, W. 1939). For a large number, N_0, of fibers (e.g. in a bundle) the number of surviving fibers (Chi et al., 1984), under an applied stress σ and unit length, is given by

$$N_s = N_0 \exp[-(\frac{\sigma}{\sigma_0})^m] \tag{4.1}$$

where σ_0 is the scale parameter of the Weibull distribution and m is the shape or flaw distribution parameter and is a constant of the fiber material: a large value of m indicates fibers with a uniform distribution of strengths or defects, while a small value of m describes fibers with a large variation in strengths or defects. From Eq. (4.1), if a Weibull distribution is an appropriate experimental description for a given set of fibers, then the data plotted as $\ln(\ln(N_s/N_0))$ against $\ln\sigma$ will give a straight line whose slope yields m. The fracture stresses are usually found by testing large numbers of individual fibers; this process is time-consuming.

Accordingly, Chi et al. (1984) discussed the determination of single fiber strength distribution from a fiber bundle tensile test. They developed a simple method for determining the parameters of the Weibull distribution function based upon the analysis of tensile curves of fiber bundles.

Xiao et al. (2006) measured the stress–strain curves of four single walled carbon nanotube (SWCNT) bundles. Worth noticing are the numerous stress drops, large and small, that appear on the stress–strain curves at nearly constant strain. These drops, presented in all the tested samples, are indicative of sub-bundle failures. The strength of a single fiber was assumed to follow the two parameter Weibull distribution. A theoretical expression of the load-strain (F-ε) relationship for the bundle was derived. Then, the two parameter of the Weibull distribution were calculated. The analysis reported in (Xiao et al. 2006), was however able to catch the mean response of the bundle but not observed catastrophic behavior; accordingly, we propose here a modification of the classical Weibull statistics able to predict the observed snap-back instabilities.

4.2 Theory

The following hypotheses are assumed in the present analytical work:
(1) The distribution of the single fiber strength, under tension follows the two-parameter Weibull distribution $W(\sigma)$, i.e.

$$W(\sigma) = 1 - \exp[-(\frac{\sigma}{\sigma_0})^m] \tag{4.2}$$

(2) The applied load is distributed uniformly among the surviving fibers at any instant during the bundle tensile test (mean field approach).

(3) The relation between applied stress and strain for single fiber, which obeys Hooke's law up to fracture, is:

$$\sigma = E_f \varepsilon \tag{4.3}$$

where E_f is the fiber young's modulus. We will relax this hypothesis in the second part of the chapter.
Eq. (4.2) may be written in an alternative form:

$$W(\varepsilon) = 1 - R(\varepsilon) = 1 - \exp[-(\frac{\varepsilon}{\varepsilon_0})^m] \tag{4.4}$$

where $R(\varepsilon)$ is the probability of survival under a strain ε. $W(\varepsilon)$ is the failure probability of a single fiber under strain no greater than ε, ε_0 is the scale parameter of the Weibull distribution, and can be given by:

$$\varepsilon_0 = \frac{\sigma_0}{E_f} \tag{4.5}$$

At an applied strain ε the number of surviving fibers in a bundle, which initially consists of N_0 fibers, is:

$$N_s(\varepsilon) = N_0 R(\varepsilon) = N_0 \exp[-(\frac{\varepsilon}{\varepsilon_0})^m] \tag{4.6}$$

The last relation is valid only for large number of fibers and we try to add an effective and simple mathematical modification to satisfy this relation with small number of fibers. Then we start our correction for single fiber.

For single fiber, N_0=1with unit length, the surviving fibers will take form:

$$N_s(\varepsilon) = N_0 R(\varepsilon) = \exp[-(\frac{\varepsilon}{\varepsilon_0})^m] \tag{4.7}$$

The mean strength of single fiber based on Weibull distribution is given by:

$$< \sigma >= \sigma_0 \Gamma(1 + \frac{1}{m}) \tag{4.8}$$

The strain corresponding to breaking point, can be obtained:

$$\varepsilon^* = <\sigma> / E_f \tag{4.9}$$

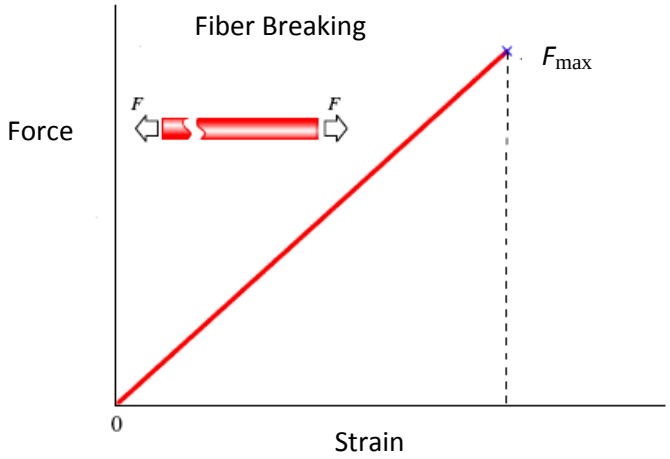

Fig. 4.1: The relation between the force and the Strain for the carbon nanotube, CNT, breaking mode.

The corresponding force are given as follows;

$$F = \begin{cases} \sigma A & \varepsilon < \varepsilon^* \\ 0 & \varepsilon > \varepsilon^* \end{cases} \tag{4.10}$$

where A is the cross-sectional area of fiber.

From Eq. (4.10), the surviving function of single fiber is given by:

$$N_s = \begin{cases} 1 & \varepsilon < \varepsilon^* \\ 0 & \varepsilon > \varepsilon^* \end{cases} \tag{4.11}$$

From Eq. (4.7), we are interested to know the survival value at $\varepsilon=\varepsilon^*$

$$N_s(\varepsilon) = \exp[-(\frac{\varepsilon^*}{\varepsilon_0})^m] \tag{4.12}$$

From Eq. (4.8) and (4.9), Eq. (4.12) can be written as:

$$N_s = \exp[-(\Gamma(1+\frac{1}{m}))^m] \tag{4.13}$$

In order to support our point of view, the curve in Fig. 4.2 shows a relation between N_s and m where N_0=1, m=1 in atomistic scale and it is raised by the hierarchical statistical model to m=10 to 50, representing the Weibull modulus on the structural scale. From Eq. (4.11), which takes form of a step function, we recommend using integer function specially round integer in Eq. (4.13), to give Ns=1.

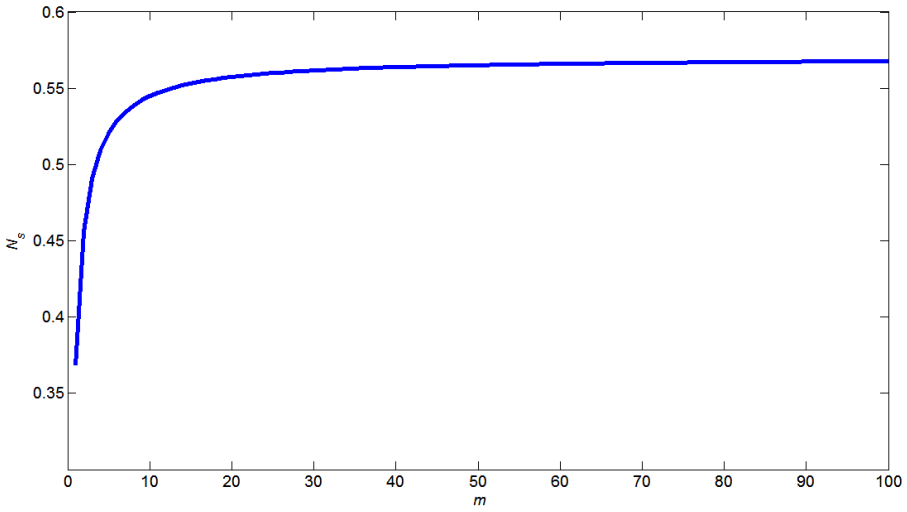

Fig. 4.2: Surviving fiber, N_0=1, vs. shape parameter.

For more clarification, here we have two methods to calculate the maximum force for single fiber: one method is mean strength divided by cross

sectional area and the other is using the survival probability with integer correction.

Here we take a single carbon nanotube as an example. The parameters of CNT used in calculation are: m=2.7, σ_0=34 GPa, E=1060 GPa, A=1.43x10^{-18}m^2.

From Eqs. (4.8) and (4.9), we find: $\langle\sigma\rangle\approx$30.06 GPa, $F_{max} \approx$ 4.3x10^{-8} N and ε^*=0.028

By inserting round integer function into Eq. (7), it will be given by:

$$N_s = \text{int}[\exp[-\left(\frac{\varepsilon}{\varepsilon_0}\right)^m]] \tag{4.14}$$

and the applied tensile load, F, is expressed as:

$$F(\varepsilon) = A\varepsilon E \ \text{int}[\exp[-(\frac{\varepsilon}{\varepsilon_0})^m]] \tag{4.15}$$

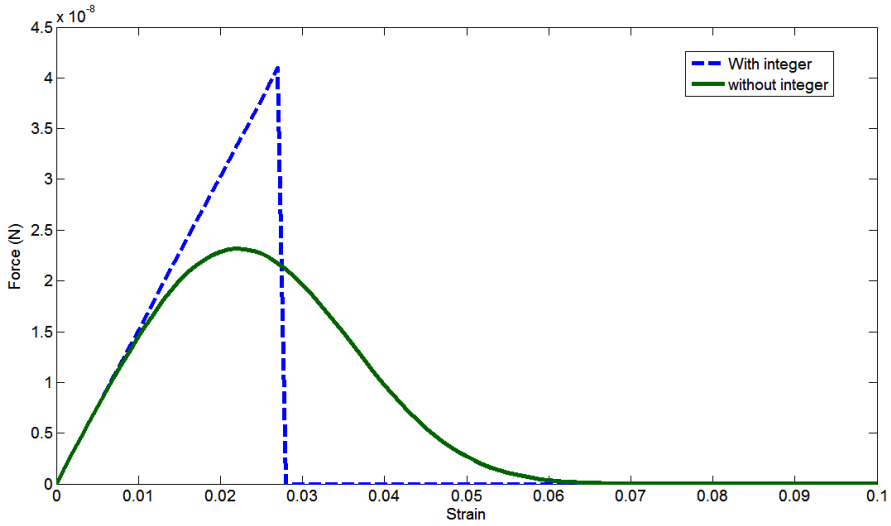

Fig. 4.3 Force-strain curves single CNT with and without integer correction.

From Eq. (4.15), F_{max}=4.1x10^{-8}N and $\varepsilon^* = 0.027$. The results from the two methods have a good agreement. From Fig. 4.3, the constitutive behavior of single CNT, which characterizes by brittle fracture, take place by employing integer correction function.

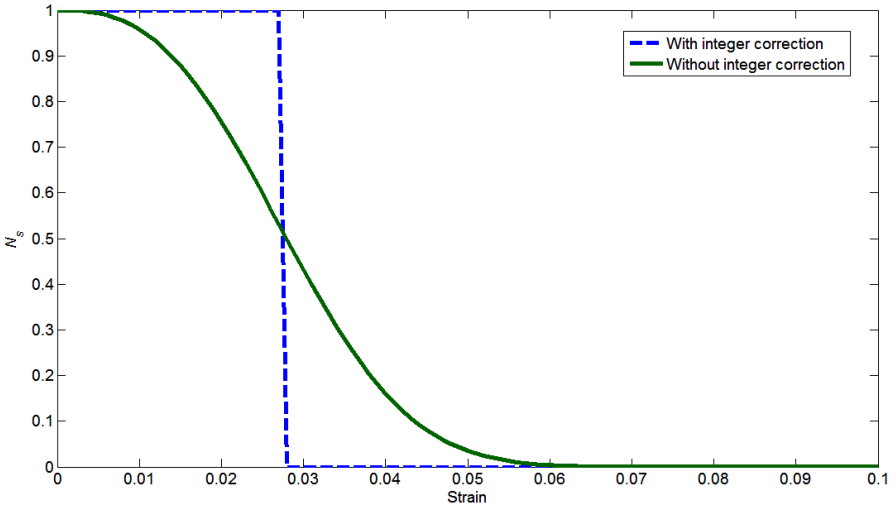

Fig. 4.4 Survival functions of single CNT, N_s vs. Strain.

For more supporting, we use another scale parameter, σ_0=44 GPa and fix other parameters. By utilizing Eqs. (8) and (9), then we get:

$<\sigma>\approx$39.2 GPa, $F_{max}\approx$5.6*10^{-8}N and $\varepsilon^* = 0.038$.
From Eq. (4.15) with integer F_{max}=5.46x10^{-8} N and $\varepsilon^* = 0.037$.

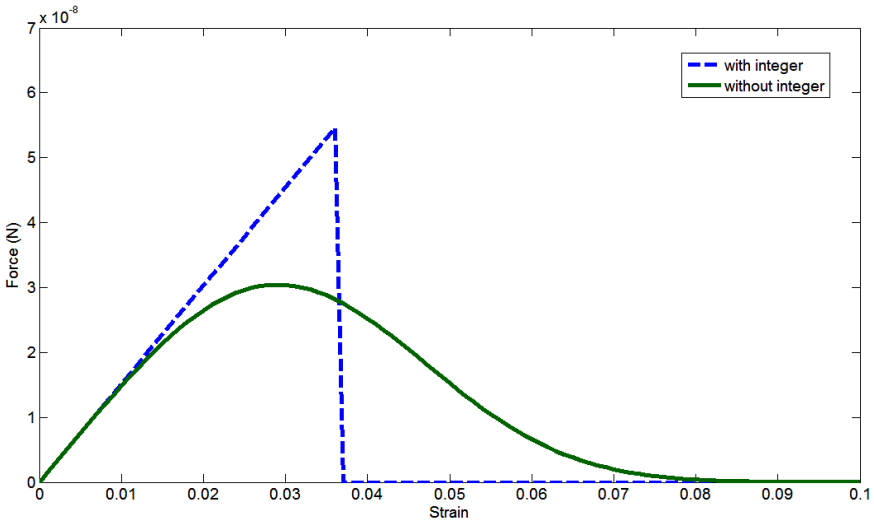

Fig. 4.5 Force-strain curves single CNT with and without integer correction.

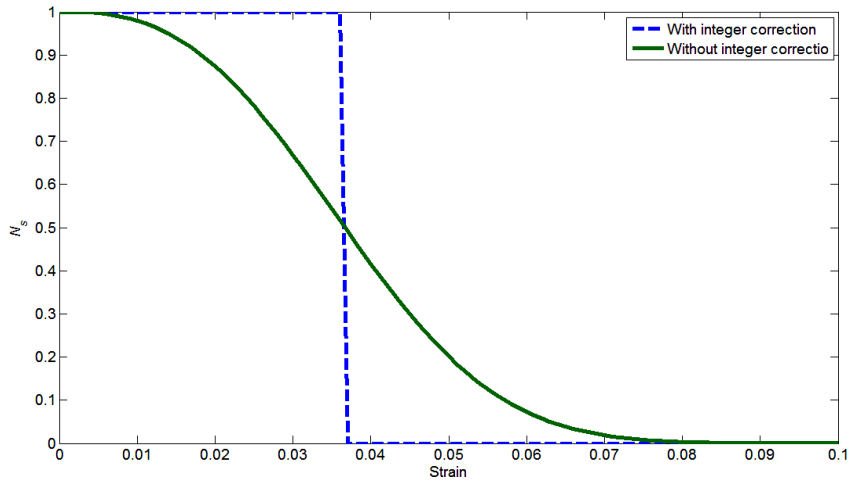

Fig. 4.6 Survival functions of single CNT, N_s vs. Strain.

The effect of integer modification for two cases i) N_0=2 and ii) N_0=3 is shown in Figs. 4.7, 4.8 and 4.9.

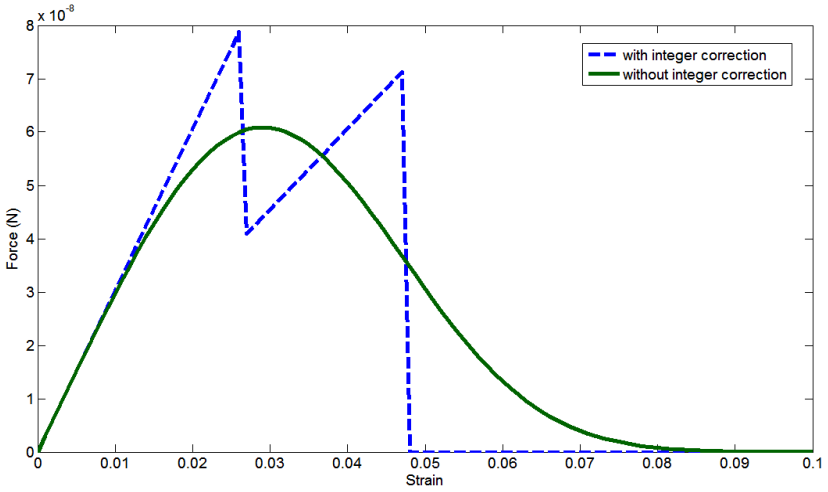

Fig. 4.7 Force-strain curves CNT bundle for N_0=2.

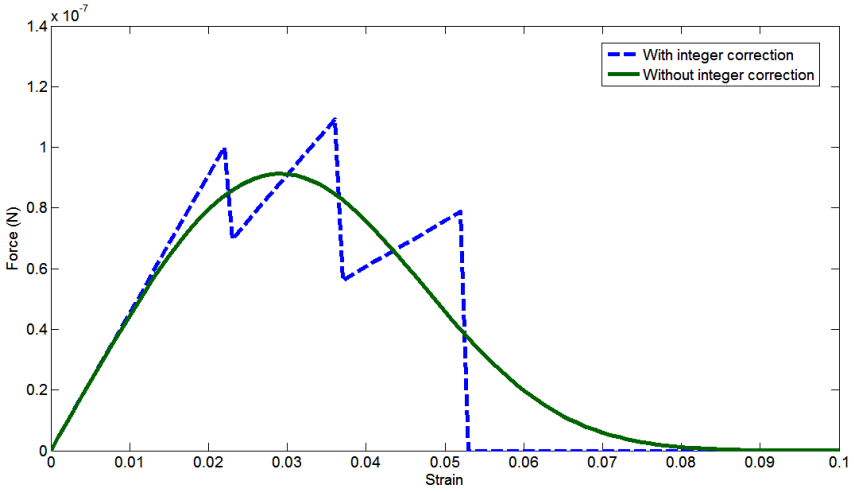

Fig. 4.8 Force-strain curves CNT bundle for N_0=3.

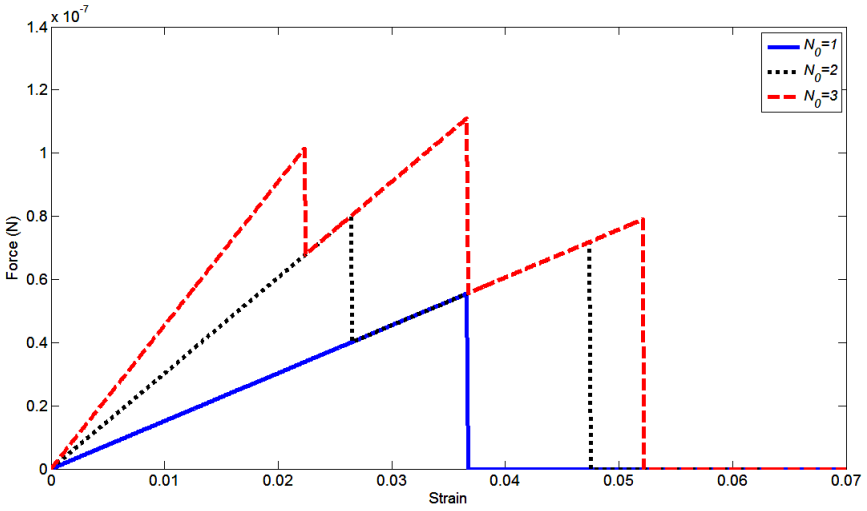

Fig. 4.9 Force-strain curves CNT bundle with for N_0=1, N_0=2 and N_0=3.

Also for large number of fibers in a bundle, the number of surviving fibers must be integer so that:

$$N_s(\varepsilon) = \mathrm{Int}[N_0 \exp[-(\frac{\varepsilon}{\varepsilon_0})^m]] \tag{4.16}$$

The introduction of the integer function in Eq. (4.16) is mathematically trivial but has remarkable physical implications, as we demonstrate.

The last expression is then related to the applied tensile load, F, by;

$$F(\varepsilon) = AE_f \varepsilon \mathrm{Int}[N_0 \exp[-(\frac{\varepsilon}{\varepsilon_0})^m]] \tag{4.17}$$

where A is the cross section area of the single fiber. Then, if A, E_f, N_0, m and ε_0 are known, the curve of load vs. strain can be drawn.

The experimental procedure to determine the probability of the single fiber strength from the experimental test of a fiber bundle was explained in detail in (Xiao et Al., 2006; Chi. et al., 1984). Empirical determination of

the initial slope of the load-strain curve, S_0, in uniaxial tension, can be derived by the following equation (Cowking et al., 1991; Mili et al., 2008):

$$S_0 = E_f A N_0 \tag{4.18}$$

4.3 Experiments on CNT bundles

We apply the model to carbon nanotube (CNT) bundles. The structure of CNT yarn or bundle, at micro scale, has two levels of hierarchy: (I) individual CNTs at the fundamental level and (II) sub-bundles, of aggregated CNTs. These sub-bundles form a continuous net, with a preferred orientation along the longitudinal axis of the yarn (Tran et al., 2009). Fig. 4.10 shows a model of CNTs pulling process from an array. According to recent studies (Iijima, et al., 1993; Bethune, et al. 1993), CNTs usually form sub-bundles containing up to 100 parallel CNTs; these have been described as nano-ropes. When pulling the CNTs from an array, it is the van der Waals attraction between CNTs which makes them joined end to end, thus, forming a continuous yarn.

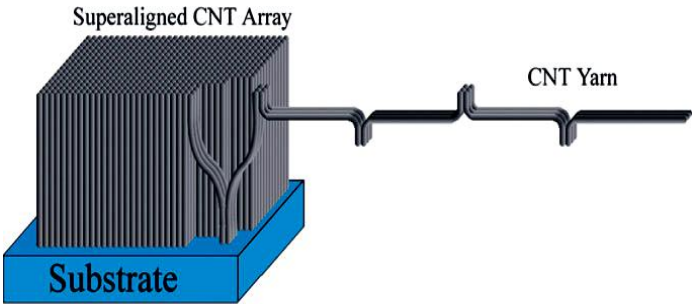

Fig. 4.10 Pulling yarn model of CNTs spinning process (Zhang et al., 2006).

The computational model (Qian et al., 2002) and the experiments of CNTs (Ajayan et al., 2000) suggest that the breaking of bundles arises from sliding rather than breakage of individual CNTs. It was furthermore noted

that the sliding of CNTs along the axial direction caused a corrugation. The mechanical properties of the yarn depend on the interaction of CNTs in bundles, itself depending on the degree of condensation (or packing) of CNT bundles in the yarn structure.

The failure mechanism of CNT-yarns is not yet clearly explained. Thus, here, mathematical modification is made to explain the mechanism of CNT-yarn failure in a simple way. In a CNT yarn, we assume that it consists of a number of bundles connected in series and each bundle consists of sub-bundles (aggregated CNTs), and we call the sub-bundle fiber.

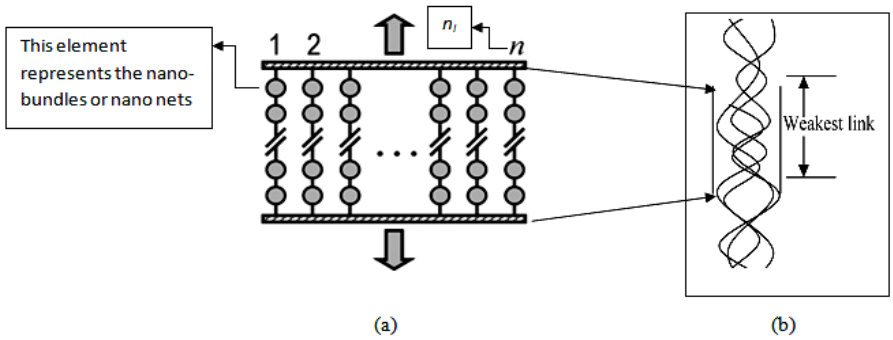

Fig. 4.11 The translation of fiber bundle to yarn.

A schematic diagram of the configuration of a bundle in the weakest part of a yarn is presented in Fig. 4.11. The weakest part has minimum number of sub-bundle, and it causes stress concentration. The weakest part will break when the tensile force acting on a fiber is greater than its breaking load. After breakage of certain number of fibers in the weakest portion, the stress on surviving fibers increases, and it causes the rupture of the yarn faster.

From the experimental force-strain curve in Fig. 4.12, we can see the failure behavior of the yarn, as the authors (Xiao et. al., 2006) noted in their previous work, the numerous kinks or load drops, are indicative of sub-bundle failures.

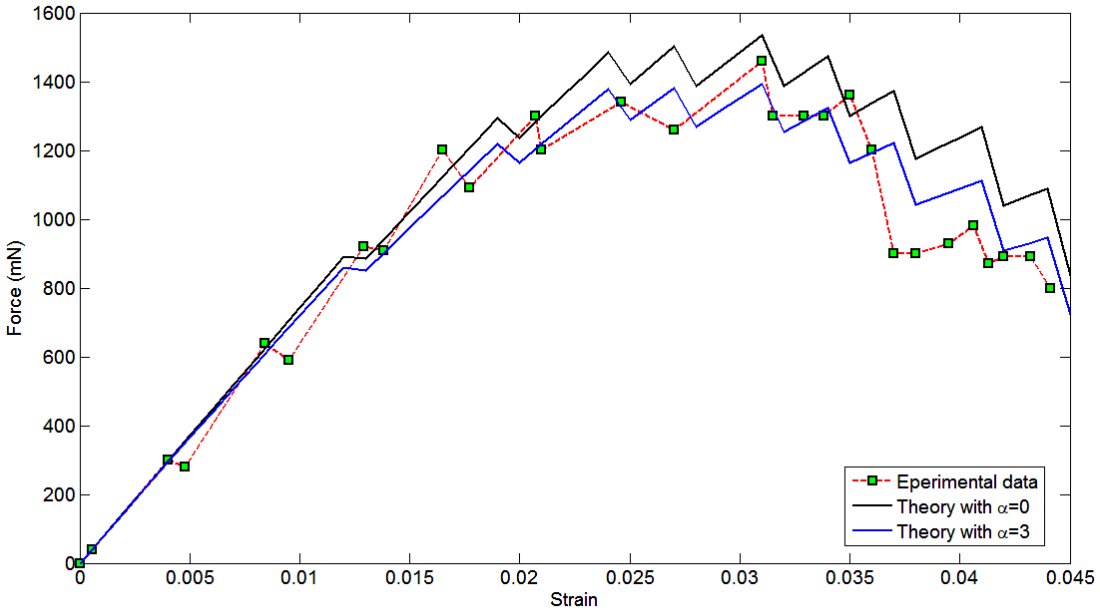

Fig. 4.12 Force-strain curves for a SWCNT bundle. The dots are the experimental results, while the solid line is our nonlinear prediction whereas the dashed line is the prediction of the linear model.

4.4 Non linear elastic constitutive law

If the number of sub-bundles is n_b and the number of individual CNTs inside each one is n_n, then the total number of CNTs in the bundle is given by:

$$N_0 = n_b n_n \tag{4.19}$$

From Eq. (4.10) we can rewrite Eq. (4.8), assuming only sub-bundle failure (the integer function applies only to n_b), as:

$$F(\varepsilon) = AE_f \varepsilon n_n \mathrm{Int}[n_b \exp[-(\frac{\varepsilon}{\varepsilon_0})^m]] \tag{4.20}$$

In Fig. 4.13 different responses, by varying n_b are plotted. Assuming non-linearity (Chi et. al. 1984), Eq. (4.20) becomes:

$$F(\varepsilon) = AE_f \varepsilon n_n (1-\alpha\varepsilon)\mathrm{Int}[n_b \exp[-(\frac{\varepsilon}{\varepsilon_0})^m]] \tag{4.21}$$

where α is the coefficient of non-linearity, expected to be (Pugno et al., 2006):

$$\alpha = \frac{E_f a^3 \gamma}{k_B} \tag{4.22}$$

where k_B is Boltzmann's constant, a^3 is the volume of a lattice unit cell and γ is the thermal expansion coefficient. Non-linearity must be considered in the case of large strains. Fitting the experimental data (Xiao et al. 2006) with the theoretical prediction of Eq. (4.12), we found that n_b=12 gives the best fit. Furthermore, in agreement with (Wang et al., 2009), we found that α=3 gives the best fit (in (Xiao et al. 2006) α=6 was used).

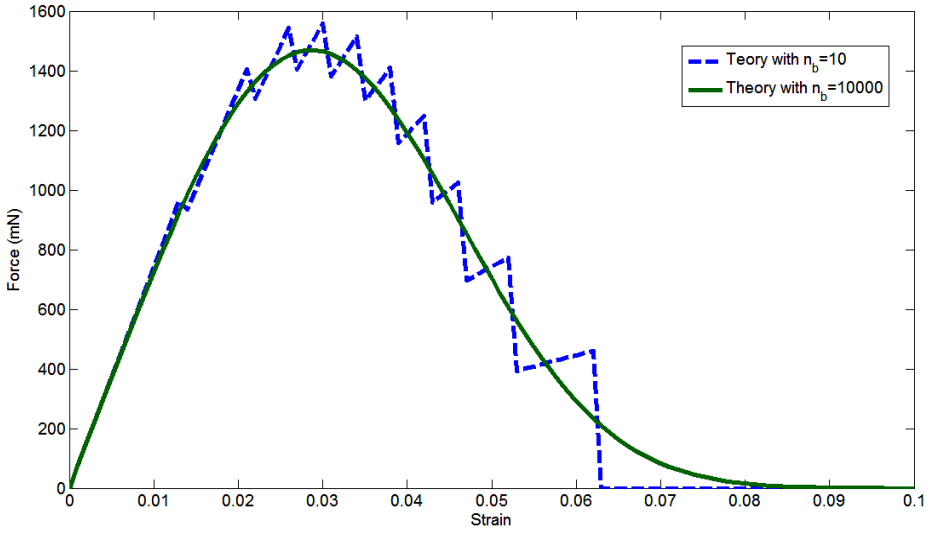

Fig. 4.13 Force-strain curves for bundle with n_b=10 or n_b=10000.

In particular, Fig. 4.12 shows the theoretical-experimental comparison. The present model, is in close agreement with the observed experimental behavior.

When we calculated the slope of each load drop, we found that it is negative and becomes higher in modulus by increasing the strain. These load drops, corresponding to a catastrophic failure of the bundle, suggest larger brittleness by increasing the strain. This tendency is also predicted theoretically by our statistical treatment, see Fig. 4.14.

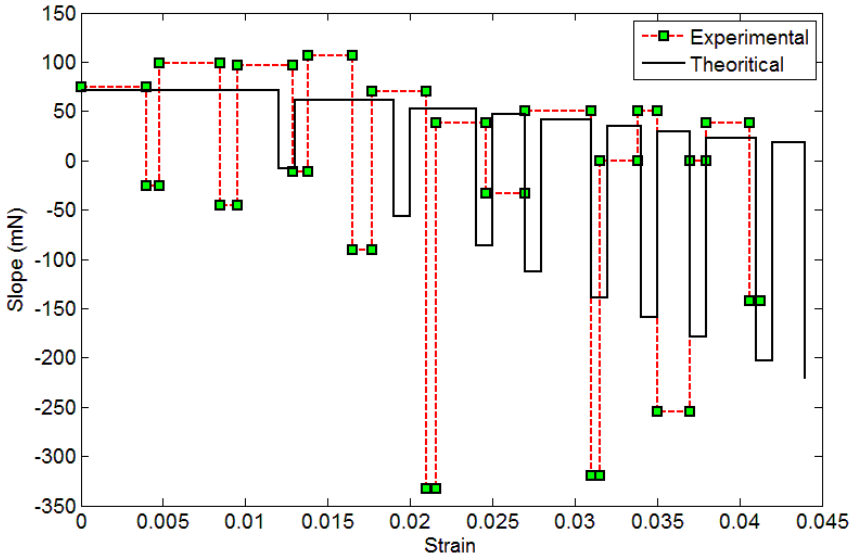

Fig. 4.14 Variation of load drop slop with strain.

4.5 Conclusion

The catastrophic failure of the nanotube bundle can be predicted by the proposed simple modification (the introduction of the integer function) of the Weibull distribution, including a nonlinear elastic constitutive law. We expect the validity of this approach for different types of bundles and not only for the relevant case of CNT bundle.

Similar treatments could be introduced in different nanotube statistics (Pugno and Ruoff. 2006), not only for the strength but also for the stiffness (Pugno, 2007e) or even adhesion (Pugno, 2007d; 2008).

Chapter 5
Investigating the role of hierarchy and fiber mixing on the strength of composite materials.

5.1 Introduction

Biological materials are hierarchically structured, beginning at the smallest scale with mineral particles, nano-fibers or platelets, which are embedded within a protein matrix. Hierarchical structuring can applied up to 7 levels of hierarchy (Launey et al., 2010) in bone and dentine, where the largest structural elements reach length scales of millimeters. Detailed descriptions of the hierarchical structures of several biological materials, such as shells, bone, teeth, sponge and spicules can be found in recently published review articles (Chen et al., 2008; Meyers et al., 2008; Fratzl and Weinkamer, 2007).

Due to the hierarchical structure, there is a variety of designs, by changing the arrangement of the components at different hierarchical levels. In the case of bone, for example, the variability at the nanoscale is in the shape and size of mineral particles, at the micronscale in the arrangement of mineralized collagen fibers into lamellar structures and at the macroscale in the porosity and the shape of the bone. The mechanical properties of bone strongly depend on all these parameters (Currey, 2003, 2002). A collection of textbooks on the relation between hierarchical structure and mechanical properties is given in the references (Currey, 2002; Thompson, 1992;

Mattheck and Kubler 1995; Vincent, 1990; Wainwright et al. 1982; Niklas, 1982). Moreover, a number of recent review articles can be referred (Jeronimidis, 2000; Ashby, 1999; Gibson et al. 1995; Jeronimidis and Atkins, 1995; Weiner et al. 2000), (Fratzl, 2003; Mattheck and Bethge, 1998; Vincent, 1999), (Launey et al., 2010; Weiner and Traub, 1992; Weiner and Wagner, 1998; Rho et al., 1998; Currey, 1999; Mann and Weiner, 1999).

Biological materials differ fundamentally from most of man-made materials in hierarchical way. The complexity of these materials is further increased because of the distribution of different chemical compositions, as the degree of mineralization, fluid content, and the resulting variation in the type and density of internal interfaces. This architecture arises from a multitude of different constituents already at the molecular level, including mainly various organic molecules, such as proteins or sugars, but also inorganic matter, mostly in the form of calcium-based minerals (Weiner et al. 2003).

This hierarchy and functional grade imply that the mechanical properties of such materials are also different at different length scales. The highest level of hierarchy in biological materials can be either the whole organism, such as a single bone of a vertebrate or an appendage segment of an arthropod. These functional units as a whole have ideal mechanical properties for their individual purposes, which are optimized for the occurring loads. The overall mechanical properties of a functional unit rarely reflect the bulk properties of their constituents, but depend on their hierarchical and functional grading architectures.

In fact, all stiff biological materials are composites with smallest components in the size-range of nanometers. In some cases (e.g. plants or insect cuticles), a polymeric matrix is reinforced by stiff polymer fibers, such as cellulose or keratin. Even stiffer structures are obtained when a (fibrous) polymeric matrix is reinforced by hard particles, such as carbonated hydroxyapatite in bone or dentin. The general mechanical behaviors of these composites are quite remarkable. In particular, they combine the two behaviors which are quite contradictory, and essential for the function of these materials. Bones, for example, need to be stiff to prevent bending and buckling (or strong to prevent crushing), and they must

also be tough, since they should not break catastrophically even when the load exceeds the normal range. How well these two conditions are fulfilled becomes obvious in the (schematic) Ashby-map in Fig. 5.1. Proteins (collagen in bone and dentin) are tough but not very stiff. Mineral, on the contrary, is stiff but not very tough.

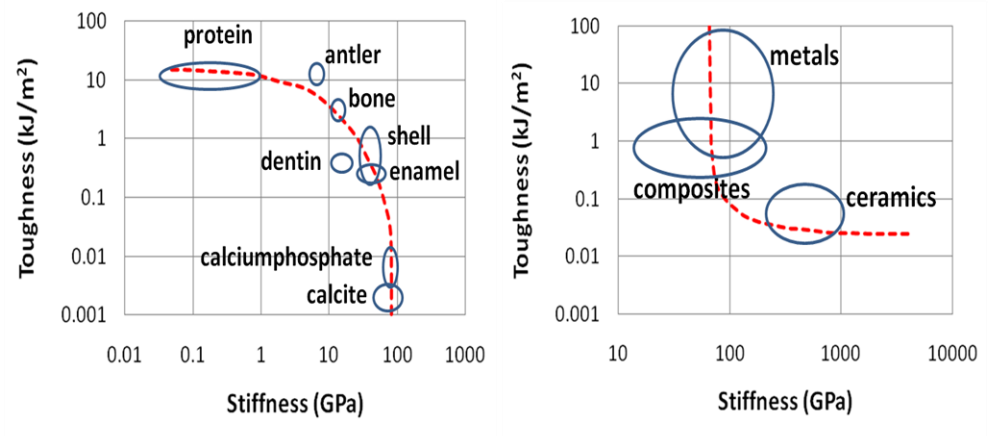

Fig. 5.1: Stiffness and toughness of proteins and mineral (hydroxyapatite and calcite), as well as a few natural protein-mineral composites and artificial materials.

As for the model of the behaviors (e.g., strength and toughness) of nanotube-based composites, starting from the properties and volume fractions of the constituents can be seen in (Bosia et al. 2010).

The rupture of disordered materials has recently attracted much technological and industrial interest and has been widely studied in statistical physics. It has been suggested by several groups that the failure of a disordered material subjected to an increasing external load shares many features with thermodynamic phase transitions.

Also, sudden catastrophic failure of structures due to unexpected fracture of their components is a concern and a challenging problem of physics as well as engineering. The dynamics of the materials failure shows interesting properties and hence there has been an enormous amount of study on breakdown phenomena (Herrmann and Roux, 1990; da Silveria, 1999; Zapperi et al. 1999). The complexity involved in fracture processes can

often be suitably modeled by grossly simplified models. A very important class of models of material failure is the fiber bundle model (FBM)

(Daniels, 1945; Coleman, 1958; Krajcinovic and Silva, 1982; Sornette, 1989 a, b; Moukarzel and Duxbury, 1994; Harlow and Phoenix, 1978; Smith, and Phoenix, 1981; Phoenix et al. 1997; Phoenix and Raj, 1992; Beyerlein and Phoenix, 1996; Curtin, 1991; Curtin, 1993; Zhou and Curtin, 1995), which has been extensively studied in the past years.

This model consists of a set of parallel fibers having statistically distributed strengths. The sample is loaded parallel to the fiber direction, and the fibers fail if the load exceeds their threshold value, the load carried by the broken fiber is redistributed among the surviving ones. Among the several theoretical approaches, one simplification that makes the problem analytically tractable is the assumption of global load transfer, which means that after each fiber breaking, the stress is equally redistributed on the surviving fibers, neglecting stress enhancement in the vicinity of failed regions (Daniels, 1945; Coleman, 1958; Krajcinovic and Silva, 1982; Sornette, 1989 a, b; Moukarzel and Duxbury, 1994; Harlow and Phoenix, 1978; Smith, and Phoenix, 1981; Phoenix et al. 1997; Phoenix and Raj, 1992; Curtin and Takeda, 1998). The relevance of FBM is manifold: in spite of their simplicity, these models capture the most important aspects of material damage, and due to the analytic solutions, they provide a better understanding of the fracture process. Furthermore, they serve as a basis for more realistic damage models.

In this chapter, we try to give an answer to the following question:
How does hierarchy affect the strength of a structure?
Only few engineering models explicitly considering the complex structures are presented in the literatures (Zhao et al. 2009; Gao, 2006; Pugno, 2006; Pugno and Carpinteri 2008). In other words, "is it possible by varying the hierarchical structure and mixing different material components to optimize the mechanical behavior of a material/structure?". To answer these questions, we introduce an analytical theory for hierarchical composite FBMs with different fiber types in the case of ELS.

The chapter is structured as follows: in Section 2, we present the analytical procedure to calculate the strength of hierarchical fiber bundle

architectures, both in the case of single-phase and composite materials; in Section 3, we present results of calculations, together with comparisons with numerical simulations to validate the procedure; finally, conclusions and outlook are given.

5.2 Theory

5.2.1 Composite fiber bundle with mixed Weibull distribution

Mixture Weibull distribution is one of the new studies which has been used a lot recently in statistical research articles and its applications are very common in reliability studies. In this section, we study composite fiber bundle, which is composed of two types of fibers with a designated percentage of each type. The classical Daniels' theory (Daniels, 1945) is applied on fiber bundle which has single type of fibers. Here, we apply it on the composite fiber bundle.

The probability that a structure subjected to a stress σ will fail when

$$W(\sigma) = x(1-\exp(-(\frac{\sigma}{\sigma_{01}})^{m_{01}})) + (1-x)(1-\exp(-(\frac{\sigma}{\sigma_{02}})^{m_{02}})) \qquad (5.1)$$

where x is the mixing parameter and, m_{01}, σ_{01}, m_{02} and σ_{02} are the Weibull's shape and scale parameters of the first and second type of fibers. The subscript 0 denotes the zero level and subscripts 1 and 2 denote the types of fibers in the bundle.

By applying Daniels' theory (Daniels, 1945; Coleman, 1958), the mean stress is expressed as:

$$\sigma = ((x)\exp(-(\frac{P}{\sigma_{01}})^{m_{01}}) + (1-x)\exp(-(\frac{P}{\sigma_{02}})^{m_{02}}))P \qquad (5.2)$$

where P is the stress sustained by surviving elements.

The maximum value of $\bar{\sigma}$ is given by;

$$\frac{d\bar{\sigma}}{dP} = 0 \qquad (5.3)$$

namely:

$$(x\exp(-(\frac{P}{\sigma_{01}})^{m_{01}})[1-m_{01}(\frac{P}{\sigma_{01}})^{m_{01}}])+(1-x)\exp(-(\frac{P}{\sigma_{02}})^{m_{02}})[1-m_{02}(\frac{P}{\sigma_{02}})^{m_{02}}]=0 \quad (5.4)$$

Eq. (5.4) can be solved numerically to obtain P_f and P_f is the value producing maximum mean strength as:

$$<\sigma_D>=[x\exp(-(\frac{P_f}{\sigma_{01}})^{m_{01}})+(1-x)\exp(-(\frac{P_f}{\sigma_{02}})^{m_{02}})]\,P_f \quad (5.5)$$

and the standard deviation θ of the strength is:

$$\theta_D=\sqrt{\frac{<\sigma>^2 N_x^{-1}}{(x\exp(-(\frac{P_f}{\sigma_{01}})^{m_{01}})+(1-x)\exp(-(\frac{P_f}{\sigma_{02}})^{m_{02}}))}[1-(x\exp(-(\frac{P_f}{\sigma_{01}})^{m_{01}})+(1-x)\exp(-(\frac{P_f}{\sigma_{02}})^{m_{02}}))]} \quad (5.6)$$

where N_x is the number of fibers in the bundle.

5.2.2 Composite fibers bundle with mixed elastic modulus and mixed Weibull distribution

When considering fiber bundles with two fiber types, it is also necessary to consider the case in which they have different elastic modulus E_1 and E_2,. Here, we use the force-displacement, see chapter 4, to obtain the mean strength of the composite bundle.

For simplicity, the relationship between applied stress and strain for single fiber obeys a linear elastic relationship up to fracture and a displacement controlled experiment is considered:

$$\sigma = E_f \varepsilon \quad (5.7)$$

where E_f is the fiber's elastic modulus.

As discussed in part 4.2, at applied strain ε, the tensile load, F is given by;

$$F(\varepsilon) = AE_f \varepsilon N_0 \exp[-(\frac{\varepsilon}{\varepsilon_0})^m] \quad (5.8)$$

where A is the cross section area of the single fiber and N_0 is the total number of fibers in the bundle. In structural engineering, the force and the displacement satisfy:

$$F=K\Delta L \tag{5.9}$$

where K is the structural stiffness and ΔL is the corresponding displacement. By considering the strain, $\varepsilon= \Delta L/L$ and from Eq. (5.8) the stiffness of fiber bundle is expressed by:

$$K = \frac{AE_f N_0 \exp[-(\frac{\varepsilon}{\varepsilon_0})^m]}{L} \tag{5.10}$$

In the case of two types of fibers (Fig. 5.2), which have different elastic moduli with different Weibull distribution, the force is given by:

$$F = \left(K_1 + K_2\right)\Delta L \tag{5.11}$$

where K_1 and K_2 are the stiffness of first and second type of fibers, respectively.

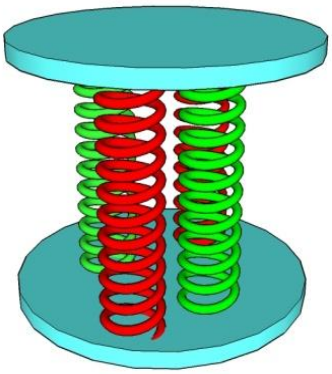

Fig. 5.2 Schematic of mixed fiber bundle.

$$F = (AE_{1f} N_{01} \exp[-(\frac{\varepsilon}{\varepsilon_{01}})^{m_{01}}] + AE_{2f} N_{02} \exp[-(\frac{\varepsilon}{\varepsilon_{02}})^{m_{02}}])\varepsilon \qquad (5.12)$$

where E_{1f} and E_{2f} are elastic modulus of the first and second types of fibers; N_{01} and N_{02} are the numbers of each type of fibers, respectively.

Thus, the mean strength of the bundle can be expressed as

$$<\sigma>= \frac{F_{max}}{AN_{01} + AN_{02}} \qquad (5.13)$$

F_{max} is the maximum force, and it is calculated from Eq. (5.12) by

$$\frac{\mathrm{d}F}{\mathrm{d}\varepsilon} = 0 \qquad (5.14)$$

$$(AE_{1f} N_{01} \exp[-(\frac{\varepsilon}{\varepsilon_{01}})^{m_{01}}](1 - m_{01}(\frac{\varepsilon}{\varepsilon_{01}})^{m_{01}}) + AE_{2f} N_{02} \exp[-(\frac{\varepsilon}{\varepsilon_{02}})^{m_{02}}](1 - m_{02}(\frac{\varepsilon}{\varepsilon_{02}})^{m_{02}})) = 0 \qquad (5.15)$$

Eq. (5.15) can be solved easily and ε which gives maximum force is obtained.

5.2.3 Hierarchical composite fiber bundle

Here, we will introduce another model called a hierarchical composite fiber bundle. This type of bundle consists of different levels. By this model, we investigate the influence of hierarchy role on random fiber bundle.

The hierarchical Daniels' theory (Pagno et al. 2011) can also be applied to a composite bundle of mixed fibers as shown in Fig 5.3. In this case, the first level has bundle of mixed fibers and by applying our hierarchical fiber bundle theory (part 2.2), we can calculate shape and scale parameters, m_{11}, σ_{11}, m_{12} and σ_{12} of the two different bundles in first level.

As shown in Fig. 5.3, we have two different composite bundles in first level, and this composite bundle constructs the second level. Thus Eqs. (5.5) and (5.6) is expressed in general hierarchical form as:

$$< \sigma_{Dn} >= [(x_n)\exp(-(\frac{P_{nf}}{\sigma_{n1}})^{m_{n1}}) + (1-x_n)\exp(-(\frac{P_{nf}}{\sigma_{n2}})^{m_{n2}})]\, P_{nf} \qquad (5.16)$$

where P_{nf} is the value of P_f at hierarchical level n. The standard deviation, θ, of the strength is

$$\theta_{Dn} = \sqrt{\frac{< \sigma_{Dn} >^2 N_n^{-1}}{(x_n \exp(-(\frac{P_{nf}}{\sigma_{n1}})^{m_{n1}}) + (1-x_n)\exp(-(\frac{P_{nf}}{\sigma_{n2}})^{m_{n2}}))}[1-(x_n \exp(-(\frac{P_{nf}}{\sigma_{n1}})^{m_{n1}}) + (1-x_n)\exp(-(\frac{P_{nf}}{\sigma_{n2}})^{m_{n2}}))} \qquad (5.17)$$

where N_n is the total number of bundles in level n.

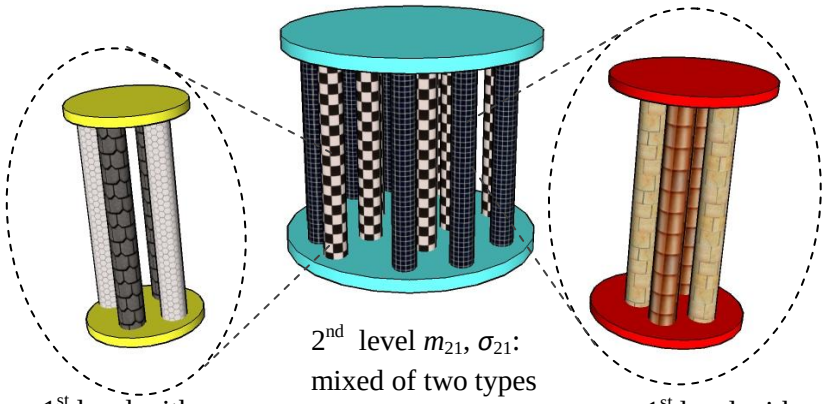

Fig. 5.3 Schematic of hierarchical composite bundle.

5.2.4 Chain of bundles under equal load sharing

We succeed to equivalent the composite bundle as single element described by Weibull distribution with scale and shape parameter σ_{11} and m_{11} respectively as mentioned in the previous part. In this case, we apply the

Previous process in chain of bundles with mixed fibers, as shown in Fig. 5.4. In the model, the chain of bundle is divided into three sublevels, i.e. the first chain of bundle:

1-Sub-level (01) is the single fibers in level 1.
2-Sub-level (11) is the bundle of fibers in level 1.
3-Sub-level (21) is the chain of bundles in level 1.

where the first number represents the sublevel and the second number is the level of hierarchy.

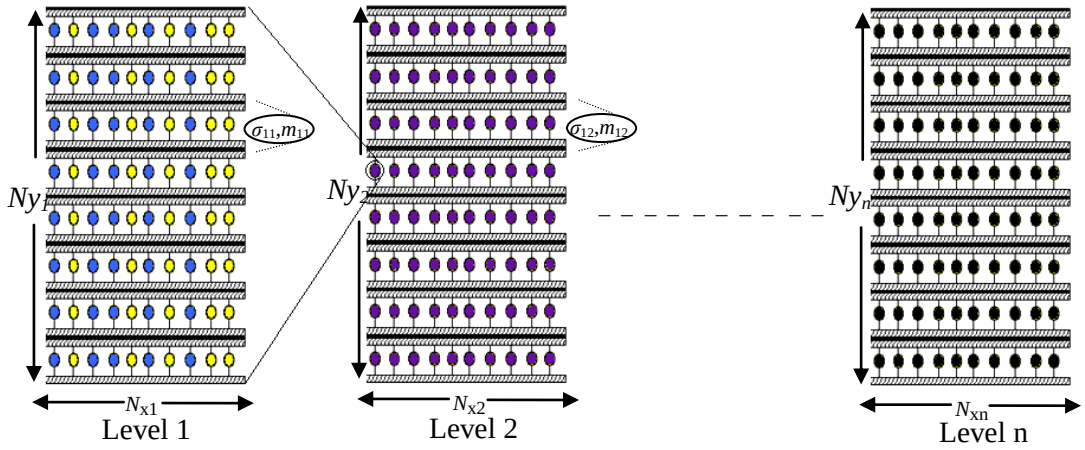

Fig. 5.4 Schematic representation of the composite fiber bundle model at the 1st level of the hierarchical chain of bundles structure.

Here, we extend the model to application in chain of N_y statistically independent bundles with N_x fibers in each bundle as shown in Fig. 5.4.

We use the weakest link theory to treat this model, the probability of the chain of bundle model, first hierarchical level, is given by;

$$W_1(\sigma) = 1 - \exp(-N_{y1}(\frac{\sigma}{\sigma_{11}})^{m_{11}}) \qquad (5.18)$$

where N_{y1} is the number of bundles in the chain. m_{11}, σ_{11} are the shape and scale parameter of each composite bundle of the first level. For each bundle, of the second chain of bundles, we apply Daniels' theory to

calculate m_{12} and σ_{12}. The probability of chain of bundles in level 2 is given by;

$$W_2(\sigma) = 1 - \exp(-N_{y2}(\frac{\sigma}{\sigma_{12}})^{m_{12}}) \tag{5.19}$$

5.3 Results and applications

5.3.1 Model: multi scale fiber bundle model with hierarchical load sharing

In this section, we use our hierarchical extension of Daniels' theory, as in chapter 2, in the analysis of the hierarchical effect on the strength of the structures. Let us consider a hierarchical fiber bundle model as shown in Fig. 5.5.

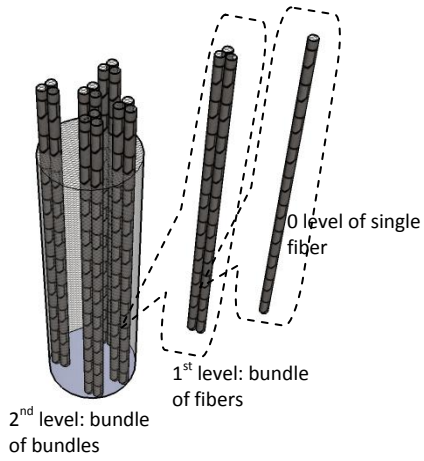

Fig. 5.5 Schematic of multi-scale (two levels) fiber bundle model.

In the following, designations: N represents total number of fibers, number of hierarchical levels is denoted by i=1, 2… M, number of elements in each hierarchical level is denoted by K=K (i). (i.e., the number of fibers in the second level bundle, Fig. 5.5). To illustrate the adopted hierarchical load sharing rule, we consider a three levels structure as an example. In this case, the load is transferred from the upper elements of the hierarchical

structure (corresponding to the ‘‘bundles-of-bundles-of-bundles-of-fibers in a three level structure) to all lower elements of the material (fibers, in this case). The load is shared equally by all the sub-elements of a given higher level element (as long as they are intact). For example, when one fiber breaks, the load will be redistributed to all fibers in the same bundle but not all the fibers in the whole structure, and also when bundle totally failed the load will redistributed on the bundles in the same levels. In other words, if the strength of a given fiber is less than the applied load, the fiber fails and the load is redistributed on the remaining fibers in the same bundle. After all the fibers in the bundle fail, the higher level element is considered as failed, the load is distributed among all the remaining elements in the same higher level (‘‘bundle of bundles’’), and so on. This means we have Equal Load Sharing, ELS, in each hierarchical level, separately, so we call it Hierarchical Load Sharing.

Explain nomenclature

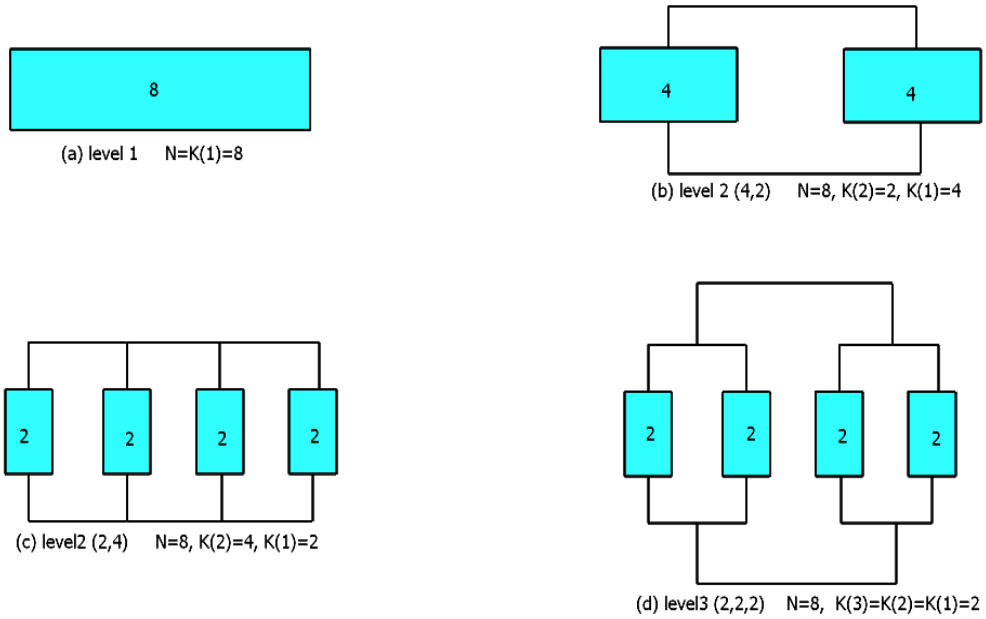

Fig. 5.6 Schematic of different levels of fiber bundle models.

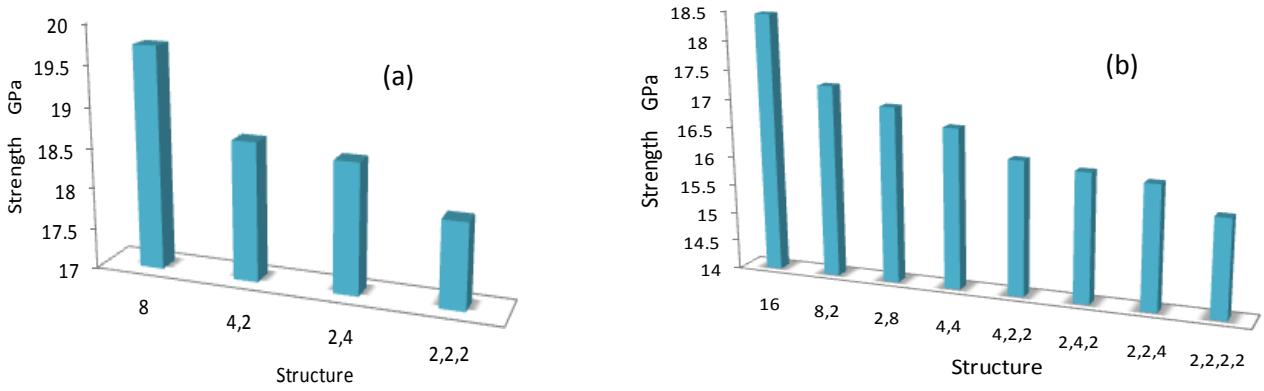

Fig. 5.7 Strength vs. Hierarchical level structure (a) *N*=8 and (b) *N*=16.

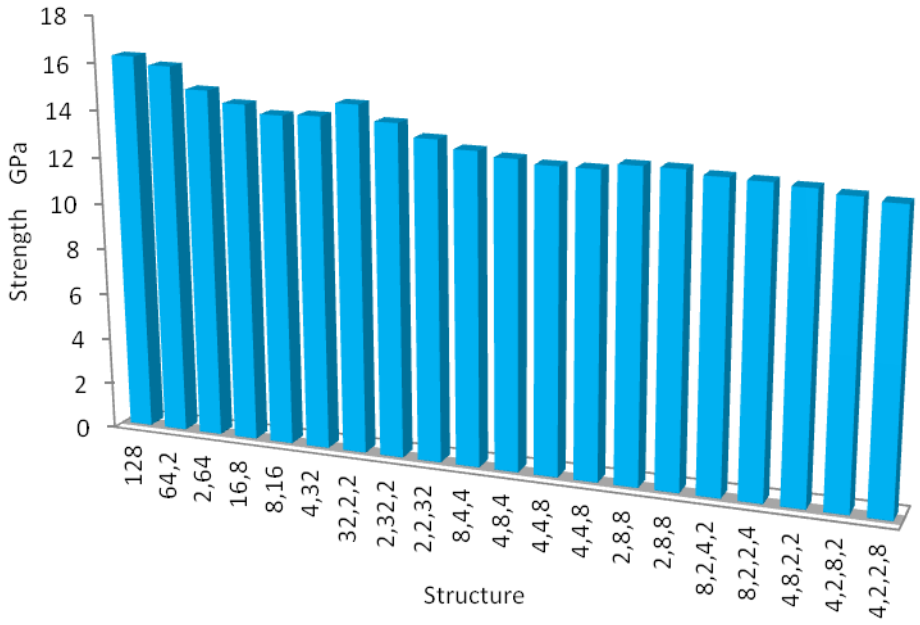

Fig. 5.8 Strength vs. Hierarchical level structure with *N*=128.

We start with a very simple example. We have four different hierarchical structures made up of N=8 fibers are compared, with one to three hierarchical levels. The single level structure is made of eight parallel fibers (indicated as "8"). Two different double-level structures are considered: two bundles of four fibers (indicated as "4,2"), and four bundles of two fibers (indicated as "2,4). Finally, the third level structure is composed by two bundles made of two bundles of two fibers (indicated as "2,2,2"). These structures are schematically shown in Fig. 5.6.

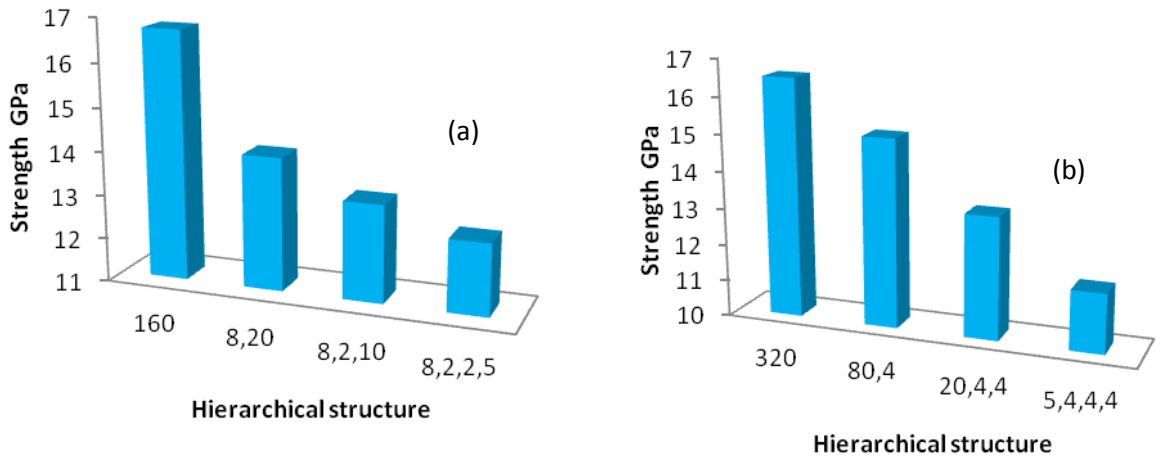

Fig. 5.9 Mean strength *vs*. different hierarchical structure, for (a) k (1) = 8, (b) k (2) =k(3) =k (4) = 4.

The level 0 fibers are assigned random Weibull distributed strengths, using carbon nanotube (CNT) properties: σ_0 = 34 GPa and m = 2.74 (Pugno and Ruoff; 2006).

Results in Fig 5.7a, b show that the lowest hierarchy level structure has the highest strength. Also, the strongest of the two double-level structures is that with the highest number of fibers in parallel (highest lower-level k). The latter would therefore seem to be the required condition for optimizing strength, i.e. the highest possible number of lower level elements set in parallel. This is confirmed by results in Fig. 5.8 relative to various 128-fiber arrangements, ranging from single-level (128 fibers in parallel) to 4-level structures. Again the highest strength is achieved by 128 fibers in parallel, then with two 64-fiber bundles, and so on. The influence of the number of

hierarchy levels on the mean strength is next evaluated again for structures with the same total number of fibers *N*. In Fig. 5.9a, structures having the same number of elements (fibers) at the lowest level are compared, i.e. $k(1)=8$, with $N=160$, as well as with the corresponding level 1 structure ($k(1)=160$) for reference. Once again a strength decrease is found from 1st level to 4th level structures, indicating that increasing hierarchy leads to decreasing strength. The same tendency is found when keeping constant the number of elements at the highest hierarchical level, as shown in Fig. 5, for

$N=320$. In Fig. 5.9b the comparison is between four different structures with $k(M)=4$, whilst in Fig. 5.10 the mean strength is plotted vs. number of hierarchical levels for three different values of $k(M)$.

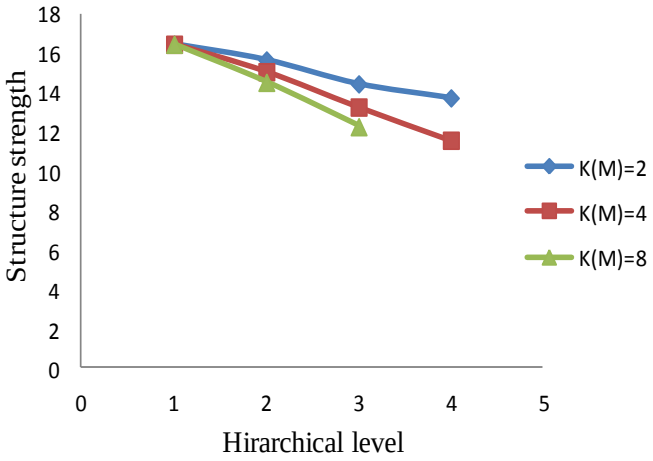

Fig. 5.10 Mean strength *vs*. the number of hierarchical levels.

The observation that the increase in the number of hierarchical levels leads to the lower strength of materials corresponding to the results of Gomez and Pacheco (1997) and Newman and Gabrielov (1991). However, it is in contrast with the observations that many natural materials, built as hierarchical fibrous composites, have extremely high strength.

Therefore, we expect that, the hierarchical theory alone isn't enough to investigate the relationship between hierarchy and strength of nature materials.

5.3.2 Composite fiber bundle

Next, we wish to apply the theory outlined in section 5.2 and evaluate the influence on the mean strength of composite fiber bundles of the chosen Weibull parameters for the two types of fibers involved.

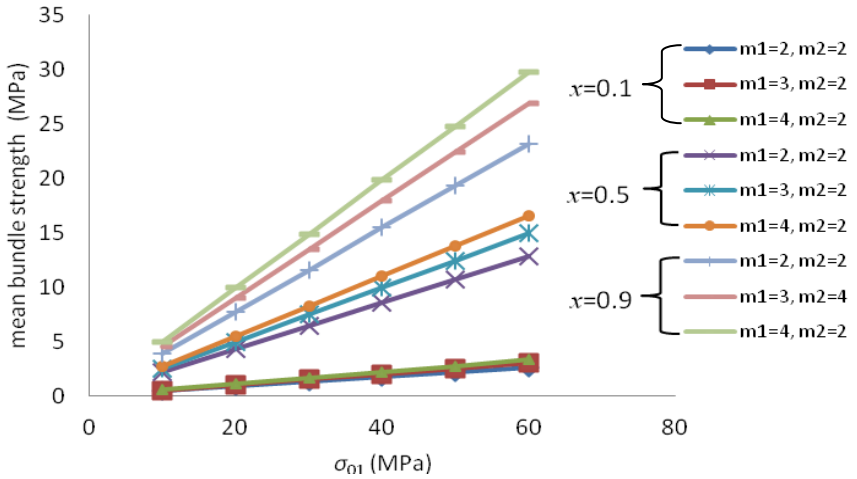

Fig. 5.11 Variation of mean strength *vs*. scale parameter of first type of fibers.

In the first example, shown in Fig. 5.11, the mean composite bundle strength is calculated for varying σ_{01}, m_{01} and m_{02} values, setting σ_{02} =0.01 MPa, and a linear dependence is highlighted. As expected, the variation of m_1 has an effect on the results in a manner which is proportional to the mixture ratio x, i.e. its effect increases with x, and increasing m_1 values yield an increase in mean strength. Also; we study the behaviour of mixed bundle with σ_{02}=0.1MPa. A linear behavior is also found between mean strength and mixture ratio as shown in Fig. 5.12. But this is not constant behaviour in all mixed bundles, we can see different behaviours of mean-strength versus. x curve with σ_{02}=10 MPa as shown in Fig. 5.16.

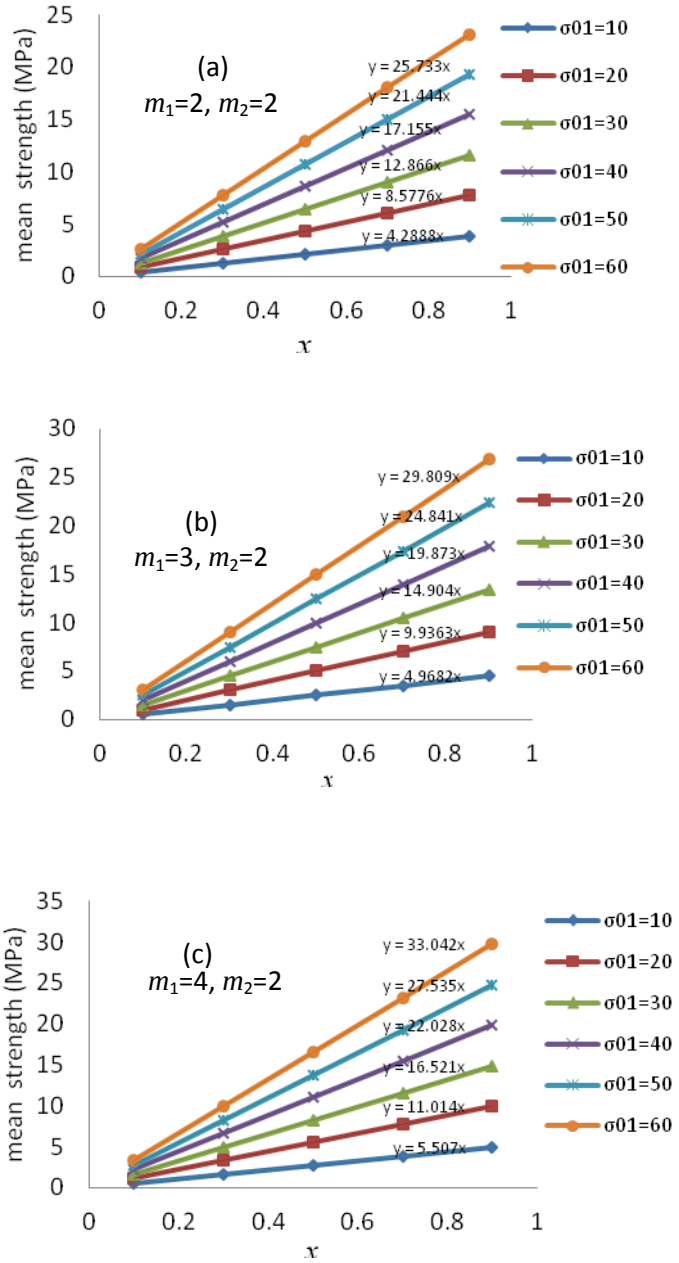

Fig. 5.12 Variation of mean strength *vs*. mixture ratio of first type of fibers with a) m_1=2, b) m_1=3 and c) m_1=4.

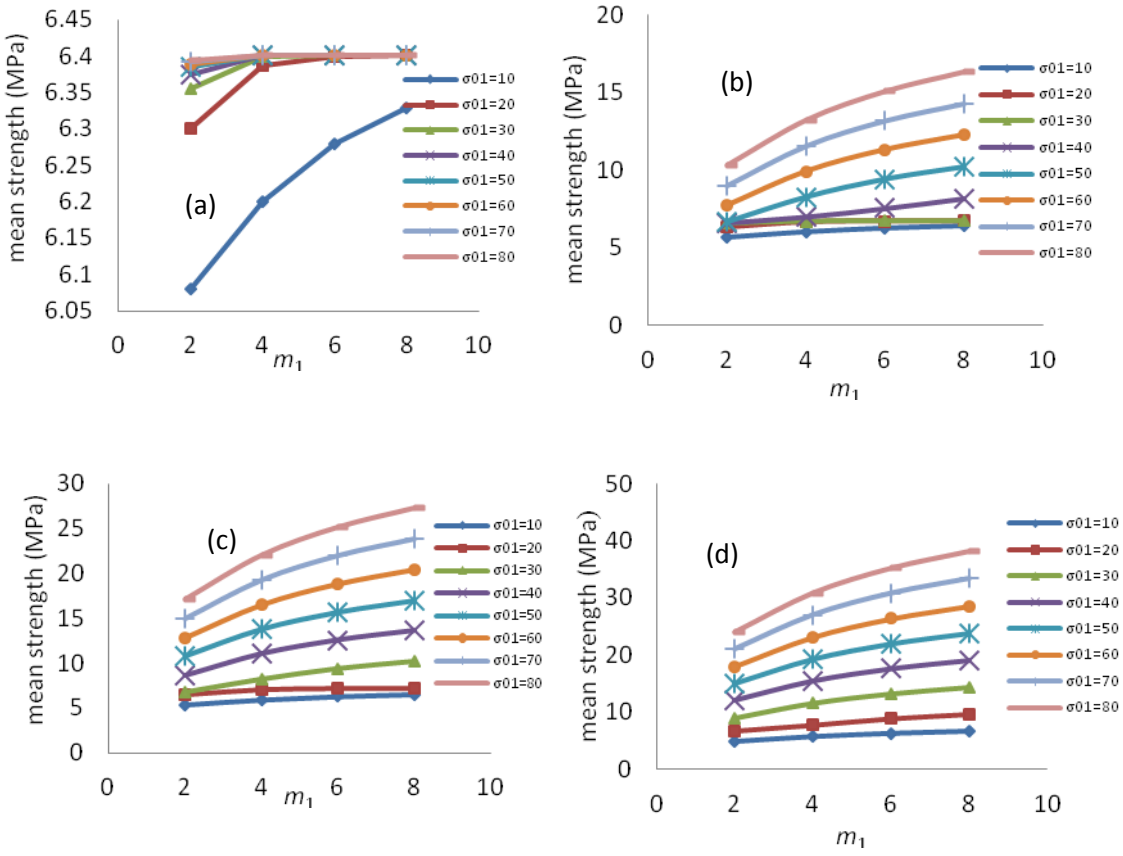

Fig. 5.13 variation of mean strength *vs*. shape parameter of first type of fibers. (a) x=0.1 (b) x=0.3 (c) x=0.5 (d) x=0.7.

In Fig. 5.13, we have four cases with different mixture ratio. In Fig. 5.13(a), the variation of mean strength approximation is too small with σ_{01} between 10 to 80 MPa. In general, the mean strength increases with m_1. The diversion between curves increases with mixture ratio. With increasing x, Fig. 5.13(b-d), the mean strength increases in regular form.

5.3.3 Comparison between rule of mixture and our model

Another issue of interest is the comparison between the results obtained with the present model (application of Daniels’ theory to a composite

bundle) and those obtained using a rule of mixtures approach. In the latter, the mean composite bundle strength $\langle \sigma_{RM} \rangle$ is calculated by using Daniels' theory to separately obtain the strengths $\langle \sigma_{1,D} \rangle$ and $\langle \sigma_{2,D} \rangle$ relative to bundles composed of 100% of first and second types of fibers, respectively, and then combining the two values using the relation:

$$\langle \sigma_{RM} \rangle = x\langle \sigma_{1,D} \rangle + (1-x)\langle \sigma_{2,D} \rangle \tag{5.20}$$

where x is the volume fraction of the first bundle. Figure 5.15 illustrates the discrepancy $\Delta = |\langle \sigma_D \rangle - \langle \sigma_{RM} \rangle|$ between the mean bundle strengths calculated using the two approaches for σ_{02}=0.1 MPa, m_{01}=4, m_{02}=2 and various values of σ_{01}. Clearly, Δ is zero for x=0 and x=1, but the discrepancy is not negligible for intermediate x values. This is due to the fact that when adopting a rule of mixtures approach, unrealistic load redistribution, Fig. 5.14, is assumed among the different types of fibers as damage progresses in the composite bundle.

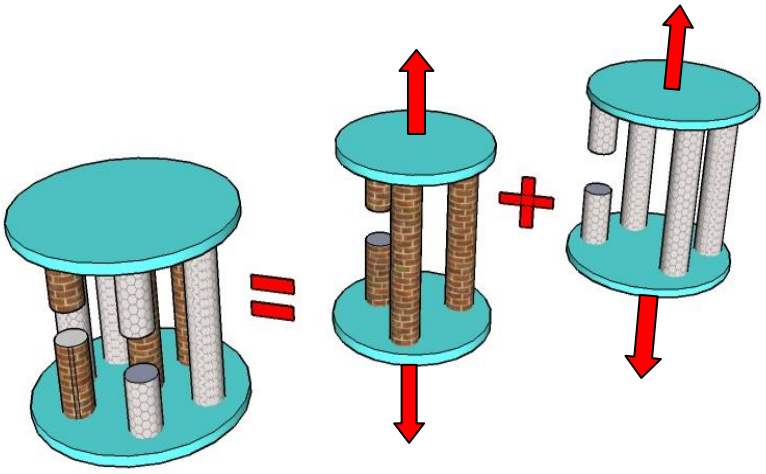

Fig. 5.14 Schematic of equivalent rule of mixture applied on composite bundle.

In composite bundle, if one fiber breaks, the load will be redistributed to all surviving fibers (two types). But when using the rule of mixtures, each bundle is treated as isolated unit. This means the load carried by the broken fiber will be redistributed to surviving fibers of the same type of broken fiber.

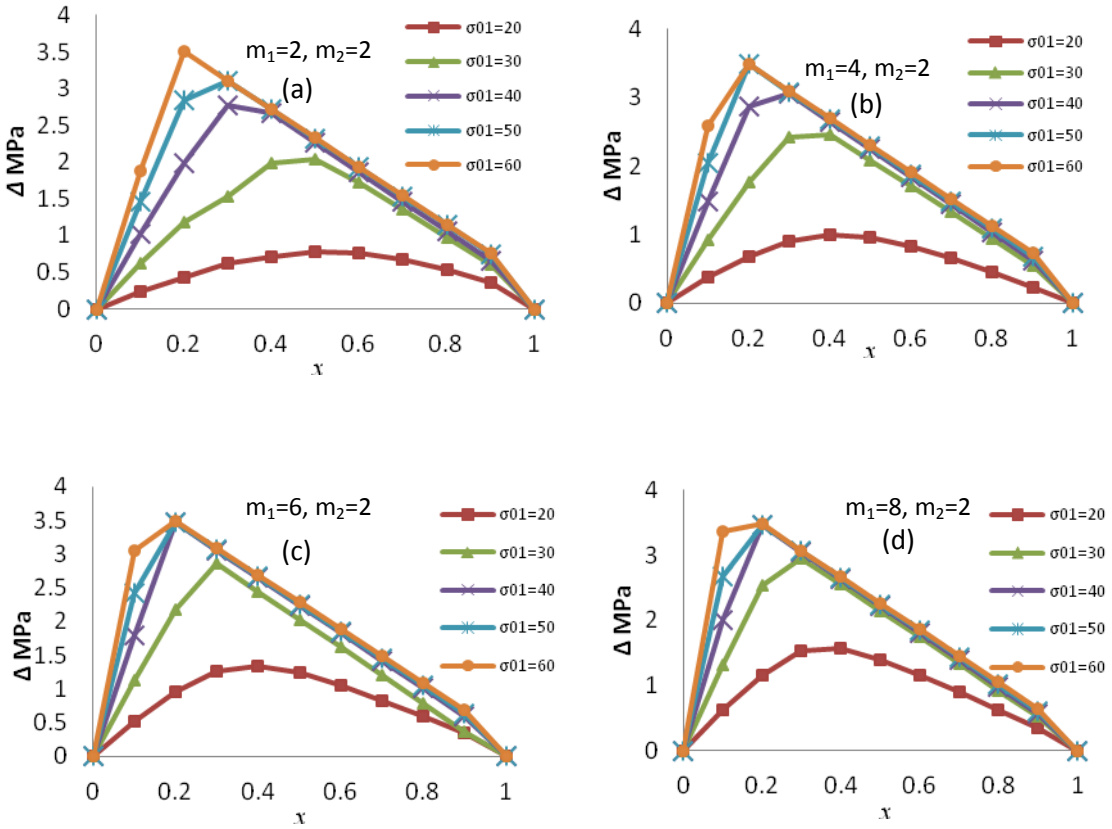

Fig. 5.15 Difference between rule of mixture *vs*. mixture ratio and Daniels’ theory *vs*. mixture ratio.

5.3.4 Comparison with numerical results

To validate the proposed approach, we now compare some analytical calculations with numerical results, (which was carried out with the Fiber

Bundle Model (FBM) (Pugno, 2006)). First, we wish to analyse the mean strength of various bundles composed of different types of fibers. As an example, we consider a mean strength calculation for a varying mixture ratio x and Weibull parameter $\sigma_{01,}$ for σ_{02}=10 MPa, m_1=2, m_2=2. The mean strength of all composite bundles is calculated analytically using the procedure described in Section 5.2 and compared to values obtained through numerical simulations. Results are shown in Fig. 5.16 and display considerable agreement between analytical and numerical calculations.

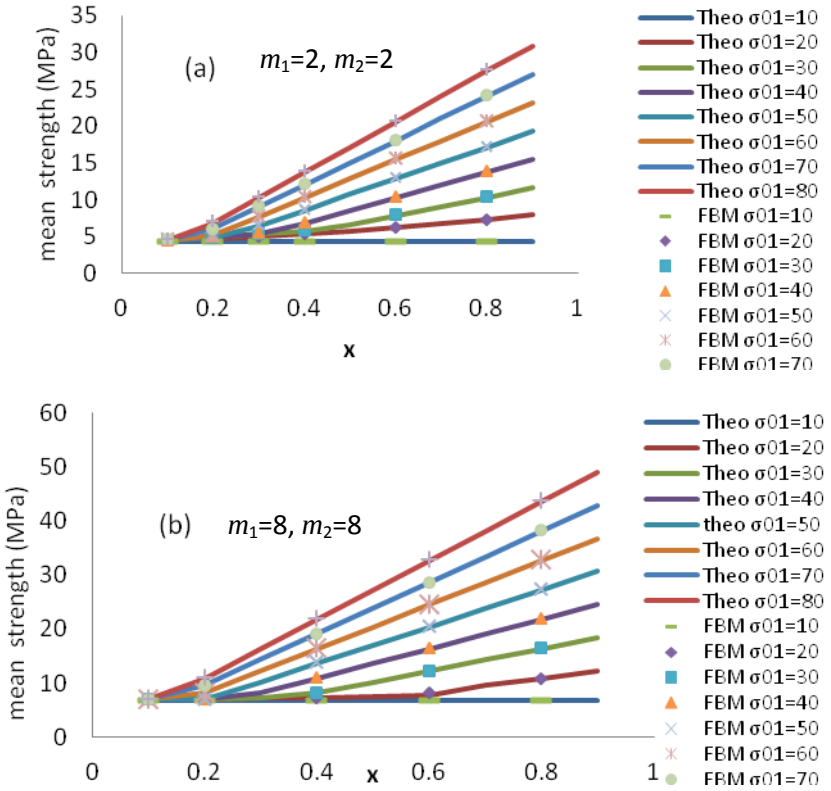

Fig. 5.16 Comparison between mean strength predictions for mixed fiber bundle where: σ_{02}=10MPa. "theo" stands for theoretical predictions, and FBM numerical simulations.

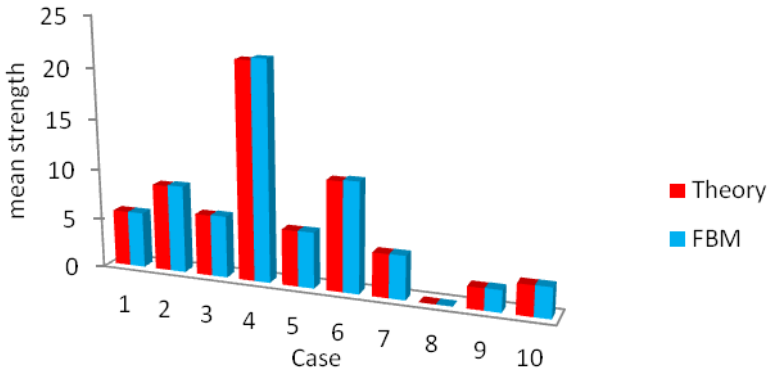

Fig. 5.17 Comparison between theory and FBM for different mixed cases.

The comparison between analytical and numerical results is extended to various different cases of composite bundles composed by fibers with different Weibull parameters and for various mixture ratios.

Table 5.1 Comparison between theory and FBM for different cases of composite bundle.

Case	σ_{01}	σ_{02}	m_1	m_2	x	Mean strength (Theo.)	Mean strength (FBM)
1	20	10	2	4	0	5.506	5.523
2	20	10	2	4	1	8.577	8.676
3	20	10	2	4	0.5	6.07	6.133
4	50	10	2	4	1	21.44	21.672
5	50	10	2	4	0	5.506	5.533
6	50	10	2	4	0.5	10.78	10.917
7	10	0.01	2	4	1	4.3	4.329
8	10	0.01	2	4	0	0.0056	0.0049
9	10	0.01	2	4	0.5	2.14	2.173
10	10	0.01	2	4	0.7	3.0017	3.021

Table 5.1 shows some different cases of composite bundle with different Weibull parameters. Here, mixture ratio equal to 0 and 1 means that the bundle is consisted of single type of fibers, even fist type or second type. We use mixture ratio equal to 0.5 in all cases except last case has x=0.7. We calculate the mean strength by Eq. (5.5) for all cases of bundles and compare it with numerical simulation. Fig. 5.17 shows the results in table 5.1, but we prefer to put it into histogram form to show clearly the agreement between the theoretical prediction and numerical simulation. Also, a good agreement has been found in different cases about elastic modulus as in table 5.2.

Table 5.2 Comparison between theory and FBM for different cases of different elastic modulus in composite bundle.

N_1, N_2	m_1	m_2	σ_{01} MPa	σ_{02} MPa	E_1 MPa	E_2 MPa	Mean Strength (MPa)	FBM mean strength (MPa)
500	2	3	4	4	10	20	1.642	1.51±0.05
500	3	6	50	400	300	800	125.4	122.94±4.35
500	2	4	40	20	110	200	9.506	8.857± 0.226

From table 5.2 we conclude that our model (part 5.2.2) is valid to treat composite bundle with different elastic modulus.

5.3.5 Hierarchical composite bundle

To illustrate the possible variations in the mechanical behavior of a hierarchical composite bundle, we consider some specific examples. First, let us analyze the case of a bundle with two types of fibers, Fig. 5.18, and a mixture ratio of x=0.5, with σ_{01}=10 MPa, σ_{02}=0.01 MPa , m_{01}=2, m_{02}=3 and N=480. In the non hierarchical case, i.e. in the case of a level 1 bundle with all 480 fibers in parallel, the expected mean strength, according to the calculation procedure in section 2.2, is $<\sigma>$=2.14 MPa.

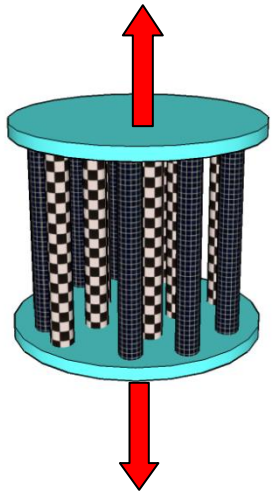

Fig. 5.18 Composite fiber bundle of two types of fibers.

Here, to investigate the effect of hierarchical arrangement on the bundle strength we study the combination between hierarchical theory and composite fiber bundle by applying our hierarchical bundle theory (Pugno, et al. 2011). In this section, we develop a model of hierarchical composite bundle where the first level is a bundle of single type of fibers (fiber bundle), but in the second level we have mixed bundle (composite bundle of bundles) as shown in Fig. 5.19.

One possibility for creating hierarchical architectures with this set of fibers is to form single-fiber bundles at level 1 and mixed bundle types at level 2. For example, we can build two types of level 1 bundles, the first one consisting of two fibers of the first type (σ_{01}=10 MPa and m_{01}=2), the second of 5 fibers of the second type (σ_{02}=0.01 MPa and m_{02}=3), and create a level 2 structure composed of the resulting 120 bundles of the first type and 48 of the second type. The chosen nomenclature for this type of structure is

[(2,5);(120,48)]. From the application of our hierarchical fiber bundle model we get: σ_{11}=8 MPa, σ_{12}=0.007 MPa, m_{01}=2.4, m_{02}=5.2, and a mean strength for the 2nd level bundle of 2.56 MPa, which is larger than the above non-hierarchical level 1 bundle.

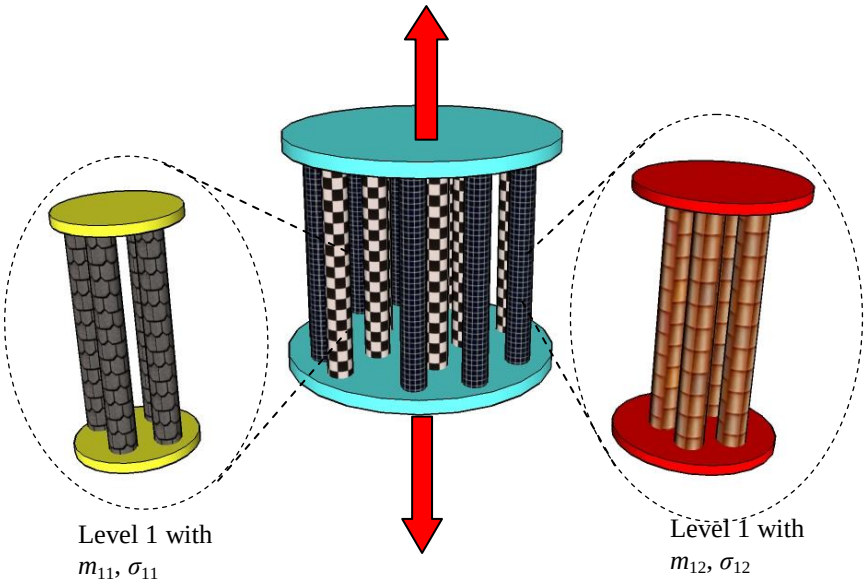

Fig. 5.19 Schematic of composite bundles of bundle.

By comparing this result with previous mean strength, we can see an increase in mean strength. This results is very interesting, because application of hierarchical theory alone leads to decrease in structure strength; but when it is combined with composite bundles structure, we obtained improvement in the mean strength. Maybe this combination between hierarchy and composite is the first key point to investigate the relationship between hierarchical structure and strength increase in nature materials. Also, this model could be used to design new bio-inspired materials.

This strength increase is obtained through various other configurations, as documented in Fig. 5.20. The general tendency is that the greatest strength increase is obtained by grouping strong fibers in small bundles and weak fibers in large bundles at level 1. Clearly, the load redistribution during specimen failure in this type of configuration favours an enhancement of the resistance to damage progression.

This may lay the foundation for a new engineering paradigm that includes the design of structures and materials starting at the molecular level, from bottom-up, to the macroscale, to create new materials and structures that mimic and exceed the properties found in biological analogs.

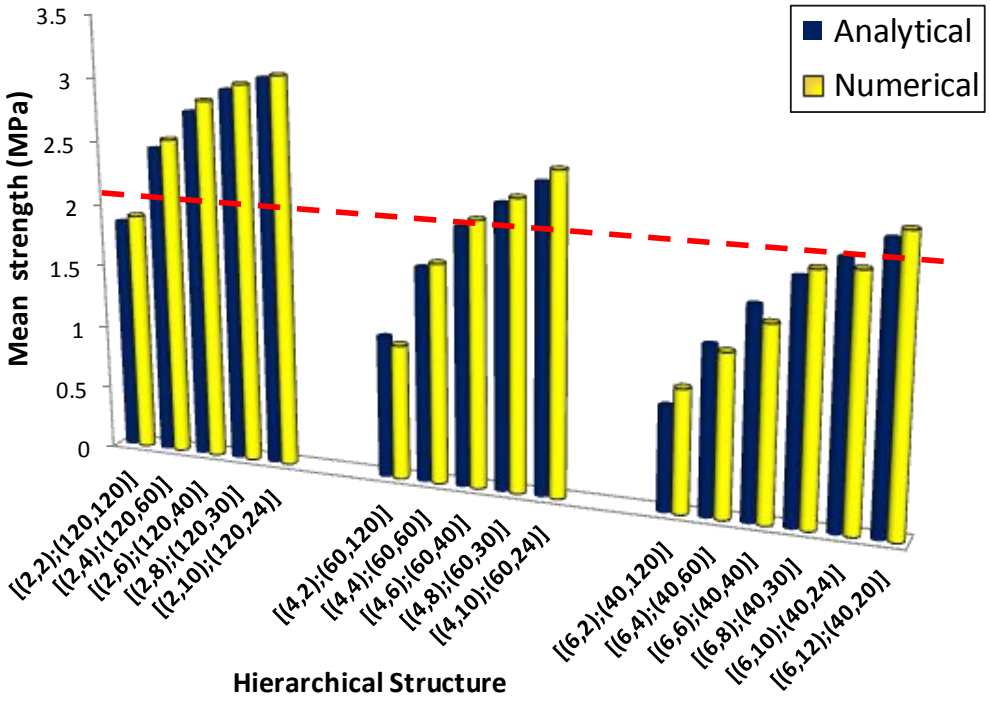

Fig. 5.20 Mean strength vs. hierarchical structure of composite bundle of bundle.

5.4 Conclusion

We have shown here that with different structural arrangements, different combinations of strength and hierarchical structure can be achieved. This finding is the most important result of the case studies put forth in this chapter: it illustrates that the conflict between strength and hierarchy can be resolved by introducing composite as an additional design variable. This provides important insight into structure–property relationships in materials. Overall our analysis illustrates that the introduction of hierarchies is the key to control material properties. Applying this insight to the design of materials will allow an extended use of hierarchies in bioinspired or biomimetic synthetic materials at nanoscale.

Chapter 6
Modeling the self-healing of biological or bio-inspired nanomaterials

6.1 Introduction

Biological systems have the ability to sense, react, regulate, grow, regenerate, and heal. Recent advances in materials chemistry and micro- and nano-scale fabrication techniques have enabled biologically inspired materials systems that mimic many of these remarkable functions. Self-healing materials are motivated by biological systems in which damage triggers a site-specific, autonomic healing response. Self-healing has been achieved using several different approaches for storing and triggering healing functionality in polymers. There are different models for the prediction of the fatigue behavior of self-healing polymers (Maiti and Geubelle, 2005; Koussios and Schmets, 2007; Jones and Dutta, 2010).
Other classes of synthetic materials can undergo healing processes, which in mechanics are basically the mechanisms leading to the recovery of strength and stiffness after damage. However, most synthetic materials require outside intervention such as the application of heat or pressure to initiate and sustain the healing process. For example, Ando et al. (2001; 2002 a, b, c) have shown the healing capability of sintered ceramics while exposed to high temperatures (1000 °C).

In addition, supramolecular materials naturally feature so-called «reversible» (non-permanent) intermolecular bonds, in contrast with polymers derived from traditional chemistry, which are based on so-called « irreversible » (permanent) bonds. This reversibility feature imparts a natural

capacity to self-heal: cracks or breaks occurring in supramolecular materials can be repaired simply by putting the fractured surfaces back together and applying light pressure; the material nearly recovers its initial strength without the need for bonding or heating.

Too model in general self-healing materials, fiber bundle models can be used. A large number of non-healing models exist for fiber bundles (e.g. - Chi et al., 1984; Xiao et al., 2008; Cowking et al., 1991; Mili et al., 2008). In contrast, according to the author's knowledge, there is no model for the prediction of the tensile behavior of self-healing fiber bundles except Carmona (2006) and Kun (2006). This model is the aim of the present chapter.

6.2 Theory

6.2.1 Engineering self healing parameter

For a large number, N_0, of fibers in a bundle, the number of surviving fibers N_{s0}, under an applied strain ε, is given by:

$$N_{s0} = N_0 \exp[-(\frac{\varepsilon}{\varepsilon_0})^m] \tag{6.1}$$

where ε_0 and m are the scale and shape parameters of the Weibull flaw distribution.
The fraction of broken fibers is given by:

$$\alpha_0 = \frac{N_{b0}}{N_0} = \frac{N_0 - N_{s0}}{N_0} \tag{6.2}$$

and in case of self-healing:

$$\alpha_h = \frac{N_{bh}}{N_0} = \frac{N_0 - N_{sh}}{N_0} \tag{6.3}$$

where N_{sh} is the actual number of surviving fibers in the presence of self-healing.

Note that Eqs. (6.2) and (6.3) resemble the definition of an engineering strain ($\varepsilon = \frac{l - l_0}{l_0}$).

We introduce the parameter λ, as the ratio between the number of broken fibers with self-healing, N_{bh}, and the number of broken fibers without healing N_{b0}:

$$\lambda = \frac{\alpha_h}{\alpha_0} = \frac{N_{bh}}{N_{b0}} = \frac{N_0 - N_{sh}}{N_0 - N_{s0}} \tag{6.4}$$

Finally, we introduce the healing parameter η, as:

$$\eta = 1 - \lambda = \frac{N_{sh} - N_0}{N_0 - N_{s0}} \tag{6.5}$$

Note that when η=1 we have N_{sh}=$N_{0,}$ whereas for η=0, N_{sh} =N_{s0}.

6.2.2 True self healing parameter

We now introduced the true parameter α_h^* as:

$$\alpha_h^* = \int_{N_0}^{N_{sh}} \frac{\mathrm{d}N}{N} = \ln N_{sh} - \ln N_0 = \ln \frac{N_{sh}}{N_0} \tag{6.6}$$

in analogy with the true strain ($\varepsilon = \int_{l_0}^{l} \frac{\mathrm{d}l}{l} = \ln \frac{l}{l_0}$).

In absence of healing it becomes:

$$\alpha_0^* = \ln \frac{N_{s0}}{N_0} \tag{6.7}$$

From Eqs. (6.4) and (6.5), the true self-healing parameter is given by:

$$\eta = 1 - \lambda = 1 - \frac{\alpha_{sh}^{*}}{\alpha_{0}^{*}} = 1 - \frac{\ln \frac{N_{sh}}{N_0}}{\ln \frac{N_s}{N_0}} \tag{6.8}$$

The introduction of the true self-healing parameter of Eq. (6.8) is needed in order to take into account the variation of the total number of fibers induced by the self-healing (similarly to the true strain that is accounting for the length *l* variation).

From Eq. (6.1) we immediately derive:

$$\ln \frac{N_s}{N_0} = (-(\frac{\varepsilon}{\varepsilon_0})^m) \tag{6.9}$$

By substituting Eq. (6.9) into Eq. (6.8) we find:

$$\ln \frac{N_{sh}}{N_0} = ((\eta - 1)(\frac{\varepsilon}{\varepsilon_0})^m) \tag{6.10}$$

and thus:

$$N_{sh} = N_0 \exp[(\eta - 1)(\frac{\varepsilon}{\varepsilon_0})^m] \tag{6.11}$$

The introduction of the self-healing into Eq. (6.11) generalizes the classical Weibull (1939) approach, Eq. (6.1).

The last expression is related to the applied tensile load, *F*, by:

$$F(\varepsilon) = AE\ \varepsilon[N_0 \exp[(\eta - 1)(\frac{\varepsilon}{\varepsilon_0})^m]] \tag{6.12}$$

where *A* is the cross sectional area of the single fiber and *E* is its Young's modulus. Then, if *A*, *L*, *E*, N_0, *m* and ε_0 are known, the curve stress vs. strain can be obtained:

$$\sigma(\varepsilon) = \frac{F(\varepsilon)}{AN_0} = E\ \varepsilon[\exp[(\eta - 1)(\frac{\varepsilon}{\varepsilon_0})^m] = E_{\text{eq}}(\varepsilon, \eta)\varepsilon \qquad (6.13)$$

6.3 Results and discussion

As an example we apply our calculation to carbon nanotube (CNT) bundle with strength randomly assigned, $\varepsilon_0 = 0.04$ and $m_0 \approx 2.7$, based on the nanoscale Weibull distribution (Pugno and Ruoff 2006). Fig. 6.1 shows the mechanism of the self-healing of a carbon nanotube. Self-healing of CNTs may accelerate the development of the CNT apace-elevator mega cable (Pugno, 2006; Pugno et al. 2008; 2009).

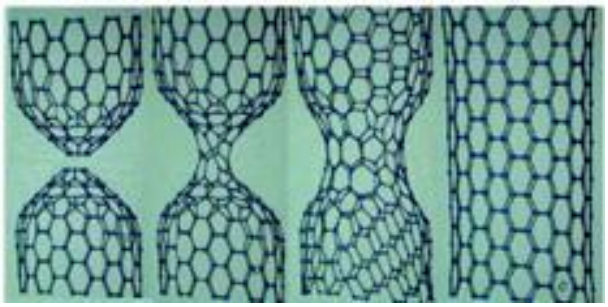

Fig. 6.1 Carbon nanotube self-healing mechanism (Prof. B. Yakobson's talk).

In Fig. 6.2, the stress–strain response is predicted for a bundle with different values of the healing parameter, η, from 0 to 1, while all the other parameters in Eq. (6.13) are kept constant. When increasing the self-healing parameter, both the maximum stress, see Fig. 6.2, and the strain at which the maximum stress is reached, increase. (This can also be seen in Fig. 6.7, where the ratio between the maximum stress with healing and maximum stress without healing is increasing in monotonic way with healing parameter increasing.) For a self-healing parameter equal to 1, the bundle will be unbreakable. Fig. 6.3 shows the variation of the number of survival

fibers as a function of the applied strain, with different values of the healing parameter.

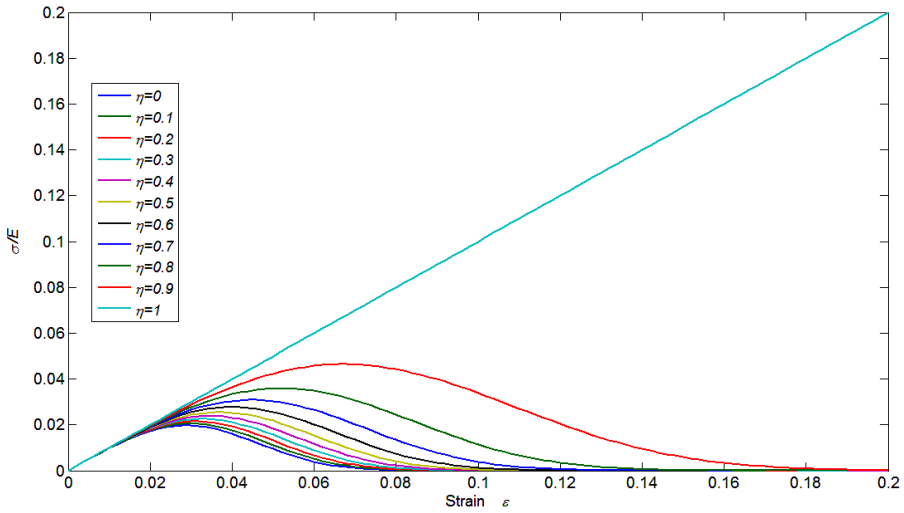

Fig. 6.2 Stress-strain response by varying the self-healing parameter.

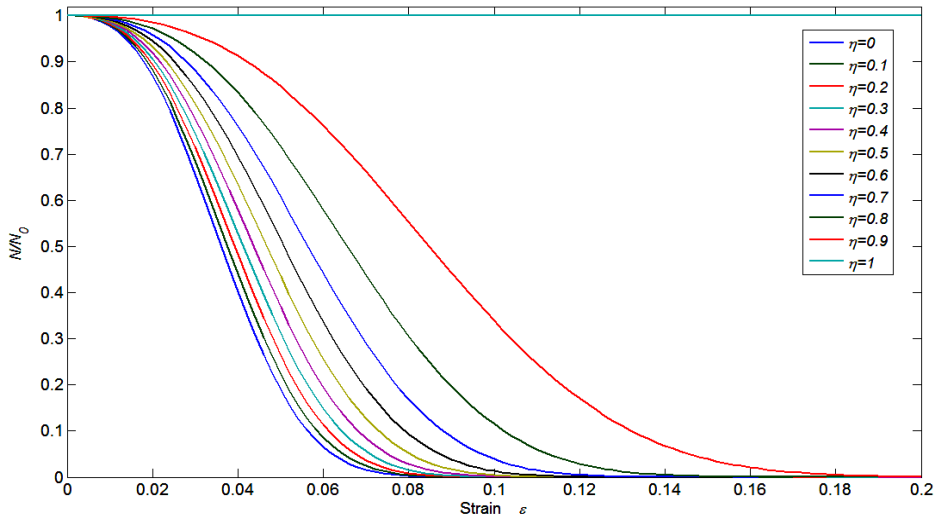

Fig. 6.3 Survival fibers, $N_{sh} \equiv N$ vs. strain, by varying the healing parameter.

Fig. 6.4 shows two different type curves. The upper curves represent the stress-strain curves of Fig. 6.2 and the lower curves are the rates of variation of the number of survival fibers in the bundle, by varying the applied strain and for different self-healing. The maxima of the lower curves represent the points at maximal failure rate of the bundle. From Fig. 6.4 we can see that the strains at which the maximum stress is reached, ε_{σ}^{*}, are lower than the strains at the maximal failure rate, ε_{n}^{*}, as specifically reported in Fig. 6.5.

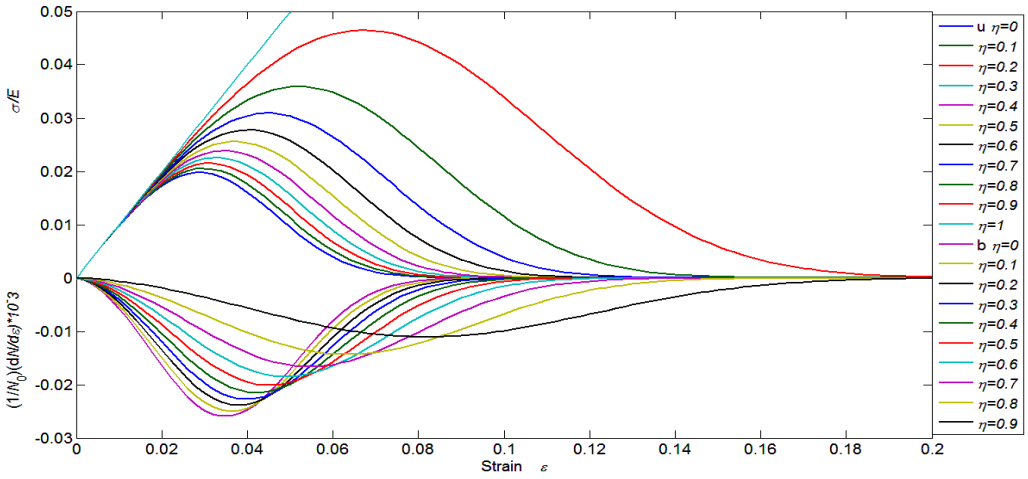

Fig. 6.4 Stress or rate of survival fibers vs. strain by varying the healing parameter.

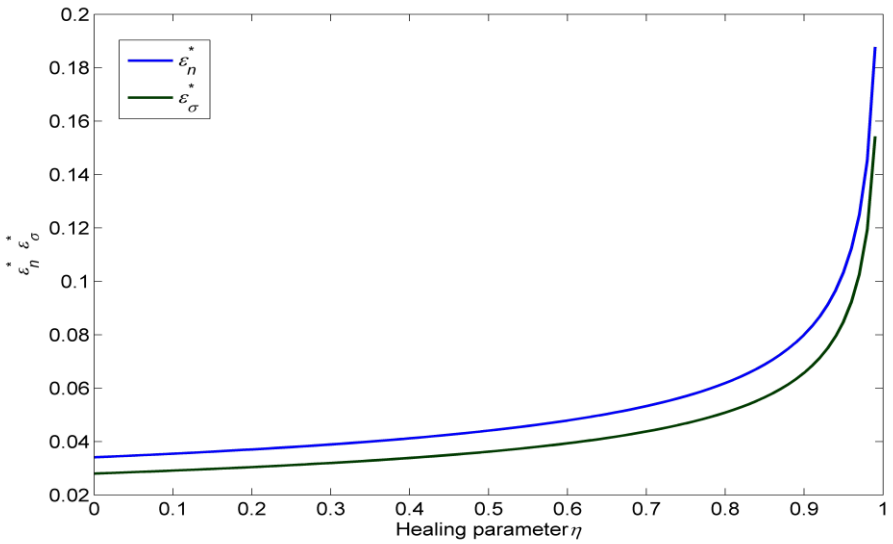

Fig. 6.5 Strains corresponding to maximum stress or failure rate vs. healing parameter.

The area under the stress-strain curve is the total dissipated energy density (in our calculations we assumed that the bundle is fractured when the stress is 1% of its maximum).

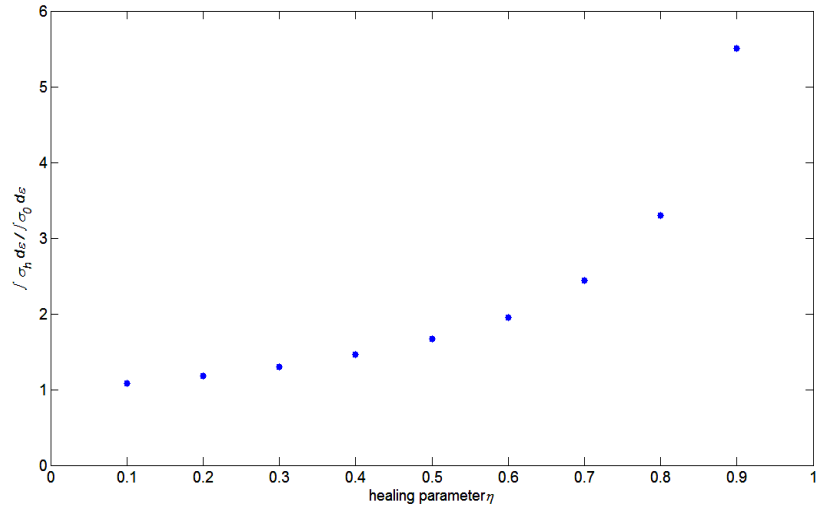

Fig. 6.6 Dissipated energy density with self-healing normalized to the non healing case vs. healing parameter.

In Fig. 6.6 the ratio between the dissipated energy density with and without healing is reported and clearly increases with increasing the self-healing parameter.

The ratio between the strains corresponding to the maximum stresses with and without healing $\varepsilon_{max,h}$ and $\varepsilon_{max,0}$ respectively and the ratio between the related maximum stresses $\sigma_{max,h}$ and $\sigma_{max,0}$ respectively are reported in Fig. 6.7: both these ratios increase by increasing the healing parameter.

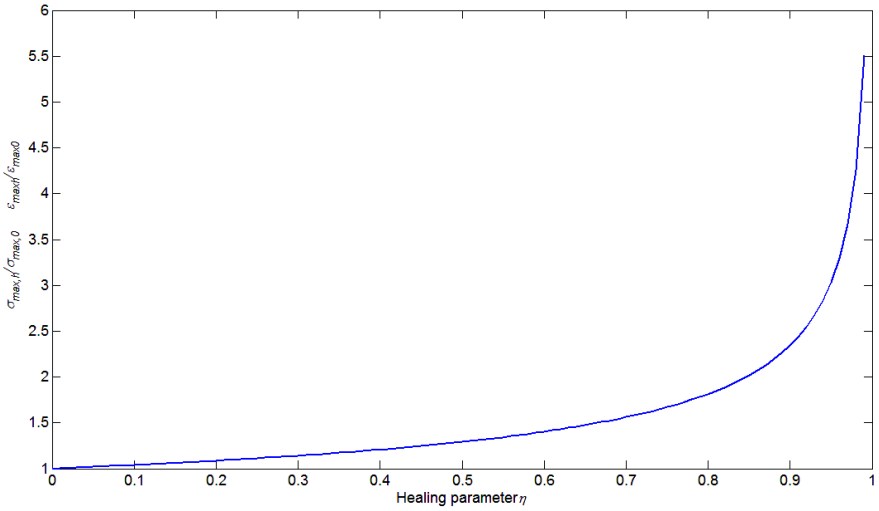

Fig. 6.7 Dimensionless maximum stress and related strain vs. healing parameter.

6.4 Conclusion

The presented simple self-healing fiber bundle model is able to quantify the increments of the mechanical performances induced by the self-healing. Applications to design a new class of bio-inspired nanomaterials are envisioned.

Chapter 7
General Conclusions

7.1 Conlclusion

In this study, an analytical model for the statistical strength of hierarchical bundle structures is developed to extend Daniels' theory. This extension is used to investigate the effect of hierarchy on the bundle mean strength. The outcome of this analytical investigation allows the evaluation of the mean strength of different hierarchical architectures.

We have proposed several models of hierarchical fiber bundles. Various specific applications were considered:

1- Hierarchical fiber bundle (bundle of bundle of fibers).
2- Hierarchical structure composed of CNT fibers (Analysis of the statistical size effect on CNT bundle strength through a weakest link model).
3- Hierarchical composite fiber bundle (bundle constituted of different types of fibers).

The adopted approach, i.e. a so-called Hierarchical Fiber Bundle Model (HFBM), is used in the analysis of the strength of different hierarchical structures of fiber bundles. Usually this type of problem is analyzed by means of phenomenological models. Our model is very efficient in describing some specific hierarchical architectures. In general, the fiber bundle model allows the simple incorporation of statistical and probabilistic effects, where as phenomenological models usually do not include basic continuum mechanics laws.

Here, the main theoretical models can be used with the engineer, rather than the statistician, in mind. As shown in chapter 2, this model is able to predict the strength of a hierarchical fiber bundle at any hierarchical level and results may be used and compared with experimental data. The

hierarchical fiber bundle model can be used to design synthetic bundles based on bio-nanofibrils which have promising mechanical properties.

We have also shown that, extending Daniels' theory using a bimodal Weibull distribution provides the means to predict the strength of CNTs yarns. The interfacial and CNT yarn strength are described by a statistical Weibull distribution. The basic result of the model indicates that the mean strength and standard deviation of CNT yarns increase with increasing interfacial Weibull parameters. The variable CNT-CNT joint strengths studied here will ultimately need to be considered in strength models for structural of CNT yarns.

We have also presented a self-consistent analytical procedure to calculate the strength of hierarchical fiber bundles constituted by two (or more) types of fibers. We have demonstrated how hierarchy alone is insufficient to yield strength enhancement, and how an increase in strength can be obtained through a suitable choice of fiber distributions at different hierarchical levels. In other words, the key to an improvement in the mechanical performance in general of multi-scale materials would seem to lie in hierarchical structuring of multi-components. This result can be of great interest, first as a mean to interpret and further investigate the exceptional mechanical performance of biomaterials, and secondly as a strategy to design and fabricate new bio-inspired materials with desired tailor-made properties. The theory and analytical procedures outlined in this work can provide a useful tool in this field.

Another important contribution presented in this thesis is the extension of the fiber bundle model for the study a self healing. The process is studied by allowing the possibility for fractured fibers to be substituted by intact ones. This model makes fiber bundles promising candidates for the understanding of the biofibrils, and possible benefits of further insight in this field can hardly be exaggerated. The analysis given in this chapter is for a single level problem, and it is clearly desirable to extend the analysis to a hierarchical level.

In conclusion, in this thesis, several types of for hierarchical bundle structures have been proposed and analyzed, and the mean strength of the corresponding structures have been explored through analytical calculations and some numerical simulations. It will be interesting to see further experimental efforts directed in this field.

7.2 A perspective

What is the future of the fiber bundle model? This study has shown that ability to extend fiber model for a hierarchical structure, which can be helpful to design strong and tough new materials. Quite a few efforts have also been undertaken for the unification of the existing statistical models of fracture, and their embedding into the formalisms of statistical physics, and remarkable progress has been made in the recent years. In this respect there are two extensions to FBM that can be implemented with moderate effort. First, our introduction of analytical correlations for mean strength and hierarchical levels can be extended to investigate the mean strength of hierarchical fibrous composite structures. Secondly, placing fiber bundle elements on the nodes of networks while retaining their disordered properties and dynamical rules could be a fascinating field to study, and a similar effort has recently been undertaken employing the random fuse model (Bakke et al., 2006). This could lead to a better understanding for the failure modes of electrical grids, or computer networks.

An increasing interest in bionic design of materials based on structures of natural biomaterials has led to the nanomechanical characterization of biomaterials. This might inspire future materials design as well as manufacturing and assembly strategies, not limited to the nanoscale. For example, using universal patterns to the fullest extent and creating diversity at the highest hierarchical level, in order to match client-specific requirements, could reduce production costs, delivery times and increase product quality. It has been suggested that the complexity of engineered systems is converging with that of biological systems. For example, a Boeing 777 has 150,000 subsystems and over 1000 computers, which are organized in networks of networks. Consequently, a better understanding of how nature designs and manages complexity will enable to maintain engineered complexity under control or even reduce it.

Finally, the fiber bundle model can be used as a tool for understanding phenomena such as creep and fatigue, as well as used to describe the behavior of fiber reinforced composites or modeling e.g. network failure, traffic jams and earthquake dynamics.

Bibliography

Ackbarow, T. and Buehler, M.J. (2009) Alpha-helical protein domains unify strength and robustness through hierarchical structures. Nanotechnology 20, 075103.

Ajayan, P., Schadler, L., Giannaris, C. and Rubio, A. (2000) Single-walled carbon nanotube–polymer composites: strength and weakness. Adv Mater. 12, 750–753.

Altman, G. H., Horan, R. L., Lu, H. H., Moreau, J., Martin, I., Richmond, J. C. and Kaplan, D. L. (2002) Silk matrix for tissue engineered anterior cruciate ligaments. Biomaterials 23, 4131–4141.

Amaniampong, G. and Burgoyne, C. J. (1994) Statistical variability in the strength and failure strain of armaid and polyester yarns. J. Mater. Sci. 29, 5141–5152.

Andersen, J. V., Sornette, D. and Leung, K. (1997) Tricritical Behaviour in Rupture Induced by Disorder. Phys. Rev. Lett. 78, 2140–2143.

Andersons, J., Joffe, R., Hojo, M. and Ochiai, S. (2002) Glass fiber strength distribution determined by common experimental methods. Compos. Sci. Technol. 62, 131–145.

Ando, K.., Chu, M., Hanagata, T., Tuji, K. and Sato, S. (2001) Crack-healing behavior under stress of mullite/silicon carbide ceramics and the resultant fatigue strength. Journal of the American Ceramic Society 84, 2073–2078.

Ando, K., Chu, M., Tsuji, K., Hirasawa, T., Kobayashi, Y. and Sato, S. (2002a) Crack healing behaviour and high-temperature strength of mullite/SiC composite ceramics. Journal of the European Ceramic Society 22, 1313–1319.

Ando, K., Chu, M., Tsuji, K., Hirasawa, T., Kobayashi, Y. and Sato, S. (2002b) Crack healing behavior of Si3N4/SiC ceramics under stress and fatigue strength at the temperature of healing (1000 °C). Journal of the European Ceramic Society 22, 1339–1346.

Ando, K., Chu, M., Tsuji, K., Hirasawa, T., Kobayashi, Y. and Sato, S. (2002c) Crack healing behavior of Si3N4/SiC ceramics under cyclic stress and resultant fatigue strength at the healing temperature. Journal of the American Ceramic Society 85, 2268–2272.

Argon, A. S. (1974) Statistical aspects of fracture, In composite material Vol. V, Academic press, New York, 184–190.

Ashby, M. F. (1999) Materials Selection in Mechanical Design, 2nd edn. Butterworth-Heinemann, Oxford.

Bakke, J. O. H., Hansen, A. and Kertesz, J. (2006) Failure and avalanches in complex networks. cond-mat/0605461.

Barber, A., Kaplan, A., Cohen, S., Tenne, R. and Wagner, H. (2006) Stochastic strength of nanotubes: An appraisal of available data. Compos. Sci. Technol. 65, 2380–2384.

Batrouni, G. G., Hansen, A. and Schmittbuhl, J. (2002) Heterogeneous interfacial failure between two elastic blocks. Phys. Rev. E 65, 036126.

Bazant, Z. P. (1997) Scaling of quasibrittle fracture: Asymptotic analysis. Int. Journal of Fracture 83, 19–40.

Bazant, Z. P. (2002) Scaling of Structural Strength. Hermes Penton Science (Kogan Page Science).

Bazant, Z. P. and Li, Z. (1995) Modulus of rupture: Size effect due to fracture initiation in boundary layer. Journal of Structural Engineering 121, 739–746.

Bazant, Z. P. and Planas. J. (1998) Fracture and Size Effect in Concrete and Other Quasibrittle Materials. CRC Press, Boca Raton Florida and London.

Bethune, D., Kiang, CH., de Vries, M., Gorman, G., Savoy, R. and Vazquez, J. and Beyers, R. (1993) Cobalt catalysed growth of carbon nanotubes with single-atomic layer walls. Nature 363, 605–607.

Beyerlein, I. J. and Phoenix, S. L. (1996a) Comparison of shear-lag theory and continuum fracture mechanics for modeling fiber and matrix stresses in an elastic cracked composite lamina. International journal of Solids and Structures 33, 2543–2574.

Beyerlein, I. J. and Phoenix, S. L. (1996b) Stress concentrations around multiple fiber breaks in an elastic matrix with local yielding or debonding using quadratic influence superposition, J. Mech. Phys. Solids 44, 1997-2039.

Bosia F., Buehler, M. J. and Pugno, M. N. (2010) Hierarchical simulations for the design of super tough nanofibers inspired by spider silk, Physical Reviewe 82, 056103.

Bratzel, G., Cranford, S. and Buehler, M. J. (2010) Bioinspired noncovalently crosslinked “fuzzy” carbon nanotube bundles with superior toughness and strength. J. Mat. Chem. 20, 10465-10474.

Beyerlein, I. J. and Phoenix, S. L. (1997) Statistics of fracture for an elastic notched composite lamina containing Weibull fibers, part I: Features from Monte-Carlo simulation. Engineering Fracture Mechanics 57, 241–265.

Carmona, H. A., Kun, F., Andrade Jr, J. S. and Herrmann, H. J. (2006) Numerical simulation of fatigue under diametrical compression. cond-mat

Carpinteri, A. (1994) Scaling laws and renormalization groups for strength and toughness of disordered materials. Int. J.Solids Struct. 31, 291–302.

Carpinteri, A. and Paggi, M. (2009) A top-down approach for the prediction of hardness and toughness of hierarchical materials. Chaos, Solitons & Fractals 42, 2546–52.

Carpinteri, A. and Pugno, N. (2005) Are the scaling laws on strength of solids related to mechanics or to geometry? Nat. Mater. 4, 421– 423.

Chakrabarti, B. K. and Benguigui, L. G. (1997) Statistical Physics of Fracture and Breakdown in Disordered Systems. Oxford University Press.

Chaplin, W. S. (1880) The relation between the tensile strengths of long and short bars. Van Nostrand's Engineering Magazine 23, 441–444.

Chaplin, W. S. (1882) On the relative tensile strengths of long and short bars. Proceeding of Engineering Club, Philadelphia 3, 15–28.

Chen, P.Y., Lin, A. Y. M., Stokes, A. G., Seki, Y., Bodde, S. G., McKittrick, J. and Meyers, M. A. (2008) Structural biological materials : Overview of current research, J. O. M. 60, 23-32.

Cheng, H., Li, F., Sun, X., Brown, S., Pimenta, M., Marucci, A., Dresselhaus, G. and Dresselhaus, M. (1998) Bulk morphology and diameter distribution of single-walled carbon nanotubes synthesized by catalytic decomposition of hydrocarbons. Chem. Phys. Lett. 289, 602–610.

Chi, Z., Chou, T. W. and Shen, G. (1984) Determination of single fiber strength distribution from fiber bundle testings. Journal of Materials Science 19, 3319–3324.

Chvapil, M., Speer, D. P., Holubec, H., Chvapil, T. A. and King,D. H. (1993) Collagen fibers as a temporary scaffold for replacement of ACL in goats. Journal of Biomedical Materials Research 27, 313–325.

Coleman, B. D. (1956) Time dependence of mechanical breakdown phenomena. J. Appl. Phys. 27, 862–866.

Coleman, B. D. (1958a) On the strength of classical fibres and fibre bundles. J. Mech. Phys. Solid. 7, 60–70.

Coleman, B. D. (1958) The Statistics and Time Dependence of Mechanical Breakdown in Fibers J. Appl. Phys. 29, 968-983.

Cosson, M., Debodinance, P., Boukerrou, M., Chauvet, M. P., Lobry, P., Crepin, G. and Ego, A. (2003) Mechanical properties of synthetic implants used in the repair of prolapse and urinary incontinence in women: which is the ideal material? International Uro-Gynecology Journal 14, 169–178.

Cowin, S. (2001) Bone Mechanics, CRC Press, Boca Raton.

Cowking, A., Atto, A., Siddiqui, A., Sweet, M. and Hill, R. (1991) Testing E-glass fiber bundles using acoustic emission. Journal of Materials Science 26, 1301–1310.

Currey, J. D. (1999) The design of mineralised hard tissues for their mechanical functions, Journal of Experimental Biology 202, 3285-3294.

Currey, J. D. (2002) Bones - Structure and Mechanics. Princeton University Press, Princeton.

Currey, J. D. (2003) How well are bones designed to resist fracture? J. Bone. Miner. Res. 18, 591-598.

Curtin, W. A. (1991) Theory of Mechanical Properties of Ceramic-Matrix Composites, J. Am. Ceram. Soc. 74, 2837- 2845.

Curtin, W. A. (1993) The “tough” to brittle transition in brittle matrix composites, J. Mech. Phys. Solids 41, 217.

Curtin, W. A. and Takeda, N. J. (1998) Tensile Strength of Fiber-Reinforced Composites: II. Application to Polymer Matrix Composites.J. Comp. Mater. 32, 2042-2059.

Curtin. W. A. (1998) Size scaling of strength in heterogeneous materials. Phys. Rev. Lett. 80, 1445–1448.

da Silveria, R. (1999) An introduction to breakdown phenomena in disordered systems Am. J. Phys. 67, 1177-1188.

Daniels. H. E. (1945) The statistical theory of the strength of bundles and threads. Proc. R. Soc. Lond. A183, 405–35.

Danzer, R. A. (1992) A general strength distribution function for brittle materials. J. Eur. Ceram. Soc. 10, 461–472.

Danzer, R. and Lube, T. (1996) New fracture statistics for brittle materials: in Fracture Mechanics of Ceramics. New York: Plenum Press 11, 425–439.

Delaplace, A., Roux, S. and Pijaudier-Callot, G. (1999) Damage cascade’ in a softening interface. Int. J. Solids Struct., 36, 1403–1426.

Dill-Langer, G., Hidalgo, R. C., Kun, F., Moreno, Y., Aicher, S. and Herrmann, H. J. (2003) Size dependency of tension strength in natural fiber composites. Physica A 325, 547–560.

Dresselhaus, M., Dresselhaus, G. and Avouris, P. Carbon Nanotubes: Synthesis, Structure, Properties, and Applications, Springer. Heidelberg, Germany 2001.

Erdmann , T. and Schwarz , U. S. (2004) Stochastic dynamics of adhesion clusters under shared constant force and with rebinding. J. Chem. Phys. 121, 8997-9017

Eppell, S. J., Tong, W. L., Katz, J. L., Spearing, W. L. and Glimcher, M. J. (2001) Shape and size of isolated bone mineralites measured using atomic force microscopy. J. Orthopaed Res 19, 1027–1034.

Epstein, B. (1948a) Statistical aspect of fracture problems. J. Appl. Phys. 19, 140–147.

Epstein, B. (1948b) Applications of the theory of extreme values in fracture problems. Journal of the American Statistical Association 43, 403–412.

Fisher, R. A. and Tippett, L. H. C. (1928) Limiting forms of the frequency distribution of the largest and smallest member of a sample. Proc Camb. Philosoph. Soc. 24, 180–190.

Fratzl, P. (2003) Cellulose and collagen: from fibres to tissues, Curr. Opin. Coll. Interf. Sci. 8, 32-39.

Fratzl, P. and Weinkamer, R. (2007) Nature's hierarchical materials. Progr. Mater. Sci. 52, 1263-1334.

Freeman, J. W., Woods, M. D. and Laurencin, C. T. (2007) Tissue engineering of the anterior cruciate ligament using a braid-twist scaffold design, Journal of Biomechanics. 40, 2029-2036.

Freudenthal, A. M. (1956) Physical and statistical aspects of fatigue. In: Advance in applied mechanics. London: Academic Press 4, 117–157.

Freudenthal,A. M. and Gumbel, E. J. (1953) On the statistical interpretation of fatigue tests. Proc. R. Soc. (Lond) A 216, 309–32.

Gao, H. (2006) Application of fracture mechanics concepts to hierarchical biomechanics of bone and bone-like materials. Int. J. Fract. 138, 101–37.

Gautieri, A., Vesentini, S., Redaelli, A. and Buehler, M. J. (2011) Hierarchical structure and nanomechanics of collagen microfibrils from the atomistic scale up. Nano Letters 11, 757–766.

Gegauff, C. (1907) Strength and Elasticity of Cotton Threads. Bull. Soc. Ind. Mulhous. 77, 153–176.

Gibson, L. J., Ashby, M. F., Karam G. N., Wegst, U. and Shercliff H. R. (1995) The Mechanical-Properties of Natural Materials .2. Microstructures for Mechanical Efficiency, Proceedings of the Royal Society of London Series a-Mathematical and Physical Sciences 450, 141-162.

Godara, A., Mezzo, L., Luizi, F., Warrier, A., Lomov, S. V., van Vuure, A. W., Gorbatikh, L., Moldenaers, P. and Verpoest, I. (2009) Influence of carbon nanotube reinforcement on the processing and the mechanical behaviour of carbon fiber/epoxy composites. Carbon 47, 2914–23.

G´omez, J. B., I˜niguez, D. and Pacheco, A. F. (1993) Solvable Fracture Model with Local Load Transfer. Phys. Rev. Lett. 71, 380–383.

Gómez, J. B. and Pacheco, A. F. (1997) Size-frequency distribution of earthquakes in hierarchically organized load-transfer models. Nonlinear Process Geophys 4, 207–11.

Grishanov, S. A., Harwood, R. J. and Bradshaw, M. S. (1999) A Model of Fiber Migration in Staple-fibre Yarn Part I, Journal of the Textile Institute 90, 298–321.

Gücer, D. E. and Gurland, J. (1962) Comparison of the statistics of two fracture modes. J. Mech. Phys. Solids 10, 365–373.

Guidoin, M. F., Marios, Y., Bejui, J., Poddevin, N., King, M. W. and Guidoin, R. (2000) Analysis of retrieved polymer fiber based replacements for the ACL. Biomaterials 21, 2461–2474.

Gumbel, E. J. (1954) Statistical theory of extreme values and some practical applications. Nat. Bur. Standards Appl. Maths. Series 33.

Gumbel, E. J. (1958) Statistics of extremes. New York: Columbia University Press.

Gurney, H. P. (1925) The distribution of stress in cotton products. J. Text. Inst. 16, 269–289.

Hansen, A. and Hemmer, P. C. (1994) Burst Avalanches in Bundles of Fibers: Local Versus Global Load-Sharing. Phys. Lett. A 184, 394–396.

Hansen, A. and Roux, S. (2000) Statistical toolbox for damage and fracture. chapter 2, 17–101. Springer Verlag.

Harlow, D. G. and Phoenix, S. L. (1978a) The Chain-of-Bundles probability model for the strength of fibrous materials I: Analysis and Conjectures. Journal of Composite Materials 12, 195–214.

Harlow, D. G. and Phoenix, S. L. (1978b) The chain-of-bundles probability model for the strength of fibrous materials. II. A numerical study of convergence. J. Compos. Mater. 12, 314–34.

Harlow, D. G. and Phoenix, S. L. (1981a) Probability distribution for the strength of composite materials, I: Two level bounds. Int. J. Fract. 17, 347–372.

Harlow, D. G. and Phoenix, S. L. (1981b) Probability distribution for the strength of composite materials, II: A convergent sequence of tight bounds. Int. J. Fract. 17, 601–630.

Harter, L. (1950) A chronological annotated bibliography on order statistics, 1, Published by USAF.

Helmer, T., Peterlik, H. and Kromp K. (1995) Coating of carbon fibres. The strength of the fibres. J. Am. Ceram. Soc. 78, 133–136.

Hemmer, P. C. and Hansen, A. (1992) The Distribution of Simultaneous Fiber Failures in Fiber Bundles. J. Appl. Mech. 59, 909–914.

Herrmann, H. J. and Roux, S. (1990) editors. Statistical models for the fracture of disordered media. Random materials and processes. Elsevier, Amsterdam.

Hidalgo, R. C., Kun, F. and Herrmann, H. J. (2001) Bursts in a fiber bundle model with continuous damage. Phys. Rev. E 64, 066122.

Hidalgo, R. C., Moreno, Y., Kun, F. and Hermann, H. J. (2002) Fracture model with variable range of interaction. Physical review E 65, 1–8.

Hillerborg, A., Mod´eer, M. and Petersson. P. E. (1976) Analysis of crack formation and crack growth in concrete by means of fracture mechanics and finite elements. Cem. Concr. Res. 6, 773–782.

Hitchon , J. W. and Phillips, D. C. (1979) The dependence of the strength of carbon fibres on length. Fiber Sci. Technol. 12, 217–233.

Horan, R. L., Collette, A. L., Lee, C., Antle, K., Chena, J. and Altmana, G. H. (2006) Yarn design for functional tissue engineering. Journal of Biomechanics 39, 2232–2240.

http://eurospaceward.org/2010/Summary_report_on_4th_ESW_conference.pdf. Prof. B. Yakobson's talk.

Hua, C. G. and Xin, D. (2005) Strength Distribution Analysis of Typical Staple Fibres. Journal of Donghua University 22, 9–11.

Huang, W., and Wang, Y. (2004) Statistical dynamic tensile strength of UHMWPE-fibres. Polymer 45, 3729–3734.

Hunt, R. A. and McCartney, L. N. (1979) A new approach of to Weibull's statistical theory of brittle fracture. Int. J. Fract. 15, 365–375.

Ibnabdeljalil, M. and Curtin, W. A. (1997) Strength and reliability of fiber-reinforced composites: localized load sharing and associated size-effects. International Journal of Solids Structures 34, 2649–2668.

Iijima, S. and Ichihashi, T. (1993) Single-shell carbon nanotubes of 1-nm diameter. Nature 363, 603.

Iwahori, Y., Ishiwata, S. and Ishikawa, T. (2003) Mechanical properties of CFRP using CNF (carbon nano-fiber) dispersed resin. In: Proceedings ICCM-14, San Diego.

Jeronimidis, G. and Atkins, A. G. (1995) Mechanics of Biological-Materials and Structures - Natures Lessons for the Engineer, Proceedings of the Institution of Mechanical Engineers Part C-Journal of Mechanical Engineering Science 209, 221-235.

Jeronimidis, G. Chapters 1 and 2, in Structural Biological Materials, Design and Structure-Property Relationships, Elices M., Editor. 2000, Pergamon: Amsterdam. 3-29.

Jiang, K., Li, Q. and Fan, S. (2002) Nanotechnology: Spinning continuous carbon nanotube yarns. Nature 419, 801.

Jones, A. S. and Dutta, H. (2010) Fatigue life modeling of self-healing polymer systems. Mechanics of Materials 42, 481– 490.

Joshi, S. P. and Ramesh, K. T. (2007) An enriched continuum model for the design of a hierarchical composite. Scripta. Mater. 57, 877–80.

Jung, T., Subramanian, R. V. and Manoranjan, V. S. (1993) Prediction of fibre strength at the critical length: a simulation theory and experimental verification for bimodally distributed carbon fibre strengths. J. Mater. Sci. 28, 4489–4496.

Kanzaki, S., Shima, M., Komeya, K. and Tsuge, A. (1999) Recent progress in the synergy ceramics project. Key Eng. Mater., 161–163, 437–442.

Kasa, Y. A. and Saito M. (1979) Weibull analysis of strengths of various reinforcing filaments. Fiber Sci. Technol. 12, 21–29.

Katz, J. L. (1976) Advances in Bioengineering, ASME, New York, NY.

Katz, J. L. (1980) Anisotropy of Young's modulus of bone. Nature, 283, 106-107.

Kelly, A. and MacMillan, N. H. (1986) Strong solids, 3rd Edn, Published by Clarendon press, Oxford.

Kim, D. H., Kim, B. J. and Jeong, H. (2005) Universality class of the fiber bundle model on complex networks. Phys. Rev. Lett. 94, 025501.

Kloster, M., Hansen, A. and Hemmer, P. C. (1997) Burst avalanches in solvable models of fibrous materials. Phys. Rev. E 56, 2615–2625.

Kolarík, J., Migliaresi, C., Stol, M. and Nicolais, L. (1981) Mechanical properties of model synthetic tendons. J. Biomed. Mater. Res. 15, 147–157.

Kolařík, J., Vaníček, J. and Migliaresi, C. (1984) Preparation and strength of poly(ethylene terephthalate) fiber bundles for model synthetic tendons. Journal of Biomedical Materials Research 18, 115–121.

Koussios, S. and Schmets,A. J. M. (2007) Hollow helix healing: A novel approach towards damage healing in fiber reinforced materials. Proceedings of the First International Conference on Self Healing Materials 18-20 April, Noordwijk aan Zee, The Netherlands.

Krajcinovic, D. and Silva, M. A. (1982) Statistical aspects of the continuous damage theory. International Journal of Solids Structures 18, 551–562.

Krajcinovic, D. and Rinaldi, A. (2005) Thermodynamics and Statistical Physics of Damage Processes in Quasi-ductile SolidsMech. Mater 37, 299–315.

Kun, F., Costa, M. H. A. S., Filho, R. N. C., Andrade Jr, J. S., Soares , J. B., Zapperi, S., and Herrmann, H. J. (2006) Damage and healing in fatigue fracture. cond-mat.

Kun, F., Raischel, R. C. Hidalgo and Herrmann, H. J. (2006) Modeling Critical and Catastrophic Phenomena in Geoscience, volume 705 of Lecture Notes in Physics, chapter Extensions of Fibre Bundle Models, 57–92. Springer Berlin.

Kun, F., Zapperi, S. and Herrmann, H. J. (2000) Damage in fiber bundle models. Eur. Phys. J. B 17, 269–279.

Launey, M. E., Buehler, M. J. and Ritchie, R. O. (2010) On the mechanistic origins of toughness in bone, Annu. Rev. Mater. Res. 40, 25-53.

Leech, C. M. (2002) The Modeling of friction in polymer fiber ropes, International Journal of Mechanical Sciences, 44, 621–643.

Leech, C. M. (2003) The modeling and analysis of splices used in synthetic ropes. Proc. R. Soc. Lond. 459, 1641–1659.

LeGeros. R. Z. (1991) in: H.M. Meyers (Ed.), Monographs in Oral Science, Karger, Basel, 121.

Li, C., Liu,Y., Yao, A., Ito, M., Noguchi, T. and Zheng, Q. (2010) Interfacial shear strengths between carbon nanotubes. Nanotechnology 21, 115704

Li, F. and Li, Z. (2001) Continuum damage mechanics based on modeling of fiber reinforced concrete in tension. Int. J. Solids Struct. 38, 777–793.

Lissart, N. and Lamon, J. (1997) Statistical analysis of failure of SiC fibres in the presence of bimodal flaw populations. J. Mater. Sci. 32; 6107–6117.

Liu, C., Cheng, H., Cong, H., Li, F., Su, G., Zhou, B. and Dresselhaus, M. (2000) Synthesis of Macroscopically Long Ropes of Well-Aligned Single-Walled Carbon Nanotubes. Adv. Mater. 12, 1190–1192.

Loan, D., Gao, S. and Mader, E. (2006) Jute/polypropylene composites. I. Effect of matrix modification. Compos. Sci. Technol. 66, 952–963.

Mahesh, S., Beyerlein, I. J. and Phoenix, S. L. (1999) Size and heterogeneity effects on the strength of fibrous composites. Physica D 133, 371–389.

Mahesh, S., Phoenix, S. L., Beyerlein, I. J. (2000) Strength distributions and size effects for 2D and 3D composites with Weibull fibers in an elastic matrix. Int. J. Fract 115, 41–85.

Maiti S. and Geubelle, P. (2005) A cohesive model for fatigue failure of polymers. Engineering Fracture Mechanics 72, 691–708.

Mann, S. and Weiner, S. (1999) Biomineralization: Structural questions at all length scales, J. Struct. Biol. 126, 179-181.

Mattheck, C. and Bethge, K. (1998) The structural optimization of trees, Naturwissenschaften 85, 1-10.

Mattheck, C. and Kubler, H. (1995) The internal Optimization of Trees. Springer Verlag, Berlin.

McCartney, L. N. and Smith, R. L. (1983) Statistical theory of the strength of fibre bundles. J. Appl. Mech. 50, 601– 608.

McClintock, F. A. and Argon, A. S. (1966) Mechanical behavior of materials. Addison-Wesley Publishing Company, 322–324

Meyers, M. A., Chen, P. Y., Lin, A. and Seki, Y. (2008) Biological materials: structure and mechanical properties. Progr. Mater. Sci. 53, 1-206.

Mili, M. R., Moevus, M. and Godin, N. (2008) Statistical fracture of E-glass fiber using a bundle tensile test and acoustic emmision monitoring. Composite Science and Technology 68, 1800–1808.

Mishnaevsky, J. L. (2007) Computational mesomechanics of composites. Wiley.

Mishnaevsky, J. L., Derrien, K. and Baptiste, D. (2004) Effect of microstructures of particle reinforced composites on the damage evolution: probabilistic and numerical analysis. Compos. Sci. Technol. 64, 1805–1818.

Moukarzel, C. and Duxbury, P. M. (1994) Failure of three-dimensional random composites, J. Appl. Phys. 76, 4086-4094.

Neckář, B. and Das, D. (2006) Mechanics of parallel fiber bundles. Fibres & Textile in Europe 14, 23–28.

Newman, W. I., Gabrielov, A., Durand, T., Phoenix, S. L. and Turcotte, D. L. (1994) An exact renormalization model for earthquakes and material failure: Statics and dynamics. Physica D 77, 200–16.

Newman, W. I. and Gabrielov, A. M. (1991) Failure of hierarchical distributions of fiber bundles. Int. J. Fract. 50,1–15.

Newman, W. L. and Phoenix, S. L. (2001) Time-dependent fiber bundles with local load sharing. Phys. Rev. E 63, 021507.

Niklas, K. J. (1992) Plant Biomechanics: an engineering approach to plant form and function. University of Chicago Press, Chicago.

Nukala, P. K. and Simunovic, S. (2005a) A continuous damage random thresholds model for simulating the fracture behavior of nacre. Biomaterials 26, 6087.

Nukala, P. K. and Simunovic, S. (2005b) Statistical physics models for nacre fracture simulation. Phys. Rev. E 72, 041919.

Olson, G. B. (1997) Computational design of hierarchically structured materials. Science 277, 1237– 1242.

Orlovskaja, N., Peterlik, H., Marczewski, M., Kromp, K. (1997) The validity of Weibull estimators-experimental verification. J. Mater. Sci. 32, 1903–1907.

Pan, N. (1993) Prediction of statistical strengths of twisted fibre structures. J. Mater. Sci. 22, 6107–6114.

Paramonov, Y. and Andersons, J. (2007) A family of weakest link models for fibre strength distribution. Compos. Part A. 38, 1227–1233.

Peirce, F.T. (1926) Tensile strength of cotton yarns, V. 'The weakest link'- Theorems on the strength of long and of composite specimens. J. Text. Inst. 17, 355–368.

Peterlik, H. (1995) The validity of Weibull estimators. J. Mater. Sci. 30, 1972–1976.

Petersson, P. E. (1981) Crack growth and development of fracture zone in plain concrete and similar materials. Tech. Rep. TVBM-1006, Division of Building Materials, Lund Institute of Technology, Lund, Sweden.

Phoenix, S. L. (1974) Probabilistic strenga.th analysis of fiber bundle structures. Fiber. Sci. Technol. 7, 15–31.

Phoenix, S. L. (1975a) Probabilistic inter-fiber dependence and the asymptotic strength distribution of classic fiber bundles. Int. J. Eng. Sci. 13, 287–304.

Phoenix, S. L. (1975b) Statistical analysis of flaw strength spectra of high modulus fibers. Composite Reliability, ASTM STP 580, 77–89.

Phoenix, S. L. (1979) Statistical theory of the strength of twisted fibre bundles with applications to yarns and cables. Text. Res. J. 7, 407–423.

Phoenix, S. L. and Ibnabdeljalil, M. and Hui, C. Y. (1997) Size effects in the distribution for strength of brittle matrix fibrous composites. Int. J. Solids. Struct. 34, 545–68.

Phoenix, S. L. and Beyerlein, I. J. (2000a) Statistical Strength Theory for Fibrous Composite Materials. In A. Kelly and C. Zweben, editors, Comprehensive Composite Materials, volume 1, chapter 1.19, 1–81. Pergamon-Elsevier Science, New York.

Phoenix, S. L. and Beyerlein,I. J. (2000b) Distribution and size scalings for strength in a one-dimensional random lattice with load redistribution to nearest and next nearest neighbors. Phys. Rev. E 62, 1622–45.

Phoenix, S. L. and Raj, R. (1992) Overview no. 100 Scalings in fracture probabilities for a brittle matrix fiber composite, Acta Metall. Mater. 40, 2813-2828.

Phoenix, S. L. and Smith, R. L. (1983) A comparison of probabilistic techniques for the strength of fibrous materials under local load-sharing among fibers. Int. J. Solids. Struct. 19, 479–96.

Phoenix, S. L. and Taylor, H. M. (1973) The asymptotic strength distribution of a general fibre bundle. Adv. Appl. Prob. 5, 200–216.

Phoenix, S. L. (1983) The stochastic strength and fatigue of fiber bundles. Int. J. Fract. 14, 327–44.

Pickering, K. L. and Murray, T. L. (1999) Weak link scaling analysis of high-strength carbon fibre. Compos. Part A. 30, 1017–1021.

Pickering, K. L., Beckermann, G. W., Alam, S. N., and Foreman, N. J. (2007) Optimising industrial hemp fibre for composites. Compos. Part A. 38, 461–468.

Porwal, P. K., Beyerlein, I. J. and Phoenix, S. L. (2006) Statistical strength of a twisted fiber bundle: an extension of Daniels' equal-load-sharing parallel bundle theory. Journal of Mechanics of Materials and Structures 1, 1425–1448.

Pradhan, S., Hansen, A. and Hemmer, P. C. (2005a) Crossover behavior in burst avalanches: Signature of imminent failure. Phys. Rev. Lett. 95, 125501.

Pradhan, S. and Hansen, A. (2005b) Failure properties of loaded fiber bundles having a lower cutoff in fiber threshold distribution. Phys. Rev. E 72, 026111 .

Pradhan, S. and Chakrabarti, B. K. (2003) Failure properties of fiber bundle models. Int. J. Mod. Phys. B 17, 5565–5581.

Pugno, N. (2006a) Mimicking nacre with super-nanotubes for producing optimized super-composites. Nanotechnology 17, 5480–5484. (chapter 5)

Pugno, N. (2006b) On the strength of the carbon nanotube-based space elevator cable: from nanomechanics to megamechanics, J. Phys.: Condens. Matter 18, 1971–1990.

Pugno, N. and Carpinteri, A. (2008) Design of micro/nano-bio-inspired hierarchical materials Philosophical Magazine Letters 88, 397 – 405.

Pugno, N. and Ruoff, R. (2006) Nanoscale Weibull statistics, J. of Applied Physics 99, 024301-4.

Pugno, N. and Ruoff, R. (2004) Quantized fracture mechanics. Philos. Mag. 84, 2829–2845.

Pugno, N. (2007a) Space elevator out of order? Nanotoday 18, 44– 47.

Pugno, N. (2007b) The role of defects in the design of space elevator cable: From nanotube to megatube. Acta Materialia 55, 5269–5279.

Pugno, N. (2007c) A general shape/size-effect law for nanoindentation. Acta Materialia 55, 1947–1953.

Pugno, N. (2007d) Young's modulus reduction of defective nanotubes Applied Physics Letters 90, 043106.

Pugno, N. (2007e) Velcro nonlinear mechanics, Applied physics letter 90, 121918.

Pugno, N. (2008) An analogy between the adhesion of liquid drops and single walled nanotubes. Scripta Materialia 58, 73.

Pugno, N., Bosia, F. and Carpinteri, A. (2008) Multiscale Stochastic Simulations for Tensile Testing of Nanotube-Based Macroscopic Cables. Small 4, 1044–1052.

Pugno, N., Bosia, F. and Abdalrahman, T. (2011) A new hierarchical fibre-bundle model theory for the calculation of the strength of bioinspired nanomaterials. Physical Review E. Submitted.

Pugno, N., Bosia, F. and Carpinteri. A. (2009) Size effects on the strength of nanotube bundles. Meas. Sci. Technol. 20, 1 –5.

Pugno, N., F. Marino, F. and Carpinteri. A. (2006) Toward a periodic table for the nanomechanical properties of the elements. International Journal of Solids and Structures 43, 5647–5657.

Qian, D., Wagner, G., Liu, W., Yu, M. and Ruoff. R. (2002) Mechanics of carbon nanotubes. Appl Mech Rev 55, 495–533.

Qin, Z., Buehler, M. and Kreplak, L. (2010) A multi-scale approach to understand the mechanobiology of intermediate filaments. Journal of Biomechanics 43, 15–22 .

Raischel, F., Kun, F. and Herrmann, H. J (2006) Failure process of a bundle of plastic fibersPhys. Rev. E 73, 066101–066112.

Ritchie, et. al http://medicalxpress.com/news/2011-08-brittleness-aging-bones-loss.html.

Rho, J., Kuhn-Spearing, L. and Zioupos, P. (1998) Mechanical properties and the hierarchical structure of bone, Medical Engineering & Physics 20, 92-102.

Rigueiro, J. P., Viney, C., Llorca, J. and Elices, M. (1998) Silkworm Silk as an Engineering Material. Journal of Applied Polymer Science 70, 2439–2447.

Rokugo, K., Uchida, Y., Katoh, H. and Koyanagi, W. (1995) Fracture mechanics approach to evaluation of flexural strength of concrete. ACI Materials Journal (Selected translation from Japan Concrete Institute) 92, 561–566.

Rosen, B. W. (1964) Tensil failure of fibrous composites. AIAA J. 2, 1985–1991.

Rosen B. W. (1965). Mechanics of Fiber Strengthening, Fibre Composite Materials, American Society for Metals, Ohio.

Roux, S. (2000) Thermally activated breakdown in the fiber-bundle model. Phys. Rev. E 62, 6164.

Saibel, E. (1969) Size effect in structural safety. Proceedings of the International Conference on Structure, Solid Mechanics and Engineering Design in Civil Engineering Materials, Southampton, Part I. 125–30.

Schmahl, W., Griesshaber, E., Merkel, C., Kelm, K., Deuschle, J., Neuser, R. D., Göetz, A. J., Sehrbrock, A. and Mader, W. (2008) Hierarchical fibre composite structure and micromechanical properties of phosphatic and calcitic brachiopod shell biomaterials–an overview. Mineral. Mag. 72, 541–62.

Scorretti, R., Ciliberto, S., and Guarino, A. (2001) Disorder enhances the effect of thermal noise in the fiber bundle model. Euro. phys. Lett. 55, 626–632.

Segurado, J. and Llorca, J. (2006) Computational micromechanics of composites: the effect of particle spatial distribution. Mech. Mater. 38, 873–83.

Shanov, V. N., Yun, Y. H. and Schulz, M. J. (2006a) Synthesis and Characterization of Carbon Nanotube Materials (Review). Journal of the University of Chemical Technology and Metallurgy 41, 377-390.

Shanov, V. N., Yun, Y. H., Tu, Y. and Schulz, M. J. (2006b) Substrate and Process Interplay During Synthesis of Millimeter Long Multi-Wall Carbon Nanotube Arrays. Sixth IEEE Conference on Nanotechnology, 215 – 218.

Shu, C., Rajagopalan, A., Ki, X. and Rajan, K. (2003) Combinatorial materials design through database science. In: Materials Research Society Symposium—Proceedings, vol. 804, Combinatorial and Artificial Intelligence Methods in Materials Science II, 333–341.

Sigl, L. (1992) Effects of the flaw distribution function on the failure probability of brittle materials. Z metallkunde 83, 518–523.

Smith, R. L. (1980) A probability model for fibrous composites with local load sharing. Proc. Roy. Soc. London, Series A 372, 539–553.

Smith, R. L. (1982) The asymptotic distribution of the strength of a series-parallel system with equal load-sharing. Ann. Probab. 10, 137–171.

Smith, R. L. and Phoenix, S. L. (1981) Asymptotic distributions for the failure of fibrous materials under series–parallel structure and equal loadsharing. J. Appl. Mech. 48, 75–81.

Sornette, D. J. (1989a) Elasticity and failure of a set of elements loaded in parallel, Phys. A 22, L243.

Sornette, D. J. (1989b) Failure thresholds in hierarchical and euclidian space by real space renormalization group, Phys. France 50, 745-755.

Sybrand van der Zwaang (1989) The concept of filament strength and Weibull modulus. Journal of Testing and Evaluation 17, 292–298.

Tran, C. D., Humphries, W., Smith, S., Huynh, C. and Lucas, S. (2009) Improving the tensile strength of carbon nanotube spun yarns using a modified spinning process. Carbon 47, 2662-2670.

Thompson, A. W. (1992) On Growth and Form - the complete revised edition. (unaltered republication of Cambridge Univ. Press, 1942) ed. Dover Publications.

Vincent, J. F. V. (1990) Structural Biomaterials. revised edition ed. Princeton University Press, Princeton.

Vincent, J. F. V. (1999) From cellulose to cell, Journal of Experimental Biology 202, 3263-3268.

Virgilii, A., Petri, A., and Salinas,S. R. (2007) A thermodynamical fiber bundle model for the fracture of disordered materials. J. Stat. Mech. P04009.

Wainwright, S. A., Biggs W. D., Currey J. D. and Gosline, J. M. (1982) Mechanical Design in Organisms. Princeton University Press.

Wan, Y. Q. and Ko, F. K. (2009) Hierarchical structure and mechanical properties of bamboo fibrils, in ICCM-17 Edinburgh, UK.

Wang, Z., Devel, M., Dulmet, D., Stuart. S. (2009) Geometry-Dependent Nonlinear Decrease of the Effective Young's Modulus of Single-walled Carbon Nanotubes Submitted to Large Tensile Loadings. Fullerenes, Nanotubes and Carbon Nanostructures 17, 1–10.

Weibull, W. (1939) A statistical theory of strength of materials. Royal Swedish Institute of Engineering Research (Ingenioersvetenskaps Akad. Handl.), Stockholm 153, 1–55.

Weibull, W. (1949) A statistical representation of fatigue failures in solids. Proc. R. Inst. Tech. No. 27.

Weibull, W. (1951) A statistical distribution function of wide applicability. J. Appl. Mech. 18, 293–297.

Weibull, W. (1956) Basic aspects of fatigue. Proceedings of the Colloquium on Fatigue, Stockholm, Berlin: Springer.

Weiner, S. and Dove, P. M. in Biomineralization, Vol. 54(Eds: P. M. Dove, S. Weiner, J. J. De Yoreo), Mineralogical Society of America, Washington D.C. 2003, 1.

Weiner, S. and Traub, W. (1992) Bone-Structure - from Angstroms to Microns, Faseb. J. 6, 879-885.

Weiner, S. and Wagner, H. D. (1998) The material bone: Structure mechanical function relations, Annual Review of Materials Science 28, 271-298.

Weiner, S., Addadi, L. and Wagner, H. D. (2000) Materials design in biology, Materials Science & Engineering C-Biomimetic and Supramolecular Systems 11, 1-8.

Wintermantel, E., Mayer, J., Blum, J., Eckert, K. L., Luscher, P. and Mathey, M. (1996) Tissue engineering scaffolds using superstructures. Biomaterials 17, 83–91.

Xiao, T., Ren, Y., Liao, K., Wu, P., Li, F., Cheng, H. M. (2008) Determination of tensile strength distribution of nanotubes from testing of nanotube bundles. Composites Science and Technology 68, 2937–2942.

Xiao, T., Ren, Y., Wu, P. and Liao, K. (2006) Force-strain relation of bundles of carbon nanotubes Applied Physics Letters 89, 033116.

Xu, Y. and Hoa, S. V. (2008) Mechanical properties of carbon fiber reinforced epoxy/clay nanocomposites. Compos Sci Technol 68, 854–861.

Yao, H. and Gao, H. (2007) Multi-scale cohesive laws in hierarchical materials. Int. J. Solids Struct. 44,8177–93.

Ye, J., Han, B. Q., Lee, Z., Ahn, B., Nutt, R. S. and Schoenung, J. M., (2005) A tri-modal aluminum based composite with super-high strength. Scripta. Mater. 53, 481–6.

Zafeiropoulos, N. E. and Baillie, C. A. (2007) A study of the effect of surface treatments on the tensile strength of flax fibres: Part II. Application of Weibull statistics. Compos. Part A. 38, 629–638.

Zapperi, S., Ray, P., Stanley, H. E. and Vespignani, A. (1999) Avalanches in Breakdown and Fracture Processes, Phys. Rev. E 59, 5049-5057.

Zhang, M., Atkinson, K. R. and Baughman, R. H. (2004) Multifunctional Carbon Nanotube Yarns by Downsizing an Ancient Technology. Science 306, 1358–1361.

Zhang, M., Fang, S., Zakhidov, A., Lee, S. B. and Aliev, A. (2005) Williams C, Atkinson K, Baughman R. Strong, Transparent, Multifunctional, Carbon Nanotube Sheets. Science 309, 1215–1219.

Zhang, X., Jiang, K., Feng, C., liu, P., Zhang, L., Kong, J., Zhang, T., Li, Q., Fan, S. (2006) Spinning and processing continuous yarn from 4-Inch Wafer Scale Super-Aligned Carbon Nanotube Arrays. Adv.Mater. 18, 1505–1510.

Zhang, S., Zhu, L., Minus, M. L., Chae, H. G., Jagannathan, S., Wong, C. P., Kowalik, J., Roberson, L. P. and Kumar, S. (2008) Solid-state spun fibers and yarns from 1-mm long carbon nanotube forests synthesized by water-assisted chemical vapor deposition. J. Mater. Sci. 43, 4356–4362.

Zhao, Q., Cranford, S., Ackbarow, T. and Buehler, M. J. (2009). Robustness-strength performance of hierarchical alphahelical protein filaments. International Journal of Applied Mechanics. 1, 85–112 .

Zhou, S. J. and Curtin, W. A. (1995) Failure of fiber composites: A lattice green function model. Acta Metalurgica Material 43, 3093–3104.

Zweben, C. (1968) Tensile failure analysis of fibrous composites. AIAA J. 6, 2325–2331.